1995

Crystallographic studies of sialidase and structure-based design of inhibitors.

Clinton Livingston White
University of Alabama at Birmingham

INFORMATION TO USERS

This manuscript has been reproduced from the microfilm master. UMI films the text directly from the original or copy submitted. Thus, some thesis and dissertation copies are in typewriter face, while others may be from any type of computer printer.

The quality of this reproduction is dependent upon the quality of the copy submitted. Broken or indistinct print, colored or poor quality illustrations and photographs, print bleedthrough, substandard margins, and improper alignment can adversely affect reproduction.

In the unlikely event that the author did not send UMI a complete manuscript and there are missing pages, these will be noted. Also, if unauthorized copyright material had to be removed, a note will indicate the deletion.

Oversize materials (e.g., maps, drawings, charts) are reproduced by sectioning the original, beginning at the upper left-hand corner and continuing from left to right in equal sections with small overlaps. Each original is also photographed in one exposure and is included in reduced form at the back of the book.

Photographs included in the original manuscript have been reproduced xerographically in this copy. Higher quality 6" x 9" black and white photographic prints are available for any photographs or illustrations appearing in this copy for an additional charge. Contact UMI directly to order.

UMI

A Bell & Howell Information Company
300 North Zeeb Road. Ann Arbor. MI 48106-1346 USA
313/761-4700 800/521-0600

CRYSTALLOGRAPHIC STUDIES OF SIALIDASE AND STRUCTURE-BASED DESIGN OF INHIBITORS

by

CLINTON LIVINGSTON WHITE

A DISSERTATION

Submitted in partial fulfillment of the requirements for the degree of Doctor of Philosophy in the Department of Biochemistry and Molecular Genetics in the Graduate School, The University of Alabama at Birmingham

BIRMINGHAM, ALABAMA

1995

ABSTRACT OF DISSERTATION
GRADUATE SCHOOL, UNIVERSITY OF ALABAMA AT BIRMINGHAM

Degree Doctor of Philosophy Major Subject Biochemistry and Molecular Genetics

Name of Candidate Clinton Livingston White

Title Crystallographic Studies of Sialidase and Structure-based Design of Inhibitors

Presented is the X-ray crystallographic structural analysis of influenza virus sialidase (neuraminidase, EC 3.2.1.18) when complexed to several inhibitors and the use of structure-based methods to develop specific bacterial sialidase inhibitors. The crystal structure of influenza virus type B sialidase (B/Mem/89 and B/Lee/40) was solved using molecular replacement phasing methods. From the complexes, the eleven strictly conserved active site residues that are critical for binding and stabilization of the substrate were identified. Crystallographic studies were also performed on the complex of influenza virus type A (N2 and N9 subtypes) and type B sialidases complexed to a sialic acid derived phosphonate analog, (4-acetamido-2,4-dideoxy-*D-glycero-D-galacto*-1-octopyranosyl) phosphonic acid or PANA, by difference Fourier techniques. Compared to sialic acid, PANA has a phosphonyl group substituted for the carboxylate group and does not possess a C2 hydroxyl. The crystal structures of the complexes between the equatorial phosphonate enantiomer, ePANA, and the type A and type B influenza virus sialidases indicated that the ePANA compound was bound to all three viral sialidases in a chair-like conformation. By

adopting a chair-like conformation, ePANA can mimic the inhibitor-protein interactions observed in the sialic acid and DANA complexes. The structural studies also indicated that the lower inhibition activity of ePANA toward the type A N9 sialidase is not due to differences in the relative binding mode of ePANA. The crystal structure of the complex between the type A N2 influenza sialidase and the axial phosphonate enantiomer, aPANA, was also solved. In this complex, the axial enantiomer must bind in a boat-like conformation to retain the inhibitor-protein interactions observed in the sialic acid and DANA complexes. Finally, the knowledge derived from analyzing the influenza virus sialidase-inhibitor complexes was applied to the structure-based design of novel bacterial sialidase inhibitors. The coordinates of the *Salmonella typhimurium*-DANA inhibitor complex and two benzoic acid based compounds and the program GRID were used to construct three classes of bacterial specific sialidase inhibitors. The program DELPHI was used to analyze the effect of the inhibitor modifications upon the calculated free energy change of complex formation.

Abstract Approved by: Committee Chairman Ming Luo

Program Director Jeffrey A. Engler

Date 7/11/95 Dean of Graduate School

DEDICATION

This dissertation is dedicated to the memory of Dr. F. L. "Bud" Suddath, Jr., without whose advice and enthusiasm, I would not have come to UAB to become a crystallographer.

ACKNOWLEDGMENTS

I would like to thank my mentor, Dr. Ming Luo, for his generosity, support, friendship, and guidance over the last five years. In addition, I would like to extend my deepest appreciation to Drs. Gillian Air, Charles Bugg, Jeffrey Esko and Stephen Harvey for serving on my committee and for their many helpful, enlightening discussions. I am grateful to the members of the Luo lab and the Center for Macromolecular Crystallography, both past and present, who have given freely of their friendship, knowledge, and expertise.

I am thankful for my father, Ray, and my mother, Susan, who instilled in me the joy of learning and always encouraged me to do my best. I love you both very much. I am also very thankful to be married to a wonderful woman, Elizabeth, whose enduring support, patience, and love made this journey possible.

TABLE OF CONTENTS

TABLE OF CONTENTS (Continued)

LIST OF TABLES

LIST OF TABLES (Continued)

LIST OF FIGURES

LIST OF FIGURES (Continued)

LIST OF SCHEMES

Scheme Page

STRUCTURE OF INFLUENZA VIRUS NEURAMINIDASE B/LEE/40 COMPLEXED WITH SIALIC ACID AND A DEHYDRO ANALOG AT 1.8Å RESOLUTION: IMPLICATIONS FOR THE CATALYTIC MECHANISM

LIST OF ABBREVIATIONS

4-guanidino-Neu5Ac2en: GANA; 2-deoxy-2,3-dehydro-4-guanidino-*N*-acetylneuraminic acid

α(hkl): structure factor phase

$\alpha(hkl)_{calc}$: calculated structure factor phase

ΔG_{el}: electrostatic contribution to the free energy change

ε_p: protein dielectric

ε_s: solvent dielectric

ρ: Rossmann and Blow defined rotation matrix

d: translation matrix

C: rotation matrix

DANA: Neu5Ac2en, 2-deoxy-2,3-dehydro-*N*-acetylneuraminic acid

EC: extracellular

f_j: atomic scattering factor

F(hkl): structure factor amplitude

$F(hkl)_{obs}$: F_o, observed structure factor amplitude

$F(hkl)_{calc}$: F_c, calculated structure factor amplitude

F(hkl): structure factor

$\mathbf{F(hkl)_{calc}}$: calculated structure factor

GBA: 4-acetylamino-3-guanidino-benzoic acid

HA: hemaglutinin

HBA: 4-acetylamino-3-hydroxyl-benzoic acid

HNBA: 4-acetylamino-3-hydroxyl-5-nitro-benzoic acid

Ki: inhibition constant

MB: membrane-bound

MUN: 4-methylumbelliferyl-α-*D*-*N*-acetylneuraminic acid

PEG: polyethylene glycol

N2: A/Tokyo/3/67 influenza virus neuraminidase strain

N9: A/tern/Australia/G70c/75 influenza virus neuraminidase strain

NA: neuraminidase; sialidase

NAG: *N*-acetyl glucosamine

NANA: Neu5Ac, α-sialic acid, *N*-acetylneuraminic acid; 5-acetylamino-3,5-dideoxy-*D*-glycero-*D*-galacto-nonulosonic acid

NANL: *N*-acetylneuraminyl lactose

PANA: phosphonate analog of neuraminic acid

aPANA: axial PANA (β-enantiomer)

ePANA: equatorial PANA (α-enantiomer)

QSAR: quantitative structure-function relationships

r.m.s.: root-mean-square

r.m.s.d.: root-mean-square difference

SA: simulated annealling

V_m: Mathew's Volume

INTRODUCTION

Sialidases

Sialidases (acylneuraminyl hydrolases, EC 3.2.1.18), also known as neuraminidases, are enzymes that cleave the α-ketosidic bond between a terminal sialic acid residue and an aglycon moiety.

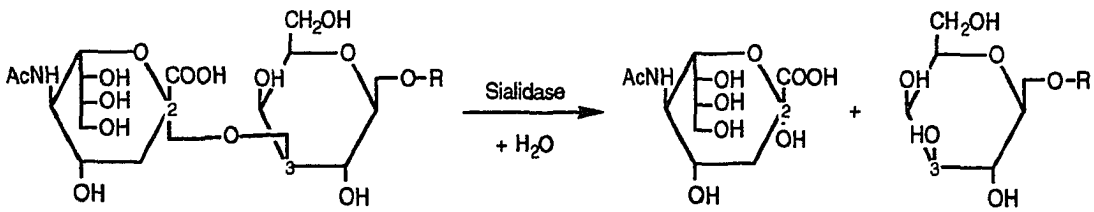

The aglycon is usually the penultimate sugar residue of a glycoconjugate carbohydrate chain. Sialidase activity was first identified almost 50 years ago due to its ability to alter red blood cell agglutination (Hirst, 1941) More than 15 years later, the first sialidase was purified and characterized from the influenza virus and the bacteria *Vibrio cholerae* (Gottschalk, 1957). Today, many sialidases, which are specific for varying ketosidic linkages, have now been identified in viruses, bacteria, parasites, and mammals (Appendix A). Sialidases play a critical role in viral, bacterial, and protozoan biology by mediating metabolism, adherence, and infection. They are also important regulators of alternate complement pathway activation, red blood cell destruction, cell growth, cell adhesion, and tumor metastasis in mammalian systems

(Ganguly *et al.*, 1976; Marchesini *et al.*, 1984; Moran *et al.*, 1986; Pitto *et al.*, 1989; Miyagi *et al.*, 1990; Miyagi *et al.*, 1992; Saito & Yu, 1992; Pilatte *et al.*, 1993; Saito & Yu, 1993; Sweeley, 1993; Kopitz *et al.*, 1994). The development of sialidase inhibitors could lead to a better understanding of these mechanisms. Given the wide prevalence and important role of sialidases in microbial infection, sialidase inhibitors have the potential to be very useful anti-viral and anti-bacterial agents.

This dissertation, and the manuscripts herein, details the use of X-ray crystallography to study several sialidase-inhibitor complexes and the use of structural information in the design sialidase specific inhibitors. The first two manuscripts represent the use of X-ray crystallography to study the structure of both native and inhibitor complexed influenza virus sialidase. These structural studies provided a better understanding of the atomic interactions responsible for the binding of different inhibitors to influenza virus sialidase. The third manuscript presents the computer-aided design of bacterial sialidase inhibitors.

Influenza virus sialidase

Three types of serotypically distinct influenza viruses have been isolated: A, B and C. Types A, B and C influenza viruses all belong to the orthomyxoviridae ("straight mucin-reacting virus") family. All three types of influenza virus can infect humans, but types A and B influenza viral infections are responsible for most cases of the disease "Flu." In fact, the name *influenza* given to flu-like symptoms originated in 18th-century Italy where astrological

and planetary influences were thought to control outbreak of the disease (Kilbourne, 1987). Since that time, we have learned a great deal more concerning the genetics, molecular biology, immunology, and structure of the related types A and B influenza viruses. We still know relatively little about the type C influenza virus, but it seems to be organized in a manner more related to the paramyxovirus family (Kilbourne, 1987). The major antigenic determinants in both types A and B influenza viruses are the hemagglutinin (HA) and sialidase (neuraminidase, NA) surface glycoproteins, which are attached to the viral membrane. Within the type A influenza category, individual subtypes have been identified, which differ in their hemagglutinin and sialidase subtypes and therefore do not show antigenic cross-reactivity. Thirteen subtypes of hemagglutinin (H1-H13) and nine subtypes of sialidase (N1-N9) are currently recognized by the World Health Organization. The name of each type A subtype, e.g. H1N1, H6N8, etc., reflects the glycoprotein subtypes present in that subtype. The type A subtypes H1N1, H2N2, and H3N2 are the only type A subtypes that have been recovered from human infections. The remaining known type A subtypes were isolated from other mammals, such as water fowl, horses or swine. To date, no subtypes of type B or C influenza have been identified. Type B influenza virus has only been isolated from human patients. Individual strains of type A and B are usually referred to by their type/origin/isolate number/year of isolation, for example, "A/Tokyo/3/67" or "B/Memphis/3/89."

The influenza virus genome is composed of eight negative stranded RNA segments. In the mature virion, the genomic RNA is

packaged with several other proteins into a ribonucleoprotein (RNP) particle, which is then encased by a lipid bilayer membrane derived from the host cell. In addition to the viral hemagglutinin and sialidase, several polymerase, polymerase-related, and structural proteins are virally encoded and found either within the virus particle or associated with the viral membrane (Figure 1).

Influenza virus sialidase activity

The influenza virus sialidase will cleave $\alpha 2 \rightarrow 3$ and $\alpha 2 \rightarrow 6$ (very low activity) but not $\alpha 2 \rightarrow 8$ linked terminal sialic acid (Neu5Ac) residues of host cell surface sialoglycoconjugates. Recent work indicates that the removal of terminal sialic acid residues from neighboring sialoglycoconjugates by the influenza virus sialidase prevents aggregation of newly budding influenza virion at the surface of an infected cell (Liu & Air, 1993; Liu *et al.*, 1995). In the absence of neuraminidase activity, the influenza virus hemagglutinin has been proposed to agglutinate the budding virions by binding the terminal sialic acid residues of (1) hemaglutinin molecules present on other virions and/or (2) sialoglycoproteins normally present on the host cell surface. The removal of sialic acid residues from the host cell mucin surfaces by the viral sialidase may also allow the virus to effectively spread throughout the nasal and bronchial mucous membranes where infection normally occurs. The sialidase protein has also been observed to induce a strong antibody immune response in infected hosts, which attenuates lethal viral infection (Webster *et al.*, 1988).

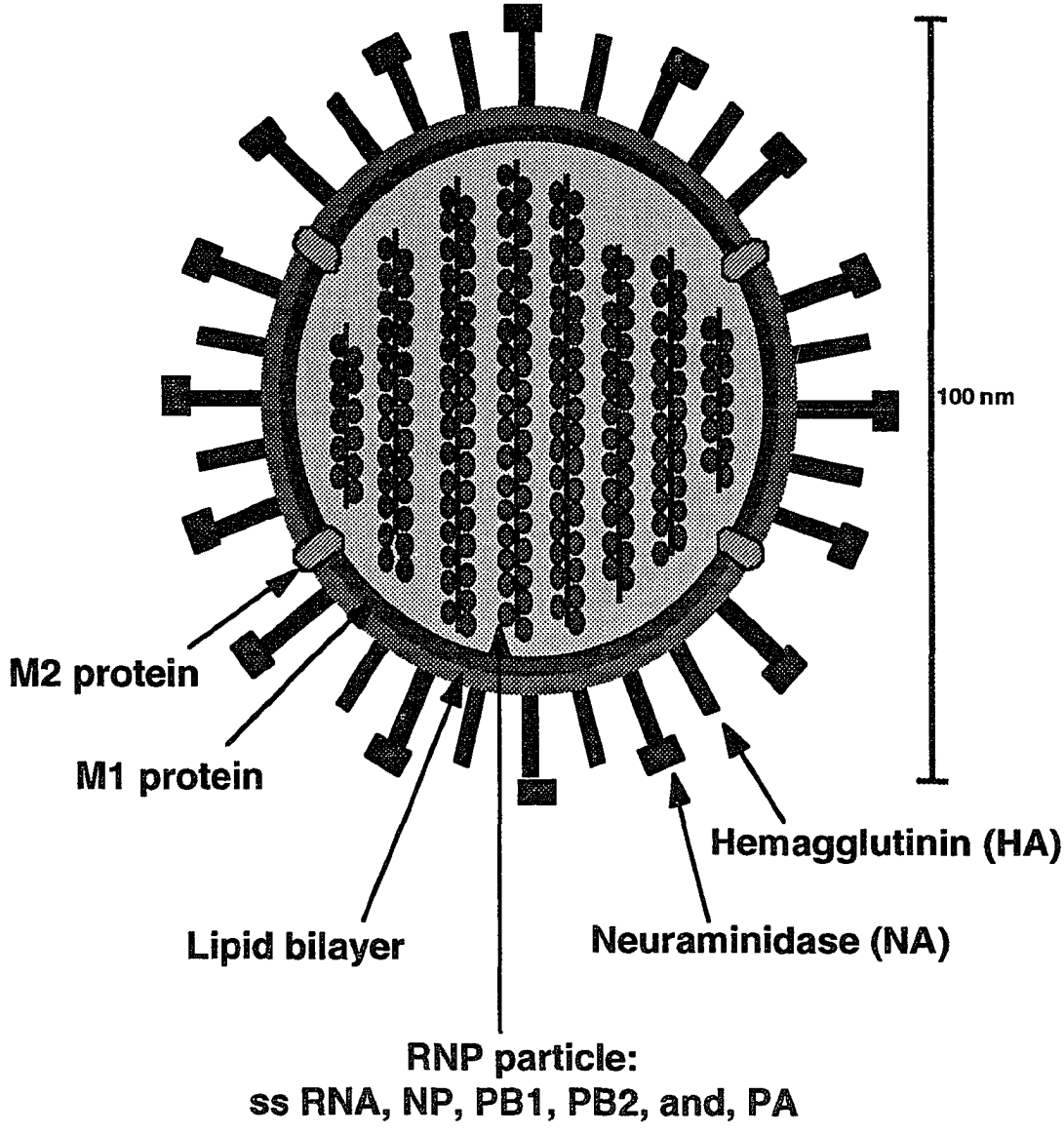

Figure 1. Influenza virus structure.

The optimum pH for influenza virus sialidase is pH 5.5-6.0, but it does show high enzymatic activity in the very broad pH range of 5.0-9.0 (Chong *et al.*, 1991a). The presence of Ca^{2+} ions has been shown to dramatically affect both types A and B influenza virus sialidase activity in a strain-dependent manner. In the A/Tokyo/3/67 strain, exhaustive dialysis or EDTA addition does not completely abolish activity, but it does decrease the sialidase activity to ~10-15% of that observed in the presence of Ca^{2+} ions (Chong *et al.*, 1991b). The crystal structure of both types A and B influenza sialidases indicate that one calcium ion binds to each subunit near the active site and another ion binds along the tetramer four-fold axis and is equally shared by four subunits. The affect of calcium ions, Ca^{2+}, on the activity of influenza virus sialidase was documented by Chong *et al.* (1991b). The observed apparent K_d for Ca^{2+} binding is 2 mM. From the crystallographic analysis of several influenza virus sialidases, two calcium ions are known to bind to the influenza virus sialidase monomer. One calcium atom is bound on the tetramer four-fold axis and can be removed by dialysis or EDTA treatment. The second calcium is bound near the active site and cannot be removed by dialysis or EDTA treatment. The bound calcium ions stabilize the tetrameric form of the active enzyme, as well as the structure of the individual monomer subunits. In addition, the calcium ions exert a non-specific ionic strength effect to enhance substrate binding. The ionic strength effect on influenza virus activity can be duplicated by the addition of NaCl. Kinetic studies on the type A N2 sialidase, using the substrate MUN, a constant ionic strength, and saturating Ca2+ conditions produced a maximal K_m =

6.8 x 10^{-5} M and turnover number = 9.5 sec^{-1}. Calcium ions also affect the inhibition activity observed using the inhibitor Neu5Ac2en, a transition state analog of sialic acid. Inhibition of the type A N2 influenza virus sialidase by Neu5Ac2en in the presence of 20 mM Ca^{2+} gave a K_i = 1.1 x 10^{-6} M. Sialic acid, Neu5Ac, which is a product of sialidase cleavage, also inhibits influenza virus sialidase with a K_i = ~1 x 10^{-3} M.

Influenza virus sialidase structure

The sialidase of influenza virus was identified nearly 40 years ago and it is one of the best studied sialidases, both in terms of protein function and structure. The influenza virus sialidase is a membrane anchored type II glycoprotein composed of four identical subunits. In the mature virion, the sialidase subunits have C4 symmetry and form a hydrophilic, box-like head attached to a long, thin stalk, which has a hydrophobic terminus anchored into the bilayer membrane of the virion. Post-translational modification of the influenza sialidase adds several N-linked glycosylation chains to both the box-like head and stalk domains. No proteolytic processing is observed for influenza sialidase, therefore, the mature protein contains an N-terminal methionine and a hydrophobic, signal sequence within the trans-membrane domain (Figure 2) (Blok *et al.*, 1982; Markoff *et al.*, 1984; Hogue & Nayak, 1992).

While types A and B sialidases only share ~25% homology in their amino acid sequences, their overall topology and active site residues are strictly conserved across all strains. The influenza virus sialidase is composed of six β-sheets arranged in a left-

handed propeller fold (β-propeller motif), shown in Figure 2. Each β-sheet contains four anti-parallel β-strands. The β-strands in each sheet are connected by large loops on the top (viral distal) surface of the box-like head and short, tight turns on the bottom (viral proximal) surface of the head. Also present in the influenza virus tetramer are several intra-subunit disulfide bonds, which stabilize the β-sheet topology. Protease treatment of whole influenza virions cleaves the viral sialidase stalk just below the box-like head to release free sialidase heads (~200 kDa) that contain all the antigenic and enzymatic functions of the wild type enzyme. The protease released heads can be easily purified and used to grow protein crystals suitable for X-ray diffraction studies (Laver, 1978). The crystalline sialidase remains enzymatically active. Therefore, small, hydrolyzible substrates, such as the tri-saccharide *N*-acetylneuraminyl lactose, and low molecular weight inhibitors, such as Neu5Ac2en, were diffused into the protein crystals to locate and study the active site of influenza virus sialidase. The influenza virus sialidase monomer active site is located in a deep depression approximately 10-12Å wide near the central pseudo six-fold rotation axis (Figure 2). The residues that make direct contact with the substrate sialic acid form the active site and are strictly conserved among all known influenza virus sialidases. The first manuscript following the introduction, "*Structure of Influenza Virus Neuraminidase B/Lee/40 Complexed with Sialic Acid and a Dehydro Analog at 1.8-A Resolution: Implications for the Catalytic Mechanism*," will describe in detail the influenza active site and the role of the individual residues in ligand binding.

Figure 2. Influenza virus sialidase structure. Above is a schematic drawing of the influenza virus sialidase structure showing the general organization of domains. The influenza virus head is released by protease treatment of the whole virion, which cleaves the stalk below the head domain as shown. Below is a ribbons drawing of the influenza virus B/Lee/40 sialidase monomer. Each of the four-stranded antiparallel β-sheets comprising the six-sheet β-propeller motif are color coded with a different color. The location of the calcium ions is also identified by the red spheres. Ca2+ 501 is located on the tetramer four-fold axis. Ca2+ 500 is located near the active site. The active site is offset from the center of the monomer and is identified by the ball-and-stick model of sialic acid. The black spheres represent amino acid residues, which differ in the B/Lee/40 strain from all other type B influenza neuraminase strains sequenced.

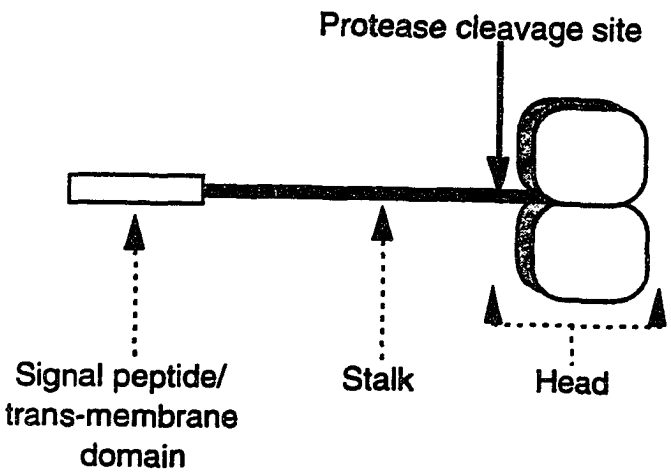

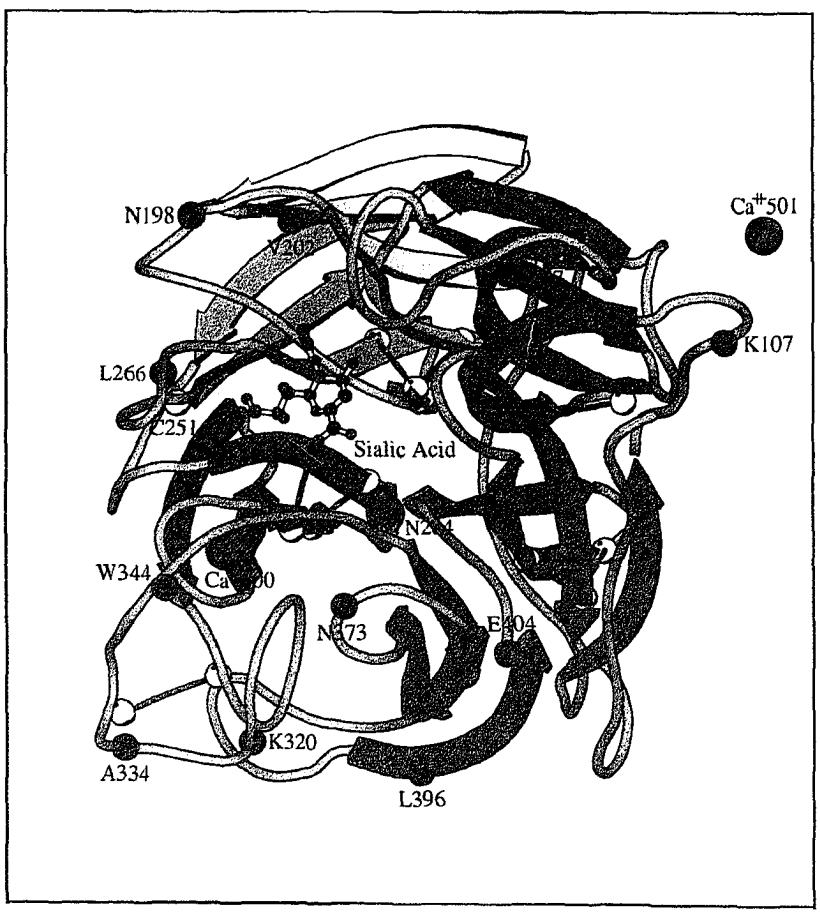

Bacterial sialidases

Though sialidases have long been identified in some bacteria, the last 20 years have seen an explosion of bacterial sialidases purified and characterized due to the advance of molecular biology techniques. The results have also shed light on the role that sialidases play in bacterial metabolism, adherence, infection, and pathogenicity. In the absence of other carbohydrates, the free sialic acid generated by the bacterial sialidase can be used by the bacteria as an alternative energy source. In addition, by cleaving the terminal sialic acid residues from host glycoconjugates, the bacterial sialidases expose new carbohydrate moieties. These non-sialic acid carbohydrate residues can then be recognized by lectin-like domains present on the bacterial surface. Except for the active site, the bacterial sialidases do not exhibit an amino acid sequence similarity to the viral sialidases (Roggentin *et al.*, 1989). Another characteristic of bacterial sialidases is the presence of other non-sialidase related domains in the whole protein. These additional domains have other functions, such as lectin-like activity, which are beneficial to the bacteria. Like the viral sialidases, several bacterial sialidases have been shown to be membrane associated (Straus *et al.*, 1993; Camara *et al.*, 1994). The majority of bacterial sialidases are excreted by the bacterium into the culture fluid and are therefore classified as extracellular. The bacterial sialidases can also be divided into two subgroups based on their requirement for divalent metal ions for activity. The bacterial sialidase subgroup that requires metal ions is represented by the *Vibrio cholerae* sialidase. The subgroup that does not require metal ions

for activity is represented by several bacterial sialidases, such as *Clostridium perfringens, Clostridium sordelli, Micromonospora viridifaciens, and Salmonella typhimurium*, among others. In addition to the high degree of sequence homology within the subgroup, the non-metal requiring sialidases also show a large amount of similarity to the N-terminal trans-sialidase domain of the trypanosomal trans-sialidase enzyme (Roggentin *et al.*, 1989). Because its crystal structure had been solved by Crennell *et al.* (1993) and because its molecular biology was one of the most extensively studied, the *Salmonella typhimurium* sialidase was chosen as a model system for the design of bacterial and trypanosomal specific sialidase inhibitors.

***Salmonella typhimurium* sialidase activity**

The sialidase gene, *nanH*, from the enteric Gram-negative bacterium *S. typhimurium*, has been cloned and the expressed bacterial sialidase has been well characterized by Dr. Vimr and colleges (Hoyer *et al.*, 1991; Hoyer *et al.*, 1992). No significant differences were detected in the expressed enzyme as compared to the wild type sialidase, except in the wild type strain, the sialidase accounts for <1% of the total protein. The postulated role of the *S. typhimurium* sialidase is to produce free sialic acid as an energy and carbon source under starvation conditions (Hoyer *et al.*, 1992).

The *S. typhimurium* sialidase has a 260-fold cleavage preference for $\alpha 2 \rightarrow 3$ versus $\alpha 2 \rightarrow 6$ linked sialic acids. In addition, the *S. typhimurium* sialidase has a high enzymatic activity for ganglioside and mucin substrates containing terminal sialic acids.

The *S. typhimurium* sialidase does not efficiently recognize α2→8 or α2→9 linked sialic acids, therefore, shows little cleavage activity for colominic acid, which is a homopolymer of sialic acid, or Group C polysaccharides.

The *S. typhimurium* sialidase is active over a broad pH range, 5.5-7.0, and does not require divalent metal ions for activity. Using 4-methylumbelliferyl-α-*D*-*N*-acetylneuraminic acid (MUN) as the substrate, the *S. typhimurium* sialidase displayed a K_m = 2.5 x 10^{-4} M and a turnover number = 2,700 sec^{-1}. The dehydro analog of sialic acid, Neu5Ac2en, inhibited *S. typhimurium* sialidase with a K_i = 0.38 mM. As compared to influenza virus sialidase, high levels of the cleavage product, Neu5Ac, did not inhibit the bacterial sialidase.

***Salmonella typhimurium* sialidase structure**

The *S. typhimurium* sialidase has a molecular weight of 41 kDa and a pI ≥ 9. The three-dimensional structure of *S. typhimurium* have been determined by Crennell *et al.* using X-ray crystallography (Crennell *et al.*, 1993). The structure was solved to 2.0Å by the multiple isomorphic replacement method and refined to a crystallographic R-factor of 18.9%. Homologous to the influenza virus sialidase, the *S. typhimurium* sialidase is folded into a lefthanded propeller motif consisting of six, four-stranded antiparallel β-sheets (Figure 3). The length of the β-strands and the loops connecting the β-strands differ markedly from the viral sialidase structure. One disulfide bond is observed in the *S. typhimurium* sialidase that links the first and second β-sheets.

The active site of the *S. typhimurium* sialidase was located by soaking the inhibitor Neu5Ac2en into crystals of the native enzyme. A detailed comparison of the *S. typhimurium* sialidase active site to the influenza virus active site is presented in the third manuscript following the Introduction, *"Modeling of Bacterial Sialidase Inhibitors."*

Trypanosomal trans-sialidase

Trypanosomes are parasitic protozoan hemoflagellates that require both insect and mammalian hosts to complete a full life cycle. *Trypanosoma cruzi* infection in humans is the etiological agent of Chagas' disease in South America, an incurable affliction that affects 15-20 million people. Recent results have indicated that the *T. cruzi* trans-sialidase enzyme is required trypanosomal infection of human host cells. Based on amino acid sequence analysis, the trans-sialidase protein is composed of a N-terminal trans-sialidase catalytic domain, a fibronectin III module-like domain, and a long tandem repeat domain, and a C-terminal 35 amino acid hydrophobic region, which may be linked to a glycosylphosphatidylinositol (GPI) anchor (Pereira *et al.*, 1991). The atomic structure of the N-terminal trans-sialidase domain of the trypanosomal trans-sialidase protein has not been solved. But, the trypanosomal trans-sialidase N-terminal domain has a high sequence homology to the *S. typhimurium* sialidase, particularly in the region of the active site residues and Asp boxes (Pereira *et al.*, 1991). Using the amino acid sequence alignment of the trypanosomal trans-sialidase to the bacterial sialidase, a three-dimensional model of

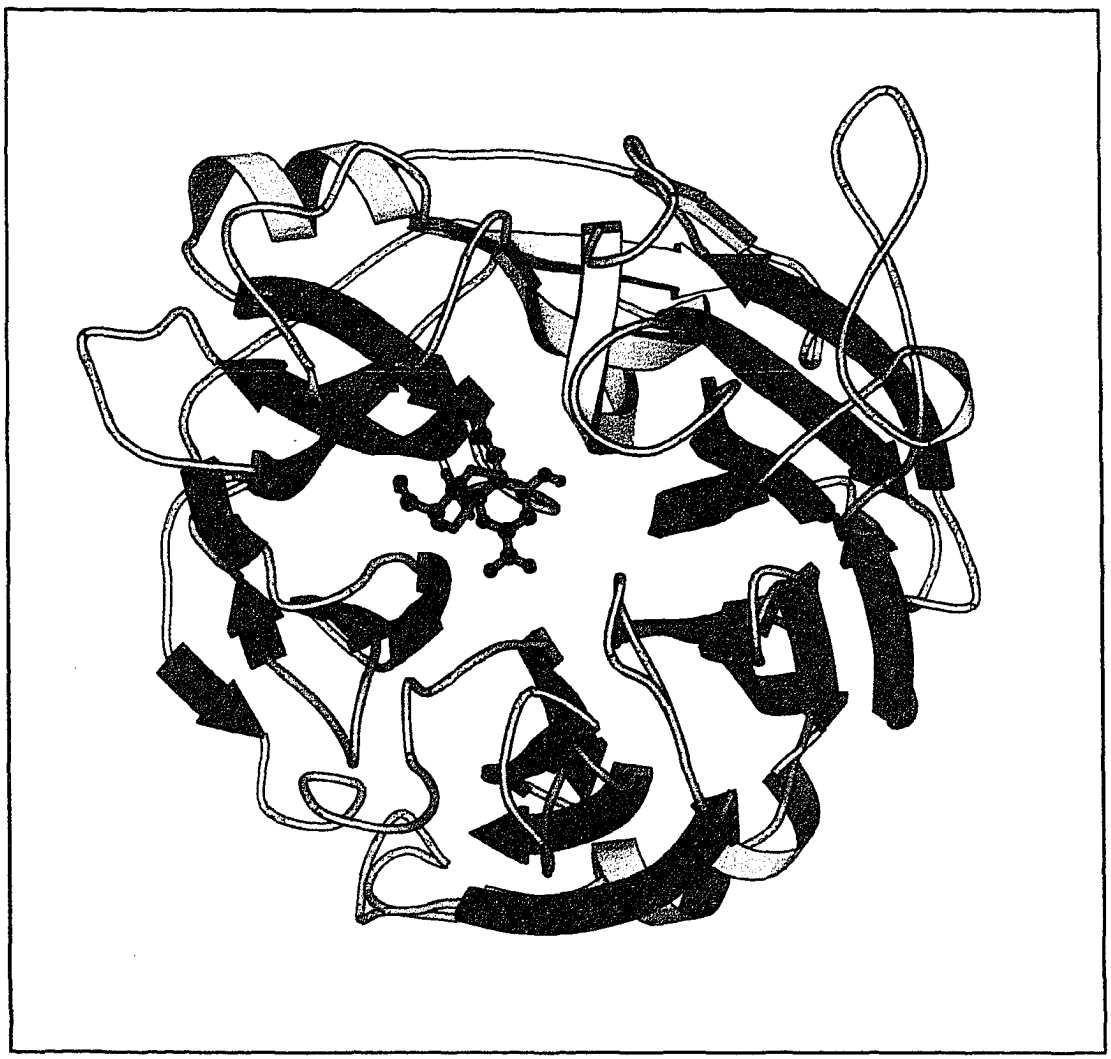

Figure 3. Ribbon drawing of *Salmonella typhimurium* sialidase-DANA crystal structure (Crenell *et al.*, 1993). The DANA molecule in the active site is shown as a ball-and-stick model. The six β-sheets comprising the β-propeller motif are color-coded.

the trans-sialidase active site was constructed from the *S. typhimurium* sialidase crystal structure. For complete details of the trypanosomal trans-sialidase homology modelin, please refer to Appendix B.

Structure-based Drug Design

Introduction

To fully appreciate the importance of structure-based drug design, one has to be familiar with earlier methods of drug development. Historically, new potential drugs have been discovered either serendipitously or by the use of screening assays. Neither method is systematic nor do they always result in a effective, safe, marketable drug. To improve the therapeutic properties of existing compounds, traditional methods, such as quantitative structure-activity relationship (QSAR) analysis, have been used. The traditional methods are useful, but interpretation of their results can be misleading or contradictory in many studies because the structure of the target and the mode of drug binding are unknown. To clearly understand the multitude of forces that affect a drug's biological activity (or lack thereof), the three-dimensional structure of the native target, or more preferably, the complex between the target and the drug, must be solved. In many cases, the structure of a particular drug-target complex can provide an immediate explanation to long-standing and perplexing biochemical questions of function and activity. For example, the design of human immunodeficiency virus (HIV) protease inhibitors has been greatly aided by the crystallographic analysis of non-cleavable substrate

and non-peptide analogs of analogs complexed to the HIV protease. In the HIV protease example, the crystallographic analysis identified the role of structural waters in the binding of substrate and stabilization of the active site loops (Wlodawer & Erickson, 1993).

The method of structure-based drug design uses the three-dimensional structure of a selected target or target-drug complex to guide the design of new compounds. By starting with the structure of the target, the structure-based drug design protocol circumvents the problems and limitations associated with traditional methods of drug development. New compounds, which will show high specificity and affinity for the target site can be quickly developed using the chemical and geometrical structure of target site at high resolution and structure-based design (Ealick *et al.*, 1991). The recent review by (Greer *et al.*, 1994) provides an excellent discussion of the structure-based drug design method and its potential for drug discovery.

Structure-based drug design is often assisted by several computer-based methods, which are used to analyze the three-dimensional structure of the target site. The first type of program is used to screen a database of known small molecule structures for compounds that match the geometric/steric constraints of the target site. The program DOCK is an example of database search/steric complementarity program (Shoichet & Kuntz, 1993). A second type of program is used to design *de novo* ligands, which fit the steric and chemical constraints of the active site. These programs first place small structural fragments into the target site based on their chemical complementarity to the target site. The

fragments located in different binding sites are then assembled into complete ligands by the program using a rules-based approach. The programs LUDI and SPROUT are examples of computer-aided *de novo* design (Bohm, 1992; Gillet *et al.*, 1994). Other programs can be used to characterize the chemical nature of the target site. One such program is GRID, which uses different chemical probe types and a grid system to systematically search the target site for favorable probe binding sites. The interaction energy between the probe and target atoms is calculated at each grid step and the resulting energy contour levels can be displayed onto the target site using computer graphics (Goodford, 1985). In addition to the ligand design programs, other computer-based methods are useful for predicting the binding energy of a designer drug for the target site. The free energy perturbation method determines the change in free energy, which results when a starting ligand is chemically transformed into the final, desired compound within the confines of a computer simulation. In small, discrete steps, the starting compound is mutated by the computer into the final structure over the course of a molecular dynamics simulation. In addition, the free energy perturbation calculations must be performed for the ligand system free in solution and when complexed to the target (Cummings & Gready, 1993). The program DELPHI can also be used to calculate the electrostatic contribution to the free energy of complex formation for a designer drug-target site complex (Gilson & Honig, 1988).

In 1987, to develop a marketable new drug by traditional methods cost an estimated $231 million and required 12 years (DiMasi *et al.*, 1991). The enormous number of potential compounds

that are chemically synthesized is one major contributor to the high cost of traditional drug development methods. Also, the traditional methods are inefficient because many of the synthesized compounds are eventually rejected due to poor activity or adverse side effects. In comparison, the time requirement and overall costs of developing a drug using structure-based design method are much lower. In this newer approach, the pool of potential compounds are first modeled into the three-dimensional structure of the target before synthesis. Only those proposed compounds that are sterically and chemical compatible with the target site are synthesized. The selection process also increases the odds that the synthesized compounds will indeed bind to the active site and exhibit high inhibition activities.

Structure-based design is also invaluable in determining the cause when a proposed compound fails to exhibit the expected increase in target site affinity. By analyzing the three-dimensional structure of the complex formed between the lackluster compound and the target site, this methodology could provide a direct explanation for the lower than expected inhibition. The information thus gained can then be used in the next design cycle to overcome the problem or quickly identify an unproductive approach.

Structure-based design of anti-influenza compounds

Today, there is no cure for influenza virus infection, though partial protection is available through yearly influenza vaccinations and the prophylactic drugs amantadine and rimantadine. Vaccination to prevent influenza virus infection has met with limited success due to the occurrence of antigenic drift and antigenic shift in

circulating influenza viruses. In short, antigenic drift occurs when single point mutations randomly occur in the viral genome which result in new amino acids being placed into the major antigenic determinants, hemagglutinin and sialidase. If the new amino acid results in a sufficiently different antigenic determinant, the antibodies of the host immune system that reacted with the parent strain may not recognize the new strain. In such an occurrence, the antibodies against the parent strain would provide no protection to the host against infection by the new strain. Antigenic drift is continuously occurring in the influenza virus population. One single mutation, or many cycles of mutation, may be required to result an antigenetically "new" hemagglutinin or sialidase protein.

Antigenic shift can occur when several type A influenza virus subtypes co-infect one cell and the RNA segments from the different viruses are shuffled to produce a progeny virus with a new combination of RNA segments. If the parent viruses, which contributed to the new combination, have not recently circulated in the human population, the new reassortment progeny virus that results could bear hemagglutinin and sialidase antigens that are not recognized by the immune systems of the general population. In such circumstances, the reassortment virus quickly becomes the dominant circulating strain in the general population, which can lead to a severe flu season or, worse, an influenza pandemic.

The result of an influenza pandemic can be devastating as shown by the influenza virus pandemic that swept the United States in 1968. The total economic loss of the '68 pandemic was estimated to be $4600 million by the U.S. Department of Health, Education, and

Welfare (Beveridge, 1978). That number represents both patient medical costs and economic losses resulting from worker absences. Annual medicare costs for treatment of influenza in people 65 and older were estimated at $225 million. Clearly, modern medicine has yet to develop an influenza vaccine that provides lifetime immunity from infection. The constant change in the influenza virus brought about by antigenic shift and drift prevents the development of an influenza virus vaccine that could bestow lifelong protection. To circumvent this problem, every year the Centers for Disease Control (CDC) attempts to predict which types and subtypes of influenza virus will be dominant in the coming year based on the types and subtypes that occurred in the previous year. Unfortunately, this implies that the new vaccine will not provide protection against influenza viruses that emerge in the coming year bearing a different hemagglutinin or sialidase subtype that was not predicted and, therefore, not included in the vaccine mixture. If an unpredicted, virulent strain of influenza was to suddenly emerge, at least six months would be required from the time of isolation of the new influenza strain to develop a vaccine against a newly emerged influenza type or subtype. Clearly, the public health service can not depend on a vaccine against the virulent strain to prevent wide spread infection in the vulnerable, high risk segments of the human population by the virulent, emerging influenza virus strain.

Two structurally-related drugs, amantadine and rimantadine, are currently licensed by the U.S. government for the treatment of influenza virus infection. These compounds work by physically blocking the function of the M2 protein, a virally encoded ion channel

located on the viral membrane surface, which is required for successful infection of host cells by influenza virus. There are several major disadvantages to the usage of amantadine and rimantadine. First, the compounds are only effective against type A influenza viruses. The types B and C influenza viruses do not have a M2 protein and are therefore impervious to amantadine and rimantadine treatment. Second, amantadine and rimantadine do not interact with strictly conserved amino acids in the M2 protein, which are essential to ion channel function of M2 (Duff *et al.*, 1994; Wharton *et al.*, 1994). Therefore, new viral strains can arise in patients treated with amantadine and rimantadine that have mutated M2 proteins no longer sensitive to the drugs, but are still functional for viral infection (Mast *et al.*, 1991). The surfacing of amantadine and rimantadine resistant strains therefore limits the usefulness of these drugs in preventing large-scale influenza outbreaks in hospital wards or nursing homes (Monto & Arden, 1992). In such cases, the patients are in very close contact and resistant strains that may arise in one patient being treated with these drugs are quickly spread to other patients in the facility. Thus, amantadine and rimantadine treatment of influenza infection is severely limited in the human population that are most at risk, who are most likely to require treatment: the immune-depressed, the young, and the elderly.

Inhibitors of influenza virus sialidase, specifically designed to target the strictly conserved active site residues found in all type A and type B influenza virus sialidases, have a significant advantage in lowering influenza virus infection when compared to vaccination and amantadine/rimantadine treatment. Unlike the latter agents, the

structure-based sialidase inhibitors should inhibit all influenza virus infections regardless of type, subtype, antigenic drift, or antigenic shift. In theory, for an influenza virus to escape treatment by a structure-based sialidase inhibitor, the virus would have to mutate the conserved active site residues, which would also diminish the enzymatic activity. Since the influenza virus sialidase does not prevent attachment and entry of the virus into the host cell, the actual role of sialidase inhibitors is to prevent virus spread, not viral infection. By limiting spread of the virus and stalling influenza infection, sialidase inhibitors would allow the host's immune system time to remove the virus before it overwhelms the host, which commonly occurs in the elderly and immune-depressed patients.

Structure-based design of anti-bacterial and anti-trypanosomal compounds

Bacterial sialidases have been implicated and correlated with several disease, such as dental caries, bacterial vaginosis, middle ear effusions, arteritis, acne, and acute streptococcal infection (Milligan *et al.*, 1978; Rogers *et al.*, 1979; Hoffler *et al.*, 1981; LaMarco *et al.*, 1984; Nakato *et al.*, 1986; Briselden *et al.*, 1992). Though many antibiotics are available to treat bacterial infections, several of the drugs are expensive or have significant side effects for the patient. Thus, there is always an interest in developing newer, more selective, and more potent bacteriocidal agents. Basic science research into the role of sialidases in bacterial biology and infection would also benefit from bacterial specific sialidase inhibitors.

There are several unique enzymes found only in trypanosomes, which are potential targets for developing anti-trypanosomal therapeutics. One such unique trypanosomal target is the glycosylphosphatidylinositol (GPI) anchored trans-sialidase protein, which is located on the cell-surface of *Trypanosoma cruzi* in the trypomastigote stage. This enzyme catalyzes the transfer of a terminal sialic acid from a host donor sialoglycoconjugate to a terminal β-1,4-linked galactose acceptor on the surface antigen protein Ssp-3. The decoration of Ssp-3 protein with sialic acid may prevent recognition of the parasite by the host alternate complement pathway (Tomlinson *et al.*, 1992; Cross & Takle, 1993). The trans-sialidase enzyme has also been postulated to play an important role in host cell invasion by the protozoan Trypanosomatidae family (de Titto & Araujo, 1987; Colli, 1993; Ming *et al.*, 1993). Some members of the Trypanosomatidae family are the etiological agents of several human ailments, such as Chagas' disease (*Trypanosoma cruzi*) and African sleepness disease (*T. brucei gambiense and T. brucei rhodesiense*), as well as the cause of animal trypanosomiasis (*T. brucei brucei*, and potentially *T. evansi, T. congolense,* and *T. vivax*). It is estimated that there are several million cases of Chagas' disease in Central and South America, as well as several million cases of African sleeping sickness in sub-Saharan Africa (Sun, 1982). Every year, several thousand new cases of Chagas' disease and African sleeping sickness occur. The rate of trypanosomiasis in the animal kingdom, which can have serious health and economic implications, is difficult to quantitate, but a conservative estimate would be several million cases in both South

America and Africa. Several drugs have been developed to treat the trypanosomal infections in humans and animals, but they suffer serious disadvantages. Either they are relatively toxic to the host, or the targeted trypanosome strains have developed a drug resistance mechanism (Kinabo, 1993). Inhibitors of trans-sialidase should be very good anti-trypanosomal agents because the trypanosomal trans-sialidase enzyme has been shown to be required for infection in humans and animals (de Titto & Araujo, 1987; Prioli *et al.*, 1991; Ming *et al.*, 1993). Using structure-based design to create new drugs specific for the trans-sialidase active site would also reduce the possibility that the new compounds were either harmful to the host or susceptible to drug resistance due to mutation of the target site.

X-ray Crystal Structure Determination

Crystallization

The protein crystals used in the diffraction studies reported in this dissertation were all grown using the hanging drop method (Blundell & Johnson, 1976). In this technique, several microliters of a very pure and highly concentrated protein solution are mixed with several microliters of a precipitating solution on the face of a plastic coverslip. The coverslip and protein drop are then inverted over a well containing a reservoir solution. The reservoir solution also contains a precipitating agent, but in a higher concentration than the protein drop. The chamber is then sealed with silicon grease to prevent evaporation loss (Figure 4). Due to the difference in precipitating agent concentrations between the two solutions, a

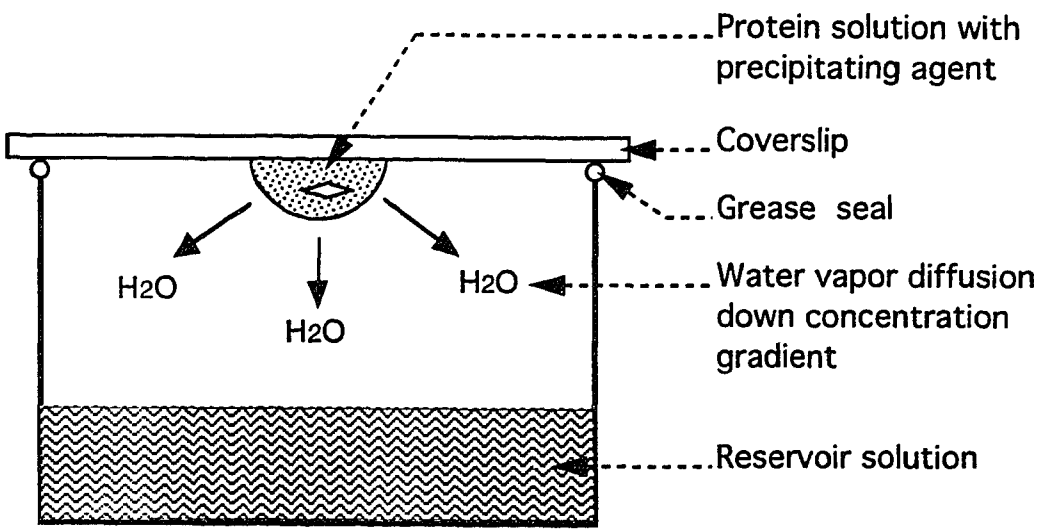

Figure 4. Schematic of hanging drop crystallization chamber.

concentration gradient forms between the reservoir and hanging drop in the sealed chamber. To equilibrate the two solutions, water vapor leaves the hanging drop and enters the reservoir, thereby slowly concentrating the protein in the hanging drop. Given enough time and the right conditions, it is likely that one or more single crystals of the protein can be grown to a size suitable for X-ray diffraction.

For the detailed crystallization conditions used to grow the influenza virus sialidase crystals, please refer to the methods and materials sections and cited references of the manuscripts. In general, crystals of the influenza virus sialidase-inhibitor complexes were prepared by soaking the native crystals in a artificial mother solution containing 5-10 mM of the inhibitor.

Data collection and processing

Optically clear, uncracked sialidase crystals were selected for X-ray diffraction analysis. The procedure for mounting a crystal for analysis is as follows. A single crystal was drawn into a quartz capillary using an attached 1.0 mL syringe. Using either a fine diameter (< 0.1 mM) glass fiber or sliver of filter paper, excessmother liquor was drained from the crystal until it was barely wet. A small amount of mother liquor was allowed to remain in the tip of the capillary to hydrate the crystal during the experiment. The capillary was then sealed at each end using a wax or oil cap. The sealed capillary is then mounted on a goniometer using modeling clay and ready for data collection.

Data collection was performed on a rotating anode Rigaku generator home source using a Siemens multi-wire proportional area

detector. For all the influenza virus sialidase crystals, the axis of highest symmetry (four-fold) was optically aligned to be perpendicular to the oscillation axis to minimize the angular phi sweep required for a full data set. In general, most data sets were collected using a framestep of 0.25°, a crystal-to-detector distance of 12.0-16.0 cm, and an exposure period of 300-400 seconds. For a particular data set, the choice of the area detector two-theta angle was determined by the diffraction quality of the crystal and the resolution requirements of the study. Please refer to the materials and methods sections of the first two manuscripts for further details about a specific data set. Because the native and inhibitor soaked influenza sialidase crystals are very stable in the X-ray beam, a single crystal was sufficient to collect most data sets.

The program XENGEN was used to process the area detector image frames that were collected for one crystal data set (Nicolet Instrument Co., 1987). The flowchart in Figure 5 details the steps required to process data using the XENGEN program. The border option removes reflections that are located near the edge of the image frame. The calibrate option is used to generate a calibration table based on the position of the direct beam. The option spots locates all the strong reflections greater than a user-defined sigma intensity cutoff on each image frame of the full data set. In the next stage of processing, the refine command is used to determine the initial crystal orientation matrix using the spots defined strong reflections and an autoindexing scalar vector method. Once an initial orientation matrix has been selected, the refine option will also allow several crystal and data collection parameters to be

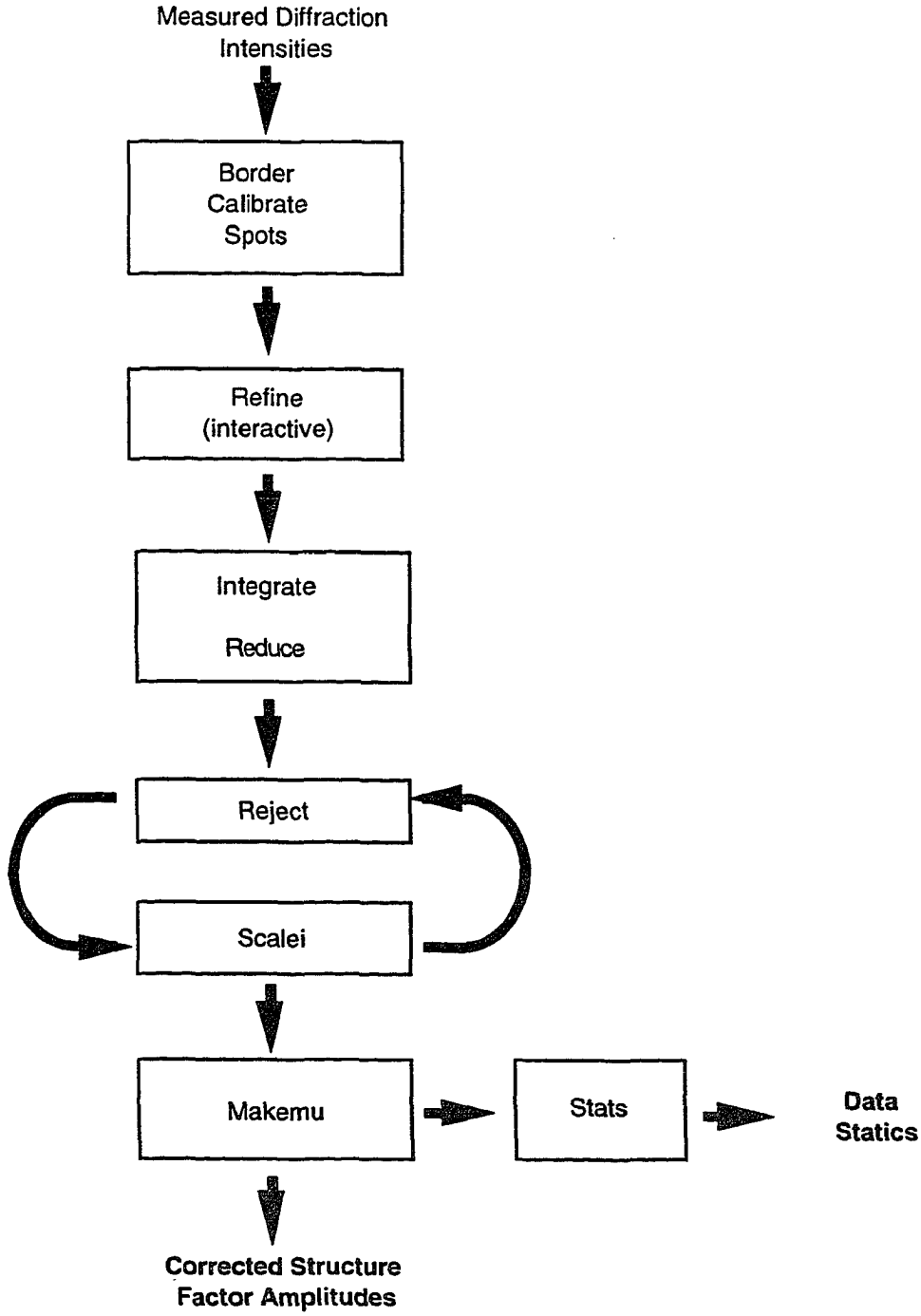

Figure 5. Flowchart of data processing using XENGEN.

refined. The third stage of processing involves integrating, sorting, and reducing each reflection using the integrate and reduce options. In the last stage of processing, several cycles of reject and scalei are used to apply rejection criteria and scaling protocols to the reflections. Also, during the integration, scaling, and rejection steps, the crystal orientation matrix is being constantly refined. Using the makemu option, the position (hkl) and structure factor of each reflection in the final data set is then exported using the makemu option. A statistical profile of the final set of reflections can be generated using the stats command.

Molecular replacement phasing

To calculate an electron density map of an unknown protein using its X-ray diffraction pattern requires knowing not only the relative intensities (amplitudes) of the diffracted X-rays, but also the relative phases of the reflections. The intensity of the reflection measured by the diffraction counter is proportional to the square of the reflection amplitude, F(hkl), but the phase of the diffracted wave can not be measured by conventional detector devices, hence the "phase problem." Three general methods are used in macromolecular crystallography to calculate starting model phases: isomorphous replacement, multiwavelength anomalous diffraction (MAD), and molecular replacement. For the diffraction studies described in this dissertation, only the molecular replacement method was used for phasing and it is the only method that will be discussed.

To discuss the method of molecular replacement and generating trial model phases, the following equations shall be introduced. Equation 1, the structure factor equation, is used to derive the structure factor, **F(hkl)**, for any given reflection using the reflection or structure factor amplitude, F(hkl), and the reflection phase, α(hkl).

$$\mathbf{F(hkl)} = F(hkl) \exp i\alpha(hkl) \qquad (1)$$

Alternatively, the structure factor can be calculated if the atomic scattering factor, *f*, and coordinate position, (xyz), of each protein atom are known. The atomic scattering factor, *f*, for a specific atom is derived directly from the electronic density distribution around the atom and is assumed to be spherical.

$$\mathbf{F(hkl)} = \sum_{j=1}^{n} f_j \exp [2\pi i(hx_j + ky_j + lz_j)] \qquad (2)$$

Hence, by setting Equation 1 equal to Equation 2, we can derive Equation 3.

$$F(hkl) \exp i\alpha(hkl) = \sum_{j=1}^{n} f_j \exp [2\pi i(hx_j + ky_j + lz_j)] \qquad (3)$$

Therefore, using Equation 3, one could derive calculated reflection phases, $\alpha(hkl)_{calc}$, if the amplitudes of the observed reflections, F(hkl), the atomic coordinates of the protein, (xyz), and atomic scattering factors, f_j, are known. Given the observed structure factor amplitudes, $F(hkl)_{obs}$, and calculated phases, $\alpha(hkl)_{calc}$, the

corresponding electron density, ρ, can be calculated using Equation 4, the electron density equation.

$$\rho(xyz) = 1/V \Sigma_{hkl} F(hkl)_{obs} \exp [i\alpha(hkl)_{calc}] \exp [-2\pi i(hx + ky + lz)] \quad (4)$$

Or, if Equation 1 is substituted into Equation 4:

$$\rho(xyz) = 1/V \Sigma_{hkl} \mathbf{F(hkl)} \exp [-2\pi i(hx + ky + lz)] \quad (5)$$

Now let us return to Equation 3. How does one determine the atomic coordinates of the protein, and by extension $\alpha(hkl)_{calc}$, if the structure of the protein is unknown? The answer to that question is the method of molecular replacement, first proposed by Rossmann and Blow (1962). The molecular replacement method uses a set of known model coordinates to derive the phases for the unknown, but structurally homologous, protein. The success of the molecular replacement method depends on the accurate superimposition of the model coordinates onto the coordinates of the unknown protein in the crystallographic asymmetric unit. The asymmetric unit is defined as the unique space of the total unit cell that can not be generated by applying the crystallographic symmetry and translation operators of the space group. By applying the proper rotation and translation operations, the model coordinate set can be aligned to the unknown molecule. Equation 6 describes in matrix notation the general rotation and translation operations, which are required to achieve superposition of the two atomic coordinate sets:

$$\begin{bmatrix} x' \\ y' \\ z' \end{bmatrix} = \begin{bmatrix} c_{11}x + c_{12}y + c_{13}z \\ c_{21}x + c_{22}y + c_{23}z \\ c_{31}x + c_{32}y + c_{33}z \end{bmatrix} + \begin{matrix} d_1 \\ d_2 \\ d_3 \end{matrix} \quad (6)$$

In a simpler form:

$$\mathbf{x'} = [\mathbf{C}]\mathbf{x} + \mathbf{d} \qquad (7)$$

The **C** matrix is referred to as the rotation matrix and the **d** matrix is referred to as the translation vector. Rossmann and Blow defined the rotation required to superimpose the rotated model onto the stationary model using the polar coordinate system and the variables ψ, ϕ, and κ (Figure 6) (Rossmann & Blow, 1962). The orientation of the rotation axis relating the stationary model and rotated molecule is defined by ψ and ϕ, while the κ determines the actual rotation value applied along the rotation axis. Hence, the Rossmann and Blow defined rotation matrix, ρ, is defined in polar terms (Figure 7) (Rossmann & Blow, 1962).

The molecular replacement method uses the rotation function, *R*, to determine the appropriate rotation matrix by superimposing Patterson functions. Equation 8 gives the general form of the Patterson function, $P(\boldsymbol{u})$, at a specific point (u,v,w) defined by vector $\boldsymbol{u}$.

$$P(\boldsymbol{u}) = {}^{2}/_{V} \Sigma_{hkl} F(hkl)^2 \cos 2\pi (hu + kv + lw) \qquad (8)$$

The value of the Patterson function depends on the electron density at point X and point X'. The Patterson function will produce a large value only if the points X and X' have high electron densities. Hence, the Patterson function describes the full set of interatomic vectors that are present for a protein in particular crystal packing. In addition, the Patterson function is only dependent on structure

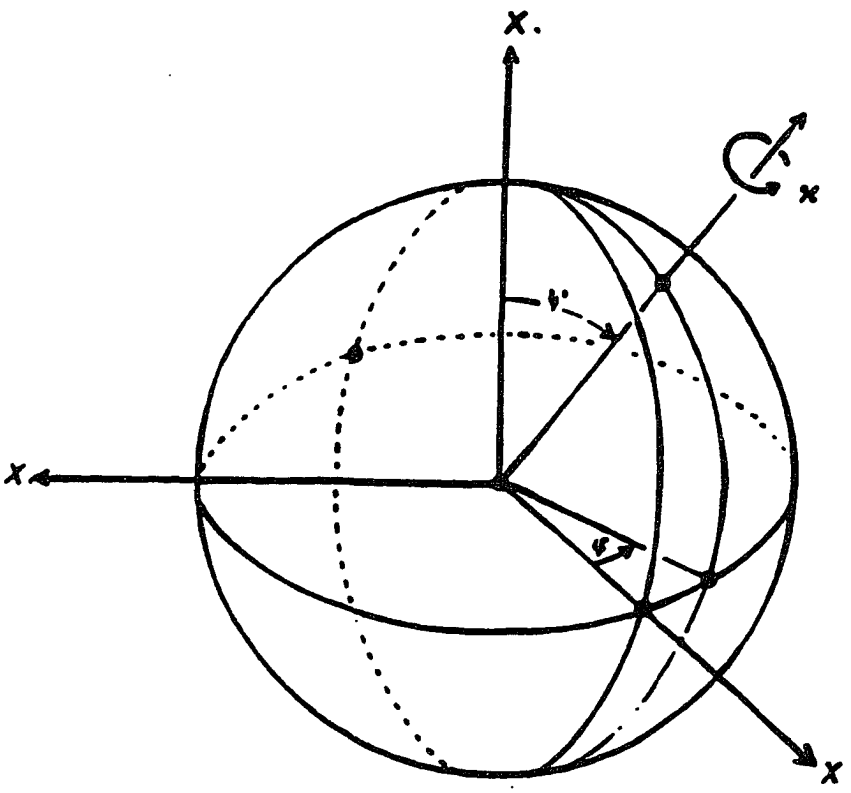

Figure 6. Polar coordinate system defined by Rossmann and Blow (1962).

$$\begin{bmatrix} \cos\kappa+\sin^2\psi\cos^2\phi(1-\cos\kappa) & \sin\psi\cos\psi\cos\phi(1-\cos\kappa)-\sin\psi\sin\phi\sin\kappa & \sin^2\psi\cos\phi\sin\phi(1-\cos\kappa)-\cos\psi\sin\kappa \\ \sin\psi\cos\psi\cos\phi(1-\cos\kappa)+\sin\psi\sin\phi\sin\kappa & \cos\kappa+\cos^2\psi(1-\cos\kappa) & \sin\psi\cos\psi\sin\phi(1-\cos\kappa)+\sin\psi\cos\phi\sin\kappa \\ -\sin^2\psi\sin\phi\cos\phi(1-\cos\kappa)+\cos\psi\sin\kappa & -\sin\psi\cos\psi\sin\phi(1-\cos\kappa)-\sin\psi\cos\phi\sin\kappa & \cos\kappa+\sin^2\psi\sin^2\phi(1-\cos\kappa) \end{bmatrix}$$

Figure 7. Rossmann and Blow (1962) rotation matrix, ρ, defined in polar terms.

factor amplitudes, F(hkl), or the reflection intensity, not **F(hkl)**, which requires knowing the reflection phase, α(hkl). Therefore, a Patterson function for the unknown protein can be directly derived from the observed diffraction pattern, and the Patterson function of a known model protein is easily calculated from its atomic coordinates.

The Patterson function can be comprised of a self-vector set and, potentially, a cross-vector set. The self-vector set represents the interatomic vectors occurring within a single protein (i.e., intramolecular). The cross-vector set represents the interatomic vectors that occur between multiple copies of the protein (i.e., intermolecular). An example of self- and cross-vector Patterson functions are present in Figure 8. Only the relative orientation of the model to the unknown protein, i.e., the rotation matrix **C** or ρ, can be determined by solving the rotation function. The translation component, ***d***, required to align the rotated model is usually determined by the R-factor search or translation function methods.

There are two types of rotation function analysis, a self-rotation function and a cross-rotation function. A self-rotation function determines the symmetry axis in the Patterson function, which results when multiple copies of the molecule are located in the crystallographic asymmetric unit. For example, a self-rotation function would be used to identify the presence and orientation of a two-fold axis in a dimeric protein. A cross-rotation function determines the angular relationship between the model molecule in one crystal unit cell and the unknown molecule in another crystal unit cell. A high structural homology between the model and

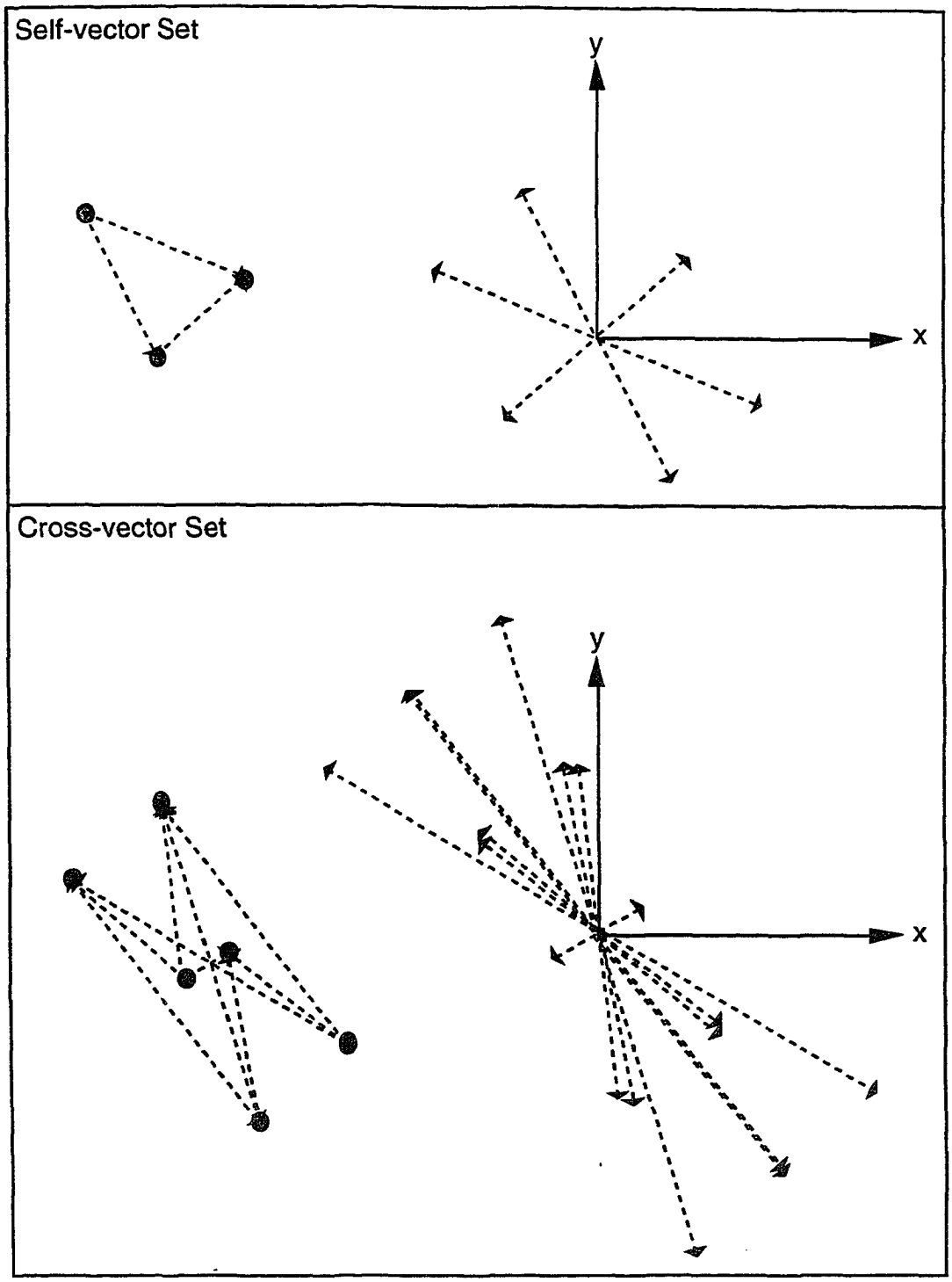

Figure 8. Examples of self-rotation and cross-rotation Patterson vector sets. The given the array of atoms shown on the left, the resulting Patterson function is shown on the right.

unknown molecule is required for the cross-rotation function to produce meaningful results.

In both self- and cross-rotation functions, an overlap function, defined as the rotation function, *R*, is used to determine the correct superposition of the Patterson function. Equation 9 gives the general, simplified version of the *R* function:

$$R = ({}^{U}/_{V3}) \Sigma_h \Sigma_p |F_h|^2 |F_p|^2 G_{h,h'} \quad (9)$$

The function expresses the superposition of two sets of interatomic vectors, one set generated by molecule P and the other set generated by the rotated molecule H, where U represents the integration volume, V represents the volume of the asymmetric unit, F_h represents the structure factor amplitudes of the stationary molecule, F_p represents the structure factor amplitudes of the rotated molecule, and $G_{h,h'}$ represents the interference function. A more detailed explanation of the importance of the interference function, *G*, can be found in the original work of Rossmann and Blow (1962).

Like the Patterson function, the calculation of the rotation function is only dependent on the value of $|F|^2$ and, therefore, does require prior knowledge of the correct phases. The rotation function will only produce relatively high values when the Patterson vectors of the stationary molecule significantly overlap the Patterson vectors of the rotated molecule. Though relatively large *R* function values can be produced by an incorrect rotation of one Patterson set onto the other Patterson set, the true rotation is usually one of the highest peaks in the rotation function. The correct rotation should

also be independent of the radius of integration chosen for the Patterson superposition, as well as the resolution of the diffraction data used to calculate the rotation function. Other factors that may affect the rotation function results are the Laue symmetry of the two Patterson vector sets being compared, the point group symmetry of the molecule in the asymmetric group, the percentage of large vectors present in the Patterson sets, and the completeness of the diffraction data.

The translation vector, **d**, which will place the rotated model molecule in the position of unknown molecule in the crystallographic unit cell, is determined by either the R-factor search method or by the translation function, *T*. The R-factor search method is performed by systematically translating the model coordinates, which have been transformed by the rotation matrix, [**C**], throughout the asymmetric unit of the unknown molecule. At each step point the model coordinates are used to calculate a predicted diffraction pattern, F_{calc}, which is then compared to the observed diffraction pattern of the unknown molecule, F_{obs}. The differences between the two diffraction patterns are represented as a residual, the crystallographic R-factor:

$$R_{crystal} = \Sigma \left| |F_{obs}| - |F_{calc}| \right| / \Sigma |F_{obs}| \qquad (10)$$

The proper translation vector is usually indicated by a minimum $R_{crystal}$ value.

There are many versions of *T* function, but the most commonly used form is that derived by Crowther and Blow (1967).

$$T(t) = \int_v P_{obs}(\boldsymbol{u})\, P_{predicted}(\boldsymbol{u})\, d\boldsymbol{u} \qquad (11)$$

This translation function compares the observed cross-vector Patterson function for the unknown protein, P_{obs}, to the predicted cross-vector Patterson function, $P_{predicted}$, of the model when rotated by [**C**] and translated by *t*. The translation function will produce a maximal value only when the two Patterson functions are superimposed.

Identification of the true translation vector, ***d***, using either the R-factor search or translation function methods can be hampered by the large number of incorrect solutions, which generated using these methods. The accuracy of rotation function, the accuracy of the measured reflection intensities, and the number of observed reflections will also affect the amount of background noise present in the translation results. To distinguish the real translation vector from an incorrect solution or noisy background, one can calculate a packing function. Given the space group of the unknown protein, the packing function predicts the amount of protein-protein contacts that would result from placing the model at a specific position defined by [**C**] and ***d***. An incorrect rotation or translation component usually will result in a packing function that produces either no protein-protein contacts in the crystal lattice or severe interpenetration of the model by symmetry-related molecules.

Model building and coordinate refinement

For the influenza sialidase studies described herein, several cycles of rigid body refinement would be carried out using the initial model following molecular replacement. Rigid body

refinement would usually result in a ~10% drop in the crystallographic R-factor. Next, a F_{obs} map, a F_{obs}-F_{calc} difference map, and a $2F_{obs}$-F_{calc} difference map would usually be calculated using the rigid body refined model. At this stage, missing sidechains and residues would be manually modeled into the difference electron density using the program FRODO on a graphics workstation (Jones, 1985). Also, if the quality of the map was sufficient, regions of the initial model, which were purposely removed before molecular replacement, such as loops or sugar residues, would now be modeled. The new set of model coordinates would then be back Fourier transformed to generate a new set of phases. The new set of phases would be combined with the observed structure factors to generate new electron difference density maps. The new maps were then used to further modifications to the model. This cycle would be repeated until no further improvement of the model was possible.

The next stage of refinement involves application of simulated annealing protocols using the program X-PLOR (Brunger, 1988). The model at this point usually contains the majority of residues and sidechains in the protein, which are well-defined by the electron density. The first step of the simulated annealing protocol is another rigid body refinement of the full model coordinates. Then, the model coordinates are subjected to a short energy minimization run to relieve poor contacts and to determine the proper weights for the crystallographic and geometric terms to use in the simulated annealing run. In the final step, the model is heated to 3000°K and allowed to cool using a molecular dynamics force field based on the

CHARMm parameters. As the temperature drops during the simulated annealing procedure, the model is assumed to adopt its minimum energy state. The coordinates of the model that are output from simulated annealing usually produce a 2-5% drop in the crystallographic R-factor. These model coordinates can then be used to calculate a new set of electron density maps, which are then used to guide improvement of the model. The improved model coordinates are then resubmitted to simulated annealing. The cycle is repeated until the electron density shows no further signs of improvement or the crystallographic R-factor no longer decreases. During the last cycles of X-PLOR simulated annealing and map calculation, individual temperature factors and water molecules can be introduced in the model for refinement. The quality and resolution of the data set and the ratio of parameters to observed reflections will determine if these factors should be considered. For example, a resolution of at least 2.5 Å is required to accurately identify and refine the placement of water molecules in the structure.

Aside from the crystallographic R-factor, several other methods can be used to assess the quality of the final, refined model coordinates. Good chemical and sterical geometry is an important criteria for any refined crystal structure. A proper structure will not significantly depart from ideal bond lengths, bond angles, and torsion angles. In addition, a Ramachandran plot can be calculated to asses the backbone geometry of the structure (Ramakrishnan & Ramachandran, 1965).

Example: molecular replacement phasing of B/Mem/89 influenza virus sialidase

The crystal structure of the B/Mem/89 sialidase was determined using molecular replacement. Crystals of B/Mem/89 sialidase were grown using the hanging drop method (Lin *et al.*, 1990). The drop contained 25 μl of protein (20mg/ml) and 25 μl of the reservoir solution (20% PEG 3350, 150mM NaCl, pH 7.0). The B/Mem/89 data collection parameters are given in Table 1. The crystallographic parameters for the B/Mem/89 crystal are given in Table 2. For solving the B/Mem/89 (and B/Lee/40) crystal structures, the C_α coordinates of one monomer of the influenza virus B/Beijing/1/87 sialidase crystal structure were used as the molecular replacement model (Burmeister *et al.*, 1992).

First, the B/Beijing/1/87 tetramer coordinates in the space group $P3_121$ were used to build a model in the P1 space group using the program MAKEP1 (M. Luo, personal communication). A prerotation operation ($\kappa = 90°$, $\psi = 120°$, $\phi = 0°$) was applied to the P1 model to align the four-fold axis of the model tetramer with the four-fold axis of B/Mem/89 sialidase tetramer in the I422 space group at $\psi = 90°$, $\phi = -90°$. A calculated structure factor data set, F_{calc}, was then determined from the P1 model over the resolution range of 15.0-3.0 Å using the program SFCU (M. Luo, personal communication). A cross-rotation function analysis was performed between the model tetramer in the P1 unit cell and the B/Mem/89 NA in the I422 unit cell using the program GRFN (M. Luo, personal communication). Given that the B/Mem/89 tetramer was sitting on the crystallographic four-fold, the cross-rotation function search for the correct orientation of the P1 model NA along the c-axis was

Table 1

Data Collection Parameters for B/Mem/89 Sialidase	
data set	NDAD0614
crystal-to-detector distance	16.0 cm
2θ, detector swing angle	17.0°
framestep	-0.25°
exposure time	400 seconds
no. frames	400

Table 2

Crystallographic Parameters for B/Mem/89 Sialidase	
data set	NDAD0614
space group	I422†
unit cell	
a=b=	123.2 Å
c=	164.8 Å
$\alpha=\beta=\gamma=$	90.0 °
$V_m = V_{a.u}{}^*/M_r=$	3.13 (one monomer in a.u.)
resolution shell ∞-2.55Å:	
unique reflections	16002
completion	76.1%
R_3 (XENGEN)§	8.28

† not $I422_1$ due to lack of systematic absences
* a.u., crystallographic asymmetric unit
§ unweighted absolute value R-factor on intensity * 100

limited to κ = 0-90°, ψ = 90°, ϕ = -90°. The cross-rotation functions were performed over the resolution ranges of 8.0-12.0 Å, 6.0-12.0 Å, and 4.0-12.0 Å. The cross-rotation function (4.0-12.0 Å, 366 large terms, 11.7%) indicated that the P1 B/Beijing/1/87 model tetramer was related to the I422 B/Mem/89 sialidase tetramer by the polar rotation κ = 24.6°, ψ = 90°, ϕ = -90°.

Using the program SFCU, a translation R-factor search on the rotated P1 monomer was performed along the c-axis to determinethe correct location of the B/Mem/89 sialidase tetramer in the I422 unit cell. Because the unit cell for the B/Mem/89 sialidase crystals is I422, the maximum fractional distance along the c-axis, which must be searched, is $0 \leq c \leq 1/2$ (0.0 to 82.2 Å along the z-axis). At each iteration step along the search axis, the coordinates of the rotated P1 monomer were translated and the structure factors calculated for that position. The calculated structure factors were then compared to the observed set of B/Mem/89 structure factors using the R-factor residual. Using a fractional step of 0.001 (0.164 Å) along the c-axis, the correct fractional translation vector was determined to be 0.0, 0.0, 0.457 (0.0 Å, 0.0 Å, 75.13 Å). This translational vector resulted in a R-factor minimum of 28.24%.

The rotated, translated model coordinates were then used to derive calculated phases, $\alpha(hkl)_{calc}$, using the program SFCU. A calculated structure factor data set, $\mathbf{F(hkl)_{calc}}$, was determined using the full atomic coordinates of the rotated and translated B/Beijing/1/87 sialidase modified at the amino acids positions, which differed from the B/Mem/89 sialidase shown in Table 3.

Table 3

Differing Amino Acids in B/Beijing/1/87 and B/Mem/89 Sialidases

B/Beijing/1/87	B/Mem/89
Lys 249	Glu 249
Asn 339	Asp 339
Arg 381	Lys 381
His 395	Pro 395

To calculate the $\mathbf{F(hkl)_{calc}}$ data set, the four differing amino acids were replaced by glycines in the B/Beijing/1/87 sialidase molecular replacement model. A difference electron density map, $\Delta\rho(xyz)$, was calculated for the observed B/Mem/89 data, F_{obs}, and the calculated data, F_{calc} and α_{calc}, using the difference Fourier synthesis shown in Equation 12.

$$\Delta\rho(xyz)=1/V\Sigma_{hkl}||F_{obs}|-|F_{calc}|| \exp[i\alpha_{(hkl)}calc] \exp[-2\pi(hx+ky+lz)] \quad (12)$$

The difference electron density map was used to locate the position of the new sidechains in the B/Mem/89 structure. The F_{obs}-F_{calc} difference map and a straight F_{obs} map, calculated using only the observed B/Mem/89 data and calculated phases, were then used to build the sidechains of the four differing amino acids into the B/Mem/89 model coordinates. The sidechain of Lys 381 could not be accurately modeled since the sidechain density was not clearly defined in the either electron density map. For the amino acids, which were identical in both type B strains, only minor differences in sidechain geometry were found in the difference Fourier analysis.

The crystal structure of the B/Mem/89 sialidase was used to confirm the molecular replacement solution for the B/Lee/40 sialidase (*"Structure of Influenza Vrus Neuraminidase B/Lee/40 Complexed with Sialic Acid and a Dehydro-analog at 1.8 Å Resolution: Implication for the Catalytic Mechanism"*). The cross-rotation peaks between the model B/Beijing/1/87, B/Mem/89 and B/Lee/40 coordinates were self-consistent indicating that the rotation peaks used to solve the B/Mem/89 and B/Lee/40 crystal structures were correct. In addition, I was responsible for

coordinating and analyzing the nuclear magnetic resonance (NMR) experiments that were performed to study influenza hydrolysis (with support from Dr. Mike Jablonsky, UAB NMR Core Facility).

STRUCTURE OF INFLUENZA VIRUS NEURAMINIDASE B/LEE/40 COMPLEXED WITH SIALIC ACID AND A DEHYDRO-ANALOG AT 1.8-Å RESOLUTION: IMPLICATIONS FOR THE CATALYTIC MECHANISM†

MUSIRI N. JANAKIRAMAN,‡,§,‖ CLINTON L. WHITE,‡,⊥ W. GRAEME LAVER,# GILLIAN M. AIR,§ AND MING LUO,*,‡,§

Center for Macromolecular Crystallography, Department of Microbiology, and Department of Biochemistry and Molecular Genetics, University of Alabama at Birmingham, Alabama 35294, and John Curtain School of Medical Research, Australian National University, Canberra 260, Australia

Received March 29,1994; Revised Manuscript Received May 16, 1994⊗
Biochemistry, Vol. **33**, No. 27, 1994

---

† This project was supported by NIH grants AI-31888 to M.L. and AI-26718 to G.M.A.

* Author to whom correspondence should be addressed.
‡ Center for Macromolecular Crystallography, University of Alabama at Birmingham.
§ Department of Microbiology, University of Alabama at Birmingham.
‖ Current address: The Upjohn Co., Kalamazoo, MI 49001.
⊥ Department of Biochemistry and Molecular Genetics, University of Alabama at Birmingham.
Australian National University.

⊗ Abstract published in *Advance ACS Abstracts*, June 15 (1994).

Abstract

Neuraminidase is one of the two glycoprotein spikes protruding from the influenza virus membrane. We have determined by X-ray crystallography the native structure of B/Lee/40 neuraminidase (NA) and the structures of its crystals soaked with a substrate, N-acetylneuraminyl lactose (NANL), and an inhibitor, 2-deoxy-2,3-dehydro-N-acetylneuraminic acid (DANA) at 1.8-Å resolution. NANL was hydrolyzed by the crystalline NA to generate the product, N-acetyl neuraminic acid (NANA, also known as sialic acid), which is still able to bind to NA. In the difference Fourier map of the presumed NA-NANA complex, the moiety bound in the active site had a distorted boat conformation of NANA, but there is no significant electron density for O2. The structure of the bound moiety is not identical to that of chemically synthesized DANA soaked into NA crystals. Prolonged incubation of NANA with NA in solution at room temperature produced only a trace amount of DANA as detected by NMR. Based on our studies, a mechanism is proposed for the enzymatic hydrolysis by influenza virus neuraminidase.

Introduction

The surface antigens found on the membrane envelope of influenza virus are two glycoproteins, haemagglutinin and neuraminidase (EC, 3.2.1.18, acylneuraminyl hydrolase). The tetrameric neuraminidase catalyzes the hydrolysis of the α-(2,3) or α-(2,6) glycosidic linkage between a terminal sialic acid and its adjacent carbohydrate moiety on a variety of glycoconjugates. In general, enzyme-catalyzed hydrolysis of biopolymers requires: (i) a nucleophile (which may be

an "activated water" molecule) or a proton donor from the enzyme to induce the formation of a transition state intermediate, (ii) a pocket to bind the specific substrate, and (iii) one or more residues to stabilize the transition state intermediate. Based on the structural analysis of the A/Tokyo/3/67 NA-NANA[1] complex, Varghese et al. (1992) implicated an aspartic acid at position 152 in the catalysis. However, this aspartic side chain is solvent exposed and, therefore, has a pK_a of 3.9, which is inconsistent with the pH range (4.5-9.0) of NA activity.

In this paper, we present the crystal structure of B/Lee/40 influenza virus neuraminidase and its complexes with presumed NANA and DANA at 1.8-Å resolution. The binding of DANA to NA ($K_i \approx 5 \times 10^{-6}$ M) is about 1000-fold higher than that of NANA, and DANA has been considered as a transition state analogue for sialic acid cleavage (Meindl et al., 1971).

Burmeister et al. (1993) described the crystal structure of influenza virus neuraminidase B/Beijing/1/87 soaked in NANL. The authors concluded that the moiety bound in the active site was not NANA, but DANA. They suggested that DANA was a side product produced at a low rate during the neuraminidase hydrolytic reaction. Our experimental data have shown some different results, which will be discussed in detail in this paper.

---

[1]Abbreviations: NA, neuraminidase; NANA, N-acetyl neuraminic acid; DANA, 2-deocy-2,3-didehydro-N-acetyl neuraminic acid; NANL, N-acetyl neuraminyl lactose; K_i, inhibition constant, F_o, observed structure factor; F_c, caluclated structure factor; SA, simulated annealing; NAG, N-acetyl glucosamine.

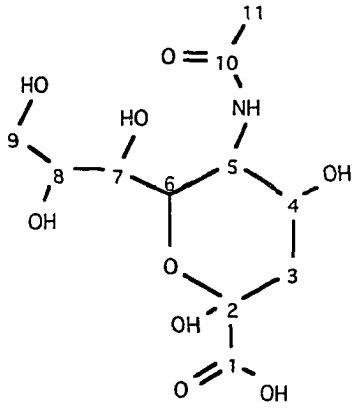

NANA
N-acetyl neuraminic acid
(*α-sialic acid*)

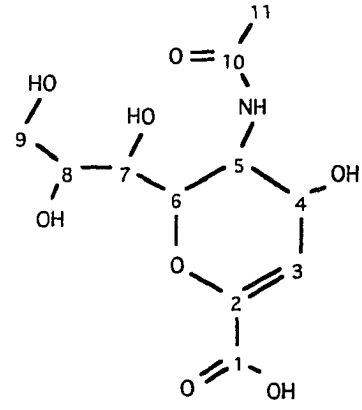

DANA
2-deoxy-2,3-didehydro-*N*-acetyl neuraminic acid

Materials and Methods

Structure Determination. Crystals of B/Lee/40 influenza virus neuraminidase were prepared following Lin et al. (1990). Complex I was obtained by soaking a crystal of NA overnight at room temperature in 5.0 mM NANL (SIGMA Chemical Co.) in mounting solution [20% (w/v) PEG 3350, 0.16 M NaCl, pH 6.6]. Complex II was prepared by soaking a crystal of NA overnight in 5.0 mM DANA (Boehringer Mannheim) in the same mounting solution. X-ray diffraction data of the native and complex crystals were recorded on a Siemens area detector at room temperature using Cu K_α radiation from a Rigaku RU-200 rotating anode generator operating at 40 KV and 100 mA. The data collection parameters were: crystal to detector distance 12.5 cm, swing angle 30°, exposure time 10 min per frame, and a frame width of 0.25°. The data thus collected (400 frames) were processed by the XENGEN (Howard et al., 1987) and CCP4 (CCP4, 1979) packages. Only reflections for which $I/\sigma_I \geq 1$ were included (Table 1). For the structure determination of the

Table 1: Crystallographic Data for Native B/Lee/40 NA and Complex I and Complex II

							Overall
NA (native): a = b = 124.56 Å, c = 71.66 Å; Tetragonal Space Group: $P42_12$							
resolution shell, Å	4.16	2.94	2.40	2.08	1.86	1.76	1.76
no. of reflections	3846	7035	6729	5564	3746	1132	28052
completeness, %	95.6	95.4	70.4	49.5	29.2	13.9	52.4
R_{sym}, %[a]	8.3	12.7	20.4	27.5	36.5	40.1	12 . 2
Complex I (NA-NANA): a = b = 125.29 Å, c = 72.04 Å; Tetragonal Space Group: $P42_12$							
resolution shell, Å	4.23	3.00	2.45	2.12	1.90	1.78	1.78
no. of reflections	3757	6879	7540	7157	5486	1511	32330
completeness, %	95.8	97.3	82.0	65.2	45.2	16.1	61.4
R_{sym}, %	7.0	11.1	19.0	20.7	22.0	21.2	12.6
Complex II (NA-DANA): a = b = 124.45 Å, c = 71.61 Å; Tetragonal Space Group: $P42_12$							
resolution shell, Å	3.18	2.52	2.21	2.00	1.86	1.77	1.77
no. of reflections	3829	7014	6432	3999	2691	755	24720
completeness, %	94.7	94.7	67.0	35.4	20.9	5.4	47.1
R_{sym}, %	9.0	14.2	22.1	41.5	36.9	36.4	13.5

[a] $R_{sym} = 100 \times \Sigma|I_j - \langle I \rangle| / \Sigma I_j$ where ΣI_j is the sum of all observations of all reflections within the resolution shell.

native B/Lee/40 NA, we used the atomic coordinates of B/Beijing/1/87 NA (Burmeister et al., 1992) (94% amino acid identity to B/Lee/40 NA) and our earlier F_o data set at 2.4-Å resolution (statistics not shown) to obtain the initial atomic model by the molecular replacement method (Rossmann & Blow, 1962). An $||F_o|-|F_c||$ difference map was calculated after removing all atoms of the 21 different side chains. The differing side chains and altered main chain atoms were modeled into the difference density using FRODO (Jones, 1985). Three rounds of PROLSQ (Hendrickson & Connert, 1981) refinement at 3.0-Å resolution and model building led to a structure with an R-factor of 22%. One more round of PROLSQ using all data to 2.4-Å resolution resulted in a structure with an R-factor of 24%. Subsequently, after ten cycles of rigid body refinement, a full cycle of simulated annealing (SA) refinement was carried out using X-PLOR (Brunger, 1992). An $||F_o|-|F_c||$ map was then calculated to locate one N-acetylglucosamine [NAG] residue (attached to Asn 284) and 125 well-defined water molecules. This resulting structure (390 amino acid residues, 1 NAG residue, 2 Ca^{++} ions and 125 water molecules per monomer) served as the native model for the refinement of the two complexes to 1.8-Å resolution. $||F_o|-|F_c||$ maps were used to place the inhibitor molecule in the enzyme active site prior to the SA refinements using X-PLOR. During such refinement runs of complex I, three different starting models were used for the molecule in the active site: model 1, NANA in its α-boat conformation; model 2, NANA in its α-boat conformation, but without O2; and model 3, DANA. Restraints on the dihedral angles C2-C3-C4-C5 and C5-C6-O6-C2 and the improper angles C2-O6-O2-

C3 (model 1 only), C2-C1-O6-C3 and C3-H31 (H3 in the case of model 3)-C2-C4 were removed to allow for any change of geometry about C2. The crystallographic R-factors are those obtained after individual temperature factor refinement using X-PLOR. Complex II was refined using exactly the same conditions as complex I, model 3. The final analysis of the structure refinement is presented in Table 2.

NMR Analysis of NA Products. Experiments were designed to detect if DANA is one of the products in hydrolysis by influenza virus neuraminidase. Since sialic acid is a substrate of viral neuraminidase (Burmeister et al., 1993) in the sense that the hydroxyl group at the C2 position is released during the formation of the oxocarbonium intermediate, it was used as the substrate in our studies. NANA (10 mM) was incubated with NA in solution (40 nM or 10 mM) at 22 °C for 48 h. The solution was then filtered through a centricon (Amicon) to remove NA and water was replaced by D_2O through repetitive lyophilization. The sample was then analyzed by NMR spectroscopy on a 600 MHz machine (Bruker). Controls of pure NANA, DANA, and a mixture of 1:1000 DANA/NANA were also scanned.

Hydration of DANA by NA. A 1 ml volume of the DANA solution (10 mM DANA, 0.5 M phosphate buffer, pH 6.0) was incubated with either B/Lee/40 NA (0.5, 1, or 2 mg), or A/tern/Australian/G70C/76 NA (2 mg). Aliquots were taken out at given times and the production of NANA was measured by the method of Aymard-Henry et al. (1973).

Table 2: Refinement Sstatistics for Native NA and Complex I and Complex II

		NA-NANA			
	native NA	model 1	model 2	model 3	NA-DANA
no. of non-hydrogen atoms	3181	3202	3201	3201	3201
no. of reflections	27321	31545	31545	31545	23998
R-factor, %[a]	20.1	20.4	19.9	19.9	21.1
$\langle B \rangle$, Å^2	21.0	10.6	10.7	10.6	19.3
rms deviation from ideality					
bond distance, Å	0.012	0.013	0.014	0.014	0.012
bond angle, deg	1.356	1.315	1.359	1.348	1.433
dihedral angle, deg	28.045	28.052	27.863	27.908	28.957
improper angle, deg	2.254	2.174	2.073	2.169	2.491

[a] R-factor = $100(\Sigma||F_o|-|F_c||/\Sigma|F_o|)$.

Results

What Binds in the Active Site? Influenza virus neuraminidase is a tetramer made up of identical subunits and each monomer has six twisted β-sheets of four anti-parallel strands arranged as a propeller. The active site is a crater located near the center of the monomer (FIGURE 1). The difference Fourier maps for complex I and complex II showed clear electron densities occupying the active site. With the exception of O2, all the non-hydrogen atoms of NANA could be fitted into the difference electron density in complex I. There is no density for O2 at a contour level of 1σ. The lack of O2 density can not be an artifact because the densities corresponding to O4, O7, O8, and O9 are clearly present. A separate difference Fourier map (not shown) between F_o's of complex I and F_c's calculated using the refined coordinates of complex I, model 2, did not show any significant electron density corresponding to O2. Thus the moiety bound in complex I seems to be a distorted form of α-sialic acid without the OH2 hydroxyl group (FIGURE 2), as was observed by Burmeister et al. (1993). In complex II, all the non-hydrogen atoms of DANA could be fitted into the difference electron density.

There is a possibility that the moiety bound in complex I is DANA, which could be produced by the loss of a proton at the C3 position of NANA during the glycosidic cleavage reaction. DANA could also be formed by a non-specific β-elimination with the participation of acidic and basic residues on the surface of the enzyme. In fact, a trace amount (<0.1%) of DANA was detected by NMR analyses when

FIGURE 1: Ribbon drawing of a monomer of B/Lee/40 influenza virus neuraminidase using RIBBONS (Carson, 1987). The yellow spheres represent amino acid residues, which differ from all other type B neuraminidases sequenced. The view is down the tetramer four-fold axis, which is passing through Ca^{++} 501. The disulfide bridges, structural Ca^{++} ion binding site (Ca^{++} 500), NAG binding site (N284) and sialic acid binding site are all highlighted.

FIGURE 2: Stereo photograph of NA-inhibitor complexes. (A) Stereo photograph of NA-NANA complex difference Fourier map calculated with the coefficients $|2|F_o| - |F_c||$ using the refined native coordinates only. A total of 31,545 unique reflections up to 1.8-Å resolution were used for this calculation and the electron density map is contoured at 1.0s level. The density corresponding to the glycerol group was left out for clarity. (B) $|F_o| - |F_c|$ map contoured at 1.0s level calculated by the same routine as in (a), but using the refined model 3 complex coordinates. (C) Same map as in (B) contoured at 0.5σ level. (D) Superposition of the refined model 3 (red) and DANA (green) as bound in the active site of NA to compare the geometry of C2 in the two complexes. (E) Superposition of the three refined NANA models: model I (blue), model II (green), and model III (red).

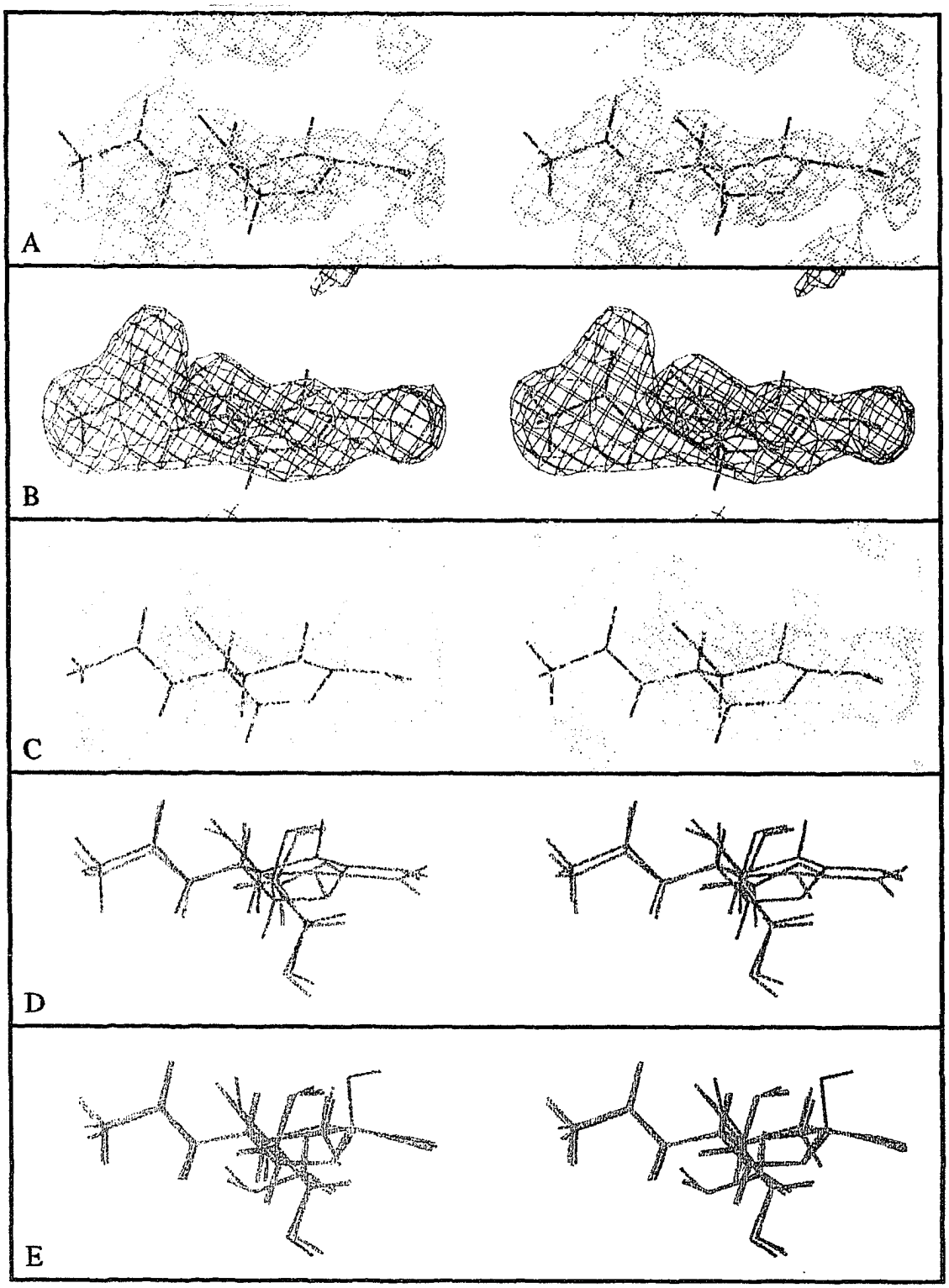

NANA was incubated with NA in solution over 48 h at room temperature (FIGURE 3).

The conversion of NANA to DANA by neuraminidase was also reported by Burmeister et al. (1993), but the experimental conditions and results were somewhat different. In contrast to their crystallographic studies, which were done at room temperature or 4 °C, Burmeister et al. (1993) incubated NANL with NA in solution for 36 h at 37 °C. Samples were then derivatized by bistrimethylsilyl trifluoroacetamide for 3 h, and DANA production was measured by coupled gas chromatography/mass spectrometry. No DANA was detected when the NA/NANL ratio was 1:12500. When the enzyme/substrate ratio was raised to 1:25 (500-fold increase of NA), a significant amount of DANA was detected.

The solution incubation experiments, as well as the crystallographic experiments, presented here were done at room temperature (≈ 22 °C). Only a trace amount of DANA was produced (<1:1000 DANA/NANA ratio) at an enzyme/substrate ratio of either 1:250000 or 1:1000 (FIGURE 3). An increase of the enzyme/substrate ratio by 250-fold did not change the yield of DANA under these conditions. Since the ratio of DANA/NANA in solution should be equal to the ratio of DANA/NANA in the solvent volume of crystalline NA, NANA should compete equally for the NA active site in the crystal even though the affinity of NANA is 1000-fold less than that of DANA.

Hence, in order to identify the major species bound in the active site of complex I crystals, we have employed a refinement strategy using three starting models: α-boat NANA (model 1), α-boat NANA

FIGURE 3: NMR analysis of the hydrolysis products of influenza virus neuraminidase B/Lee/40 using NANA (sialic acid) as the substrate. The experimental conditions were specified in the text. (A-C) The control experiments showed that 0.1% of DANA mixed with NANA could be detected by this method. The shifting of the DANA characteristic peaks (e.g., 6.2 ppm to 5.8 ppm) in the mixture could be due to the additional hydrogen bonds of DANA to NANA. (D, E) The experimental data for the given NA/NANA starting ratios indicate that the conversion of NANA to DANA by NA was approximately 0.1% of NANA as judged by comparison of the NANA/DANA peak height ratio in the experimental spectra to the NANA/DANA peak height ratio in the 0.1% DANA/NANA control spectrum.

Control

A. 10mM NANA

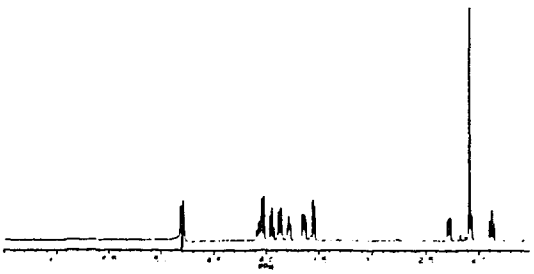

B. 10mM DANA

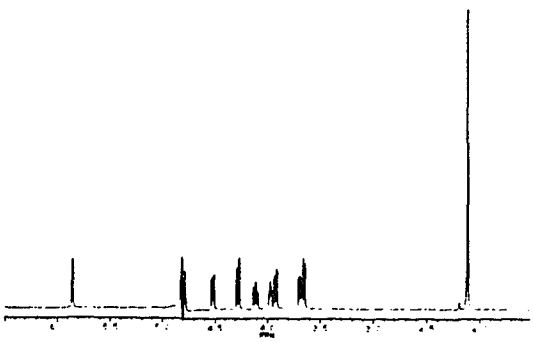

C. DANA/NANA 1:1000

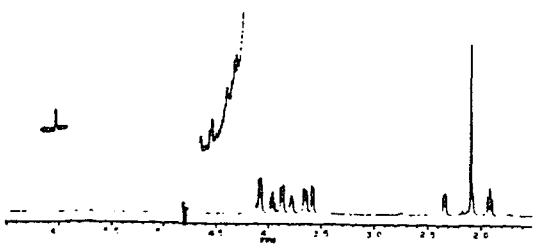

Experimental

D. NA/NANA 1:250000

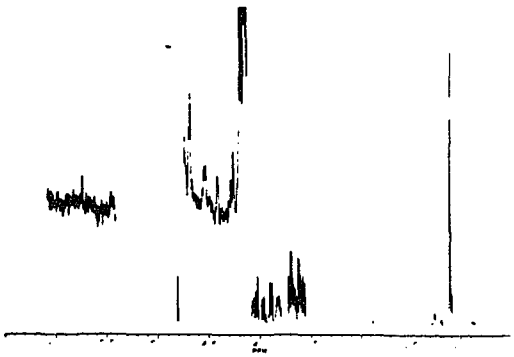

E. NA/ NANA 1:1000

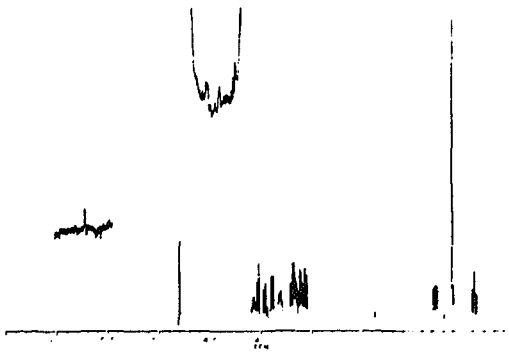

omitting O2 (model 2), and DANA (model 3). The restraints on geometry around C2 were relaxed for each model (for details see structure determination). When models 1 and 2 were used, C2 retained to a large extent its tetrahedral geometry, but there was still no significant density for O2 in the corresponding $|IF_o|-IF_c|$ difference maps where F_c was calculated using the refined coordinates of NA in complex I. When model 3 was used, C2 clearly moved away from the plane defined by C1, C3, O6 of the starting DANA model. The coordinates from this refinement had the best fit to the $|IF_o|-IF_c|$ electron density map (FIGURE 2A, Table 3). When DANA in complex II was refined using the same starting model and restraint relaxations as previously used for complex I, model 3, no significant changes to the DANA geometry occurred in complex II. Therefore, the refined coordinates of complex I, model 3, are clearly different from those of chemically synthesized DANA (FIGURE 2C, Table 3). Thus, the question is what chemical species are present in the NA active site? Since the occupancy resulted from X-PLOR refinement could not be interpreted as a true measurement of O2 presence in the complex, a series of F_c electron density maps were calculated using the refined model 1 coordinates with arbitrarily assigned O2 occupancies. The F_c electron density map for 20% O2 occupancy appears to be compatible with the $|IF_o|-IF_c|$ map calculated by use of the refined model 3 coordinates. Very weak density at the expected O2 position appeared when the contour level was reduced to 0.5σ (FIGURE 2C). This may be an indication that a low percentage of the bound compound is NANA. Therefore, NANA could only account for 20% or less of the total bound species in the

Table 3: Occupancies, Normalized Electron Densities, and Geometrical Data for NANA and DANA in Their Respective Complexes with NA

	NA-NANA			
	model 1	model 2	model 3	NA-DANA
occupancies[a]				
inhibitor	0.94	0.95	0.99	0.98
O2	0.65			
B-factors, Å^2				
inhibitor	9.46	8.66	9.44	
O2	21.59			
distances, Å[b]				
C2 - O2	1.46 (1.41)			
C2 - O6	1.38 (1.43)	1.39 (1.43)	1.41 (1.43)	1.37 (1.43)
C6- O6	1.42 (1.43)	1.43 (1.43)	1.43 (1.43)	1.37 (1.43)
C1 - C2	1.56 (1.52)	1.55 (1.52)	1.42 (1.38)	1.39 (1.38)
C2 - C3	1.55 (1.52)	1.57 (1.52)	1.40 (1.38)	1.41 (1.38)
C3 - C4	1.54 (1.52)	1.56 (1.52)	1.56 (1.52)	1.50 (1.52)
angles, deg[c]				
C1 - C2 - C3	114.30 (108.72)	115.65 (108.72)	124.82 (122.25)	134.02 (122.25)
C1 - C2 - O6	103.05 (107.24)	102.16 (107.24)	112.48 (118.75)	112.41 (118.75)
O2 - C2 - C1	106.90 (109.50)			
O2 - C2 - C3	111.17 (110.10)			
O2 - C2 - O6	110.40 (111.55)			
O6 - C2 - C3	110.67 (109.40)	109.09 (109.40)	112.00 (109.40)	111.45 (109.40)
C2 - C3 - C4	112.53 (110.70)	112.53 (110.70)	120.93 (120.00)	119.39 (120.00)
C2 - O6 - C6	121.58 (113.80)	121.87 (113.80)	126.53 (113.80)	117.54 (113.80)

[a] Occupancies are with respect to the protein atom occupancy of 1.0. [b,c] The equilibrium distances and angles within the brackets are those parameters employed by X-PLOR.

NA active site. If the remaining 80% was DANA, the refined coordinates of complex I, model 3, would have been the same as those of complex II, DANA. The final structure of complex I, model 3, strongly suggests that a third species other than NANA and DANA is bound in the NA active site at a significant percentage. One likely candidate is the NANA derived oxocarbonium ion, which was shown to be present in the pathway of influenza virus neuraminidase hydrolysis (Chong et al., 1992). The geometry of the refined complex I, model 3, is compatible with that of the postulated oxocarbonium ion.

Mechanism of Action. Based on competitive inhibition studies with *Arthrobacter sialophilus* neuraminidase, Miller et al. (1978) postulated that a salt bridge forms between a positively charged group on the enzyme and the carboxylate group of the substrate, which results in the distortion of the substrate to the half-chair conformation and the formation an oxocarbonium ion with a positive charge at C2. Similarly, Chong et al. (1991) showed that a positively charged residue was involved in substrate binding and hydrolysis by an influenza virus neuraminidase (A/Tokyo/3/67). Using site directed mutagenesis, Lentz et al. (1987) identified amino acids involved in enzyme activity without the full knowledge of the NA three-dimensional structure. Although the enzyme mechanism proposed by Lentz et al. (1987) is incompatible with the three-dimensional structure, the results showed the critical role of at least five conserved active site residues in neuraminidase activity. Recent studies of kinetic isotopic effects by Chong et al. (1992) have provided evidence for the formation of an oxocarbonium ion in

the neuraminidase reaction. The prior results implicated that the formation of the oxocarbonium ion at C2 is a key step in neuraminidase hydrolysis, but as yet no mechanism for its induction and stabilization has been proposed that is fully compatible with all the structural, biochemical, and kinetic data.

Based on the refined structure of complex I, we propose the enzyme mechanism shown in Scheme 1 for influenza virus neuraminidase. As the sialyl group of the substrate binds to the active site, it undergoes a ring distortion probably due to the strong ionic interactions between the carboxylate of the substrate and the three guanidinium groups of arginines 116, 292, and 374. These conformational changes induce the formation of the strained oxocarbonium ion in the active site, which results in the cleavage of the glycosidic bond. The aglycon moiety leaves the active site with the glycosidic oxygen, which becomes protonated by solvent. Stabilization of the positively charged oxocarbonium ion could result from keeping the C2 carbonium planar. This is achieved by multiple interactions between the functional groups of the intermediate and the active site residues. Such a strong binding is only possible when the C2 atom is in a planar conformation similar to DANA. Although the side chain carboxylate of Asp 149[2] and the partial negative charge on Tyr 409 OH (enhanced by hydrogen bonding with Glu 276 OE1) could contribute in part to the direct neutralization of the positive charge of the C2 carbonium, their major role in the overall stabilization is to maintain the C2 carbonium ion planarity in the transition state. In the rate limiting

[2]Asp149 in B/Lee/40 NA is equivalent to Asp152 in A/Tokyo/3/67.

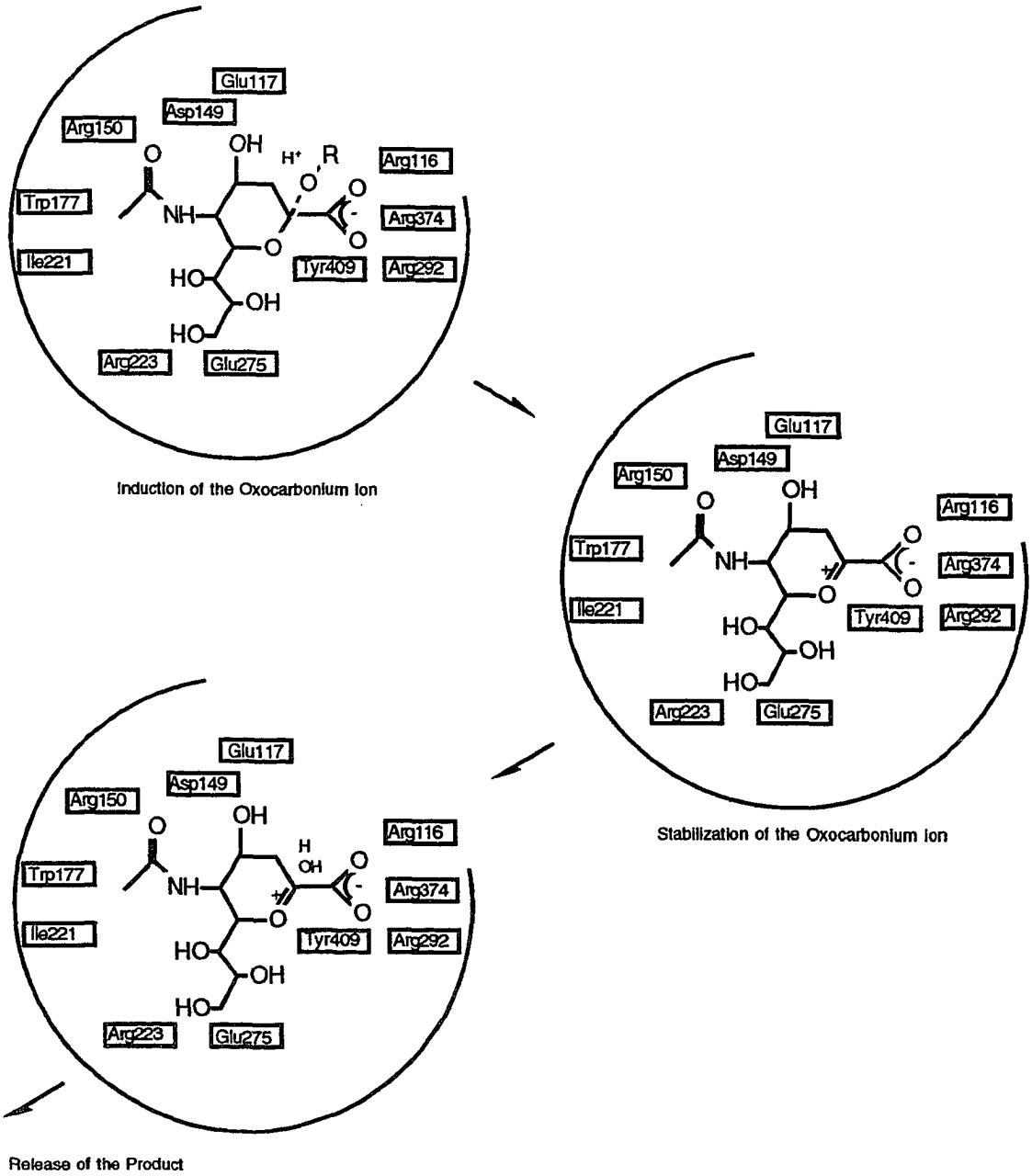

Scheme 1: Proposed influenza virus sialidase mechanism.

step of the reaction, the oxocarbonium ion picks up a hydroxyl molecule from solvent and leaves the active site as NANA. This mechanism clearly rationalizes the data from site directed mutagenesis because it requires the participation of all the active site residues in the stabilization of the transition state. It is also consistent with the kinetic isotopic effects, which predict the same number of steps in the reaction. Finally, sTable binding of the positively charged intermediate by keeping it in a planar conformation must be an inefficient step, and, therefore, the mechanism would result in the slow turn-over number of 9 s^{-1}, which we have measured (data not shown).

Discussion

We propose a mechanism of influenza virus neuraminidase reaction in which the driving force comes solely from the induction and stabilization of the oxocarbonium ion intermediate. The activation of the substrate does not involve any nucleophile or proton donor as found in other hydrolases. The stabilization is through concerted interactions between the positively charged intermediate and the active site residues, which maintain the planarity of the C2 oxocarbonium intermediate. The suggestion by Burmeister et al. (1993) that the sialyl cation is stabilized primarily by the charge on Tyr 409 OH (Tyr 408 in B/Beijing/1/87 NA) is inconsistent with the result that mutations of active site residues other than Tyr 409, including Asp 149 and Glu 275, could abolish the enzyme activity. All the active site residues must contribute not only to the binding of the substrate, but also to the

stabilization of the oxocarbonium intermediate. This is supported by evidence that a newly synthesized analogue of DANA, which lacks the 4-hydroxyl and 6-glyceryl groups, can still bind crystalline NA efficiently without interactions to Asp 149 and Glu 275 (unpublished data of our ongoing experiments).

The mechanism proposed by Burmeister et al. (1993) also suggested an irreversible production of DANA as a side product by proton elimination at C3 of the oxocarbonium intermediate. In contrast, our experiments showed that DANA was gradually hydrated by influenza virus NA, both types A and B (FIGURE 4).

Acknowledgments

We are grateful to Drs. Burmeister, Ruigrok and Cusack, EMBL Outstation, France, for providing the atomic coordinates of B/Beijing/87 NA prior to the publication of their work. We thank Mr. Paul A. Demuth and Dr. Mike Jablonsky for help on the NMR studies and Lily Yang for help in making FIGURE 2. Excellent technical assistance was provided by Aulikki Koskinen.

References

Aymard-Henry M., Coleman, M.T., Dowdle, W.R., Laver, W.G., Schild, G.C., & Webster, R.G. (1973) *Bull. W. H. O. 48(2)*, 199-202.

Brunger, A.T. (1992) *X-PLOR Version 3.0 Manual*, Yale University, New Haven, CT.

Bucher, D., & Palese, P. (1975) in *The Influenza Viruses and Influenza* (Kilbourne, E.D., Ed.) pp 83-123, Academic Press, New York.

Burmeister, W.P., Henrissat, B., Bosso, C., Cusack, S., & Ruigrok, R.W.H. (1993) *Structure 1*, 19-26.

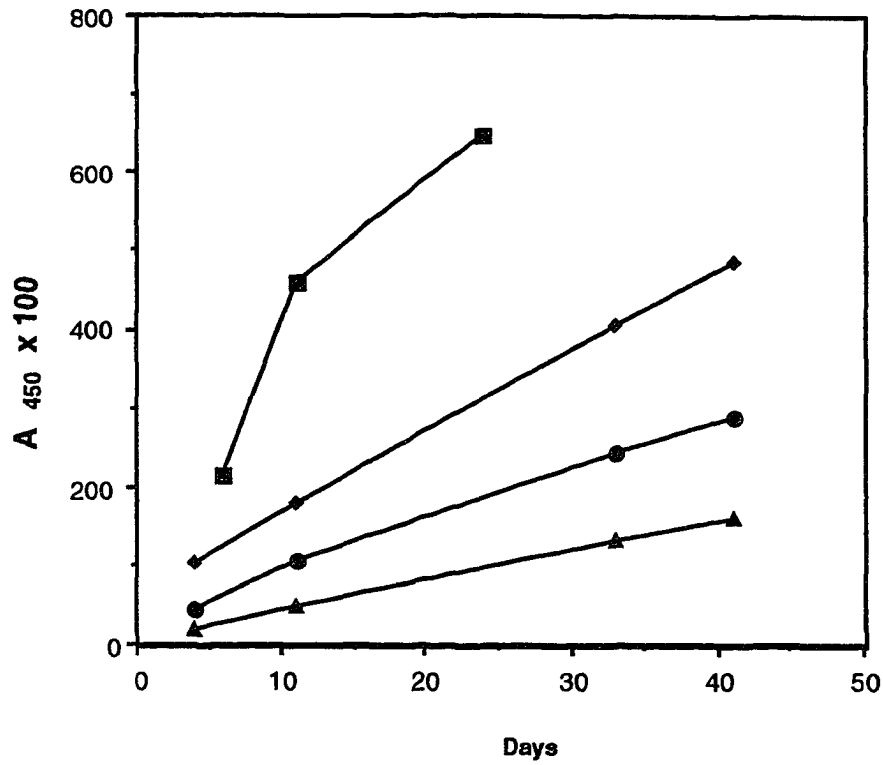

FIGURE 4: Hydration of DANA by influenza virus neuraminidase. Either B/Lee/40 NA at a concentration of 0.5 mg/ml (▲), 1.0 mg/ml (●), and 2.0 mg/ml (◆), or A/tern/75 (N9) NA at a concentration of 2 mg/ml (■) was incubated with an initial concentration of DANA (10 mM) at 20 °C. Aliquots were removed at the indicated time points, and the relative amount of NANA in the sample was determined by optical absorbtion at 450nm assaying for NANA as described by Aymard-Henry et al. (1973).

Burmeister, W.P., Ruigrok, R.W.H., & Cusack, S. (1992) *EMBO J. 11(1)*, 49-56.

Carson M., & Bugg, C.E. (1986) *J. Mol. Graphics 4*, 121-122.

CCP4 (1979) *The SERC (UK) Collaborative Computing Project No. 4, A Suite of Programs for Protein Crystallography*, Daresbury Laboratory, Warrington, U.K.

Chong, A.K.J., Pegg, M.S., & von Itzstein, M. (1991) *Biochem. Int. 24(1)*, 165-171.

Chong, A.K.J., Pegg, M.S., Taylor, N.R., & von Itzstein, M. (1992) *Eur. J. Biochem. 207(1)*, 335-343.

Hendrickson, W.A., & Connert, J.H. (1981) in *Structure, Conformation, Function and Evolution* (Srinivasan R., Subramanian, E., & Yathindra, N., Eds.) pp43-57, Pergamon Press, Oxford.

Howard, A.J., Gilliland, G.L., Finzel, B.C., Poulos, T.L., Ohlendorf, D.H. & Salemme, F.R. (1987) *J. Apl. Crystallogr. 20*, 338-387.

Jones, T. A. (1985) *Methods Enzymol. 115*, 157-171.

Lentz, M.R., Webster, R.G., & Air, G.M. (1987) *Biochemistry 26*, 5351-5358.

Lin , Y., Luo, M., Laver, W.G., Air, G.W., Smith, C.D., & Webster, R.G. (1990) *J. Mol. Biol. 214(3)*, 639-640.

Miller, C.A., Wang, P., & Flashner, M. (1978) *Biochem. Biophys. Res. Commun. 83*, 1479-1487.

Meindl, P., Bodo, G., Lindner, J., & Palese, P. (1971) *Z. Naturforsch. 263*, 792-797.

Rossmann, M.G. & Blow, D.M. (1962) *Acta Cryst. 15*, 24-31.

Varghese, J.N., McKimm-Breschkin, J.L., Caldwell, J.B., Kortt, A.A., & Colman, P.M. (1992) *Proteins 14*, 327-332.

A SIALIC ACID-DERIVED PHOSPHONATE ANALOG INHIBITS DIFFERENT STRAINS OF INFLUENZA VIRUS NEURAMINIDASE WITH DIFFERENT EFFICIENCIES

CLINTON L. WHITE[1,2], MUSIRI N. JANAKIRAMAN[1,3], W. GRAEME LAVER[4], CÉDRIC PHILIPPON[5], ANDREA VASELLA[5], GILLIAN M. AIR[3] AND MING LUO[1,3]

[1]Center for Macromolecular Crystallography,
[2]Department of Biochemistry and Molecular Genetics,
[3]Department of Microbiology,
University of Alabama at Birmingham, Birmingham, Alabama, 35294, USA,
[4]John Curtin School of Medical Research,
Australian National University, Canberra 2601, Australia
[5]Laboratorium für Organische Chemie,
ETH-Zentrum, CH-8092 Zürich, Switzerland

(Received 9 August 1994; accepted 14 October 1994)
Journal of Molecular Biology, Vol. 245, 1995

Keywords: antiviral; PANA; neuraminyl phosphonic acid; X-ray structure; structure-based drug design

*Corresponding author
Present address: M.N. Janakiraman, Upjohn Corporation, Kalamazoo, Michigan, U.S.A.

Abbreviations used: HA, hemaglutinin; NA, neuraminidase; NANA, *N*-acetylneuraminic acid or α-sialic acid; DANA, 2-deoxy-2,3-dehydro-*N*-acetylneuraminic acid; N2, A/Tokyo/3/67 neuraminidase strain; N9 A/tern/Australia/G70c/75 neuraminidase strain; PANA, phosphonate analog of neuraminic acid; ePANA, equatorial PANA; aPANA, axial PANA; PEG, polyethylene glycol; MUN, 4-Me-umbelliferyl-*N*-acetylneuraminic acid; F_{obs}, observed structure factors; F_{calc}, calculated structure factors; r.m.s., root-mean-square; r.m.s.d, root-mean-square difference.

Abstract

A phosphonate analog of N-acetyl neuraminic acid (PANA) has been designed as a potential neuraminidase (NA) inhibitor and synthesized as both the α (ePANA) and β (aPANA) anomers. Inhibition of type A (N2) and type B NA activity by ePANA was approximately a 100-fold better than sialic acid, but inhibition of type A (N9) NA was only ten-fold better than sialic acid. The aPANA compound was not a strong inhibitor for any of the NA strains tested. The crystal structures at 2.4 Å resolution of ePANA complexed to type A (N2) NA, type A (N9) NA, and type B NA and aPANA complexed to type A (N2) NA showed that neither of the PANA compounds distorted the NA active site upon binding. No significant differences in the NA-ePANA complex structures were found to explain the anomalous inhibition of N9 neuraminidase by ePANA. We hypothesize that an increase in the ePANA inhibition compared to sialic acid is due to (1) a stronger electrostatic interaction between the inhibitor phosphonoyl group and the active site arginine pocket and (2) a lower distortion energy requirement for binding of ePANA.

Introduction

The two glycoproteins found on the influenza virus membrane envelope are the haemagglutinin (HA) and neuraminidase (NA, acylneuraminyl hydrolase, EC 3.2.1.18) proteins. The trimeric haemagglutinin is responsible for viral attachment to the cell surface receptor, which is a terminal sialic acid residue (Hirst, 1941; Gottschalk, 1959). The functional neuraminidase exists as a tetramer of identical subunits. The NA tetramer forms a box-like

head on top of a long stalk domain and is anchored in the viral membrane by a hydrophobic sequence near the N-terminus (Blok *et al.*, 1982; Air & Laver, 1989). The neuraminidase is thought to enhance viral mobility via hydrolysis of the α-(2,3) or α-(2,6) glycosidic linkage between a terminal sialic acid residue and its adjacent carbohydrate moiety on the host receptor (Gottschalk, 1957, 1959). It has been shown in tissue culture that NA activity is required to facilitate the release of progeny virions from infected cells and prevent self-aggregation (Palese & Schulman, 1974; Liu & Air, 1993). Tetrameric heads of NA can be released from the viral surface by proteolytic cleavage. The purified heads still maintain full neuraminidase activity in the crystalline state (Laver, 1978; Air *et al.*, 1990).

The amino acid sequence identity between most strains of influenza type A and type B neuraminidases heads has been found to be approximately 30% (Blok *et al.*, 1982; Air *et al.*, 1990; Bossart-Whitaker *et al.*, 1993). The crystal structure of several native NA heads, as well as the complexes of NA to α-sialic acid (NANA), a weak inhibitor, and 2-deoxy-2,3-dehydro-*N*-acetyl neuraminic acid (DANA), a moderate inhibitor, have been reported (Varghese *et al.*, 1983, 1992; Tulip *et al.*, 1991; Varghese & Colman, 1991; Burmeister *et al.*, 1992; Bossart-Whitaker *et al.*, 1993). Both types A and B NA strains are composed of six, four-stranded anti-parallel β-sheets arranged in a right-handed propeller motif. Early workers identified DANA as a potent inhibitor of neuraminidase and a possible analog of the enzymatic transition state (Meindl *et al.*, 1974; Palese & Schulman, 1974). Crystallographic studies of DANA

complexed to influenza virus neuraminidase have shown that DANA binds in a similar fashion as NANA in the active site (Meindl *et al.*, 1974; Palese & Schulman, 1974; Burmeister *et al.*, 1992; Varghese *et al.*, 1992; Bossart-Whitaker *et al.*, 1993). From these studies, several highly conserved active site residues were identified that directly interact with the substrate, although the detailed enzyme mechanism is still not completely understood (Colman *et al.*, 1983; Varghese *et al.*, 1983; Lentz *et al.*, 1987; Chong *et al.*, 1991; Varghese & Colman, 1991; Chong *et al.*, 1992; Janakiraman *et al.*, 1994; Taylor & von Itzstein, 1994).

The crystallographic results have also led to the speculation and design of novel inhibitors, which either (1) enhance the existing interactions between the substrate and the protein or (2) make new contacts in previously unoccupied active site regions. Thus substitution of the C4 hydroxyl group of DANA with a guanidino group reportedly resulted in a 10,000-fold increase on the potency of DANA (Holzer *et al.*, 1993; Woods *et al.*, 1993). The inhibitor presented in this paper, PANA, is a sialic acid derived phosphonate analog, which replaces the monobasic carboxyl group with a dibasic phosphonoyl group. This substitution should strengthen the charge-charge interaction with the arginine pocket in the active site of neuraminidases while maintaining the favorable interactions of the remaining inhibitor functional groups to the NA active site (Wallimann & Vasella, 1990; Vasella *et al.*, 1991; Vasella & Wyler, 1991). Figure 1 describes the enzyme-bound structure and the proper name for NANA and several NANA analogs. Note that the atom numbering of NANA is different from the atom numbering of the

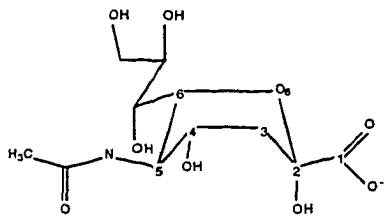

NANA
α-*N*-acetyl neuraminic acid

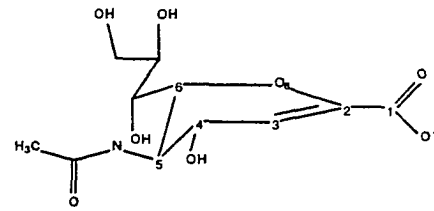

DANA
2-deoxy-2,3-dehydro-*N*-acetyl neuraminic acid

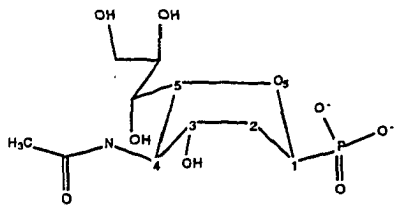

aPANA
(4-Acetamido-2,4-dideoxy-D-*glycero*-β-D-*galacto*-1-octopyranosyl) phosphonic acid

pKa_1= 1.67 pKa_2=6.30

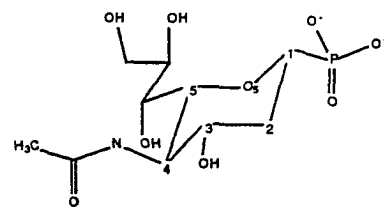

ePANA
(4-Acetamido-2,4-dideoxy-D-*glycero*-α-D-*galacto*-1-octopyranosyl) phosphonic acid

pKa_1= 1.63 pKa_2=6.35

Figure 1. Comparison of the NANA, DANA and PANA structures. The structures are shown in the conformation assumed by the inhibitor when bound to neuraminidase (the NA active site is located above the inhibitor ring). The pK_a values for the PANA inhibitors are according to Wallimann & Vasella (1990). Note, both the unbound NANA and aPANA at equilibrium in solution will favor alternative conformations. The spontaneous anomerization of NANA in solution results in an equilibrium ratio of 95:5, β-anomer:α-anomer. The aPANA in solution at equilibrium favors the lower energy $^2C_5$ conformation. No anomerization occurs with the PANA inhibitors due to the lack of a C2 hydroxyl group.

PANA analogs. Unless otherwise stated, the active site residue numbering reference scheme is that of the B/Lee/40 NA-ePANA complex. The subject of this study is the inhibitory activity and crystal structure of the PANA compounds complexed to different influenza neuraminidases: N2, a type A NA (A/Tokyo/3/67); N9, a type A NA (A/tern/Australia/G70c/75); and B/Lee/40, a type B NA.

Results and Discussion

Inhibition and IC_{50} assays

The inhibitory activity of ePANA and aPANA was tested for several strains of influenza virus neuraminidase using a standard NA assay and fetuin substrate (Aymard-Henry *et al.*, 1973). The inhibition of N2 and B/Lee/40 NA by ePANA was approximately 100-fold better than NANA inhibition, with the exception of N9 inhibition levels. The ability of ePANA to inhibit the N9 strain when compared to other NA strains tested was decreased by ten-fold. The aPANA inhibition activity was comparable to that of NANA (data not shown). The IC_{50} values for PANA inhibition were also measured by a fluorometric assay using 4-Me-umbelliferyl-*N*-acetylneuraminic acid (MUN) as the substrate (Figure 2; Potier *et al.*, 1979). Again, the ePANA compound showed a decrease in inhibition efficiency for N9 NA versus other NA strains. The N9 NA IC_{50} was ten-fold higher than the type B (B/Mem/89) NA IC_{50}, which is representative of other types A and B NA IC_{50} values. In both of the assays, an identical amount of NA activity was used for testing each sample. Therefore the observed ten-fold difference in the binding studies between influenza N9 NA and the remaining influenza NAs studied is

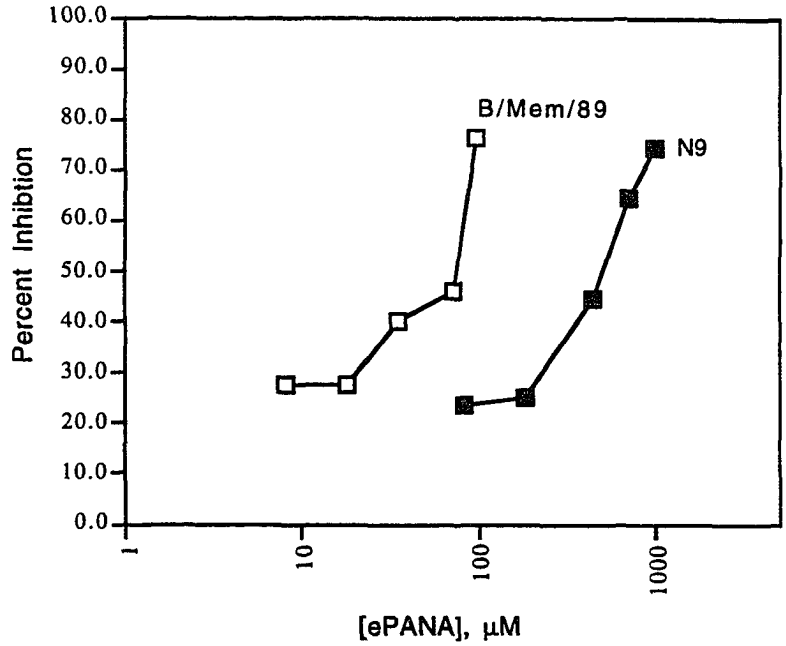

Figure 2. IC_{50} values for ePANA inhibition of a type A N9 subtype (A/tern/Australia/G70c/75) neuraminidase and a type B (B/Mem/89) neuraminidase. The IC_{50} values were determined using purified virions as the neuraminidase source and 4-Me-umbelliferyl-*N*-acetylneuraminic acid as the substrate in a standard fluorometric assay (Aymard-Henry *et al.*, 1973). See Material and Methods for details.

valid. Without accurate measured K_i values, the authors can only speculate that the observed binding difference for N9 NA may be approximately equal to a free energy change of ~3kcal/mol.

Equatorial phosphonate binding

The interactions between the equatorial phosphonate and the neuraminidase active site were examined by X-ray crystallography. The structures of the ePANA complexed to the N2, N9, and B/Lee/40 strains were determined to 2.4 Å resolution. The electron density corresponding to the phosphonate inhibitor was clearly present in the active site of the neuraminidase in the initial $||F_{obs}|-|F_{calc}||$ maps calculated using the native phases, where F_{calc} represents structure factors calculated from the native coordinates. After modeling the phosphonate compound in the active site, the complex structure was carefully refined to produce the final coordinates used in the current analysis (Figure 3).

The neuraminidase active site is a shallow pocket that is lined by a central shell of 11 strictly conserved amino acids that directly interact with the substrate (Burmeister *et al.*, 1992). Surrounding the central active site residues is a second shell of mostly conserved or homologous residues that interact with the central shell through an extensive hydrogen bonding network. Figure 4 shows the B/Lee/40 NA-ePANA complex active site. The general position of the ePANA in the B/Lee/40 NA active site is consistent with the inhibitor position in the other influenza virus NA-PANA complexes.

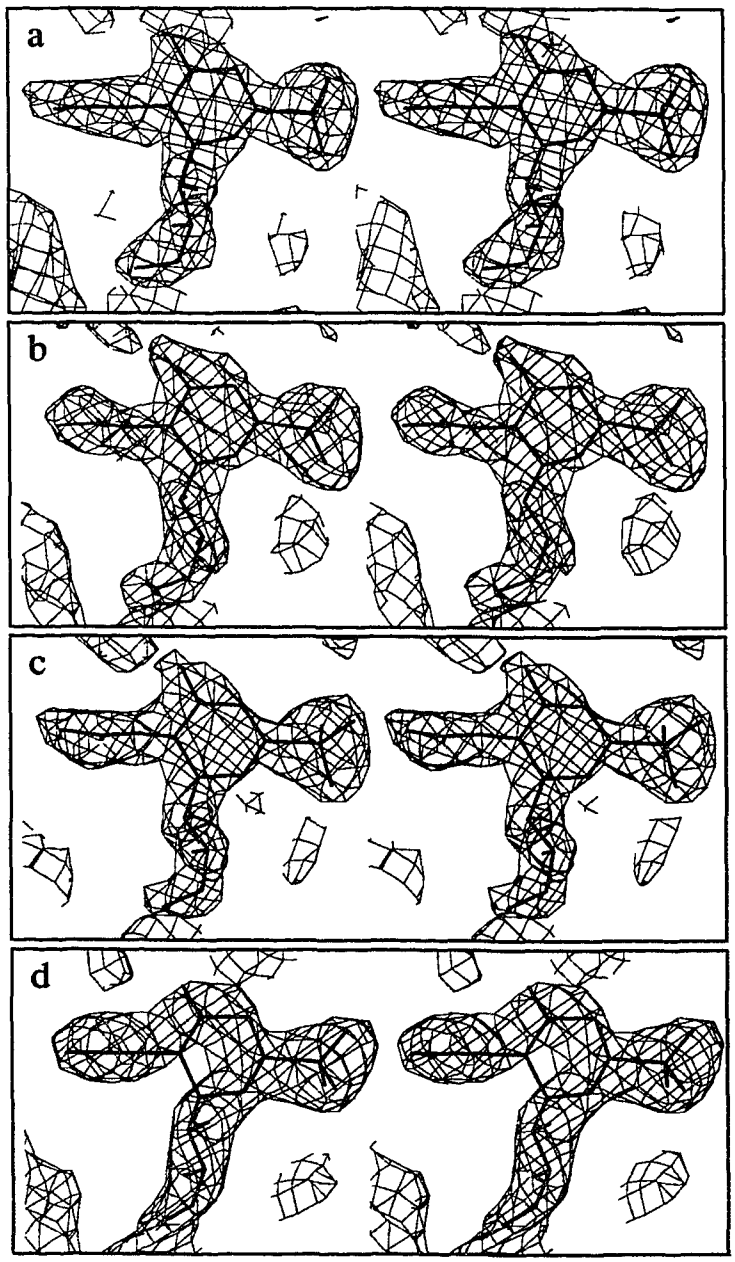

Figure 3. $|2|F_{obs}|-|F_{calc}||$ electron density maps for the refined PANA-NA complexes at 2.4 Å resolution generated using calculated phases (X-PLOR) and contoured at 1.5σ. Also shown are the refined coordinates of the PANA inhibitor for each neuraminidase complex: (a) B/Lee/40 NA-ePANA complex, (b) N2 NA-ePANA complex, (c) N9 NA-ePANA complex and (d) N2 NA-aPANA complex.

The binding of the phosphonate inhibitor is dominated by the charge-charge attraction between the phosphonate dianion and a pocket of three positively charged arginine residues (R116, R292 and R374) in the active site. Opposite the arginine pocket, the methyl group of the acetamido moiety fits into a small hydrophobic pocket formed by residues I221 and W177, as well as the side chain of R223. The acetamido carbonyl oxygen forms a hydrogen bond with the guanidinium group of R150. The hydroxyl group at C3 forms hydrogen bonds with D149 and E117, while the last two hydroxyl groups of the glycerol moiety form hydrogen bonds with E275. The Y409 hydroxyl is directly underneath the C1 and O5 sugar ring atoms. The phosphonoyl group substitution should not only increase the charge-charge interaction with the active site arginine pocket, which is advantageous, but may also introduce deleterious steric effects due to its larger size and the inherent rigidity of the NAactive site. Our results clearly show that the binding of the ePANA inhibitor does not induce any significant disturbance in the active site structure, as evidenced by the low root-mean-square (r.m.s.) difference (0.265 Å) between the backbone atoms of the 11 active site residues in the native B/Lee/40 NA and the B/Lee/40 NA-ePANA complex. This r.m.s. value is not much higher than the r.m.s. difference between the B/Lee/40 native NA and NANA complex active site backbone atoms (0.202 Å) at 1.8 Å resolution (Janakiraman *et al.*, 1994).

Because the coordinates of the NANA, DANA, and ePANA B/Lee/40 NA complexes are available, we are able to directly compare the characteristics of ePANA binding versus NANA and DANA using the

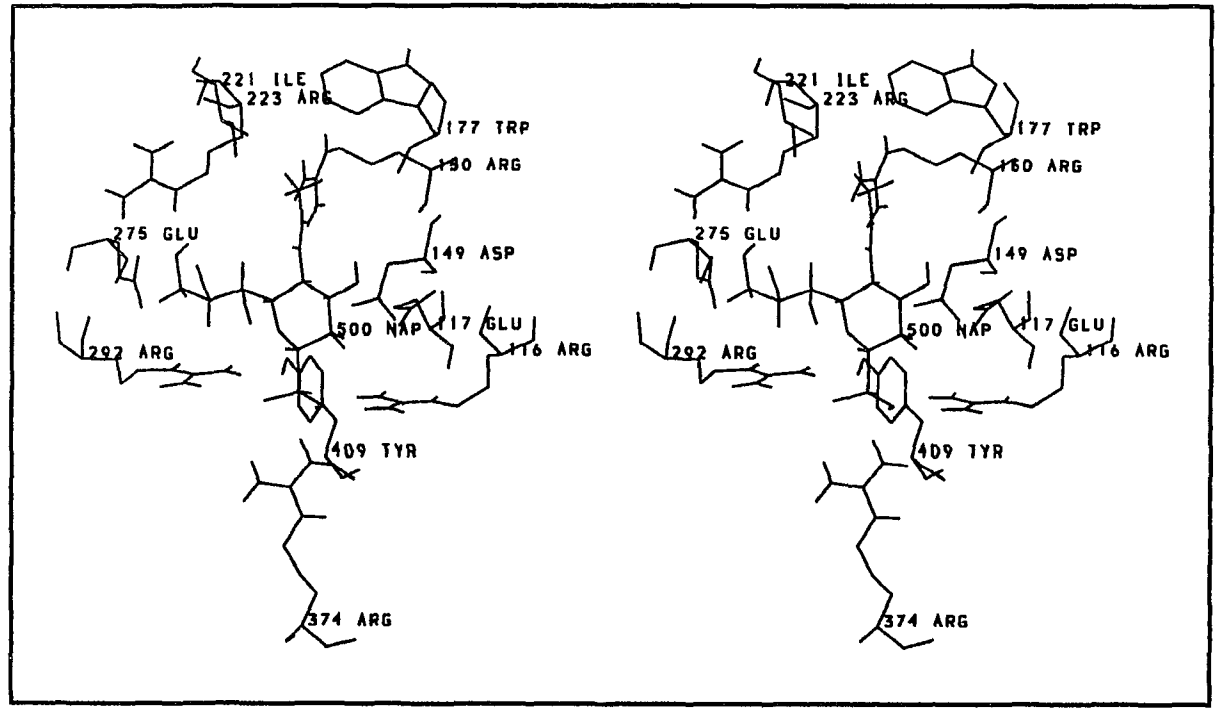

Figure 4. Final refined coordinates of the B/Lee/40 NA-ePANA complex showing orientation of inhibitor in the NA active site. Shown are the ePANA residue (500 NAP), which binds influenza virus neuramnidase in the chair conformation, and the active site residues, which directly interact with the ePANA functional groups (R116, E117, D149, R150, W177, I221, R223, E275, R292, R374, and Y409). The strong charge-charge interaction between the ePANA phophonyl group and the active site arginine pocket (R116, R292, and R374) must be maintained for tight inhibitor binding.

same NA strain. The low r.m.s. deviations for the hydroxyl, acetamido, and glycerol functional groups between the ePANA, NANA and DANA B/Lee/40 NA complexes after superposition by the active site backbone atoms demonstrate that the inhibitor substituants away from the inhibitor acidic group maintain approximately the same position in all the inhibitor complexes (Figure 5 and Table 1).

We were also interested in any possible differences that may occur when ePANA is bound to different strains of influenza virus NA. The superposition of the active site residues from the native B/Lee/40 NA and the B/Lee/40 NA-ePANA complex, as well as the complexes of ePANA bound to different NA strains (N2, N9, and B/Lee/40), shows that the active site geometry of the enzyme is nearly identical in the absence and presence of ePANA (Table 2). Any r.m.s. differences less than the maximum Luzatti estimated coordinate error determined for the ePANA complexes (0.31 Å) should be considered insignificant.

When examining the active site residues, one can conclude that the binding of ePANA does not markedly disturb the backbone atoms of the active site residues, though some subtle changes do occur. Excluding the three arginines (R116, R292, and R374), which anchor the inhibitor acidic group, the side chains of the hydrophobic residues in the active site display less positional variation than the hydrophilic residues. A possible explanation for this difference in side-chain positional variation is that the hydrophobic residues do not make directional interactions with the inhibitor and are therefore more forgiving to variations in the position of the inhibitor functional groups when the inhibitor is bound to the active

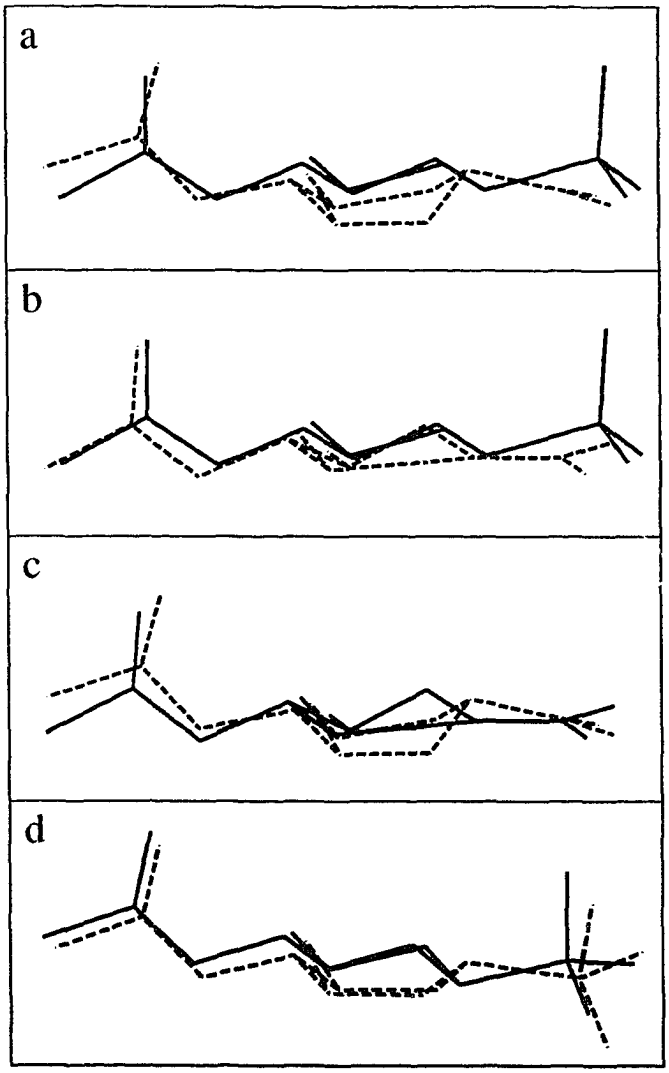

Figure 5. Superposition of neuraminidase bound inhibitor structures using the C1, sugar ring (C2-C6, O6), N5 and C7 inhibitor atoms (X-PLOR). The glycerol side chain has been intentionally cut away to clearly expose the ring atoms. In the B/Lee/40 NA-NANA complex, the authors did not model the O2 atom of NANA due to a lack of corresponding electron density in their experimental data (Janakiraman *et al.*, 1994). The following pairs of NA complexed inhibitors have been superimposed: (a) B/Lee/40 NA-NANA (dashed) and B/Lee/40 NA-ePANA (solid), (b) B/Lee/40 NA-DANA (dashed) and B/Lee/40 NA-ePANA (solid), (c) B/Lee/40 NA-NANA (dashed) and B/Lee/40 NA-DANA (solid), and (d) N2 NA-aPANA (dashed) and N2 NA-ePANA (solid).

Table 1

r.m.s. differences (Å) of inhibitor functional groups for different inhibitor neuraminidase complexes* after superposition by active site backbone atoms

Group	B/Lee/40 NA-NANA *versus* B/Lee/40 NA-ePANA	B/Lee/40 NA-DANA *versus* B/Lee/40 NA-ePANA	B/Lee/40 NA-NANA *versus* B/Lee/40 NA-DANA	N2 NA-aPANA *versus* N2 NA-ePANA
Active site backbone atoms	0.167	0.212	0.171	0.106
C-1 (P) atoms†	0.750	0.846	0.238	0.377
Ring atoms:				0.564
C2 (C1)	0.423	0.394	0.442	
C3,O6 (C2,O5)	0.785	0.389	0.776	0.741
C4,C5,C6 (C3,C5,C6)	0.412	0.473	0.144	0.587
Hydroxyl O4 (O3) atom	0.298	0.276	0.134	0.485
Acetamido group	0.395	0.359	0.428	0.593
Glycerol group	0.457	0.551	0.295	0.566

†NANA/DANA atom numbering followed by equivalent PANA atom numbering in parentheses.

Table 2

r.m.s. *differences* (Å) *of active site residues for* B/Lee/40 NA-NANA and B/Lee/40 NA-ePANA neuraminidase complexes and different ePANA neuraminidase complexes (N2, N9, B/Lee/40)* after superposition by active site backbone atoms

Group	B/Lee/40 NA-NANA *versus* B/Lee/40 NA-ePANA	N2, N9, and B/Lee/40 NA-ePANA complexes
Active site backbone atoms	0.265	0.201
Active site side chain atoms	0.449	0.448
R116 side chain	0.103	0.327
E117 side chain	0.313	0.204
D149 side chain	0.833	0.704
R 150 side chain	0.205	0.459
W177 side chain	0.147	0.187
I221 side chain	0.432	0.173
R223 side chain	0.317	0.645
E275 side chain	0.959	0.749
R292 side chain	0.238	0.367
R374 side chain	0.144	0.480
Y409 side chain	0.233	0.199

† B/Lee/40 NA residue numbering

site. The hydrophilic residues in the active site must make compensatory movements with respect to the inhibitor to retain the proper bonding geometry and therefore should have a higher r.m.s. difference. Residue E117 is an exception among the hydrophilic residue because it only forms a long hydrogen bond to the inhibitor C3 hydroxyl group and is therefore much less dependent on changes in the inhibitor position. Although the active site substituants of different neuraminidase strains are roughly in the same position, the slight variations in side chain geometry among the inhibitor-NA complexes may explain to some extent the small differences in the observed inhibition affinity.

Table 3 lists the r.m.s. differences for the ePANA inhibitor when bound to different NA strains. When the bound ePANA molecules in the N2, N9 and B/Lee/40 NA-ePANA complexes are compared with each other, it is clear that the binding of ePANA to different influenza virus NA strains is nearly identical. The phosphonate group is tightly restrained to the position that maintains the strongest electrostatic interactions with the active site arginines. The remainder of the inhibitor functional groups, and in particular the glycerol group, seem to have more flexibility in their interactions with the active site residues.

The most striking difference between bound ePANA and the other inhibitors occurs in the conformation of the pyranosidic ring in the NA-ePANA complexes. Upon binding of NANA to NA, the pyranosidic ring must be converted from the more stable chair conformation, $^{2}C_{5}$, into an energetically unfavorable boat-like ($B_{2,5}$) conformation. The slightly flat boat conformation of bound NANA properly

Table 3

r.m.s. differences (Å) of ePANA functional groups for different neuraminidase (N2, N9 and B/Lee/40) ePANA complexes after superposition by active site backbone atoms

Group	N2, N9, and B/Lee/40 NA-ePANA complexes
P atoms	0.143
Ring atoms:	
C-1	0.123
C-2, O-5	0.212
C-3, C-5, C-6	0.199
Hydroxyl atom O-3	0.221
Acetamido group	0.206
Glycerol group	0.258

positions the inhibitor carboxyl group to make a strong interaction with the active site arginine pocket and allows the remaining part of the substrate beyond the glycosidic oxygen of the terminal sialic acid to exit the active site unhindered. In contrast, the ePANA (α anomer) adopts a $^2C_5$ conformation both in solution and when bound to NA. It is the lack of a C1 hydroxyl group in ePANA that makes it possible for the pyranosidic ring to assume a $^2C_5$ conformation when bound to NA. Modeling shows that a steric clash would occur between the ePANA C1 hydroxyl group and the Y409 hydroxyl group on the active site floor if the C1 hydroxyl was present on the sugar ring of bound ePANA. By analogy to ePANA binding, this may partially explain why the β anomer of NANA does not bind influenza virus NA. Assuming that the β-NANA would bind NA in a $^2C_5$ conformation similar to ePANA, which would be required for the correct positioning of the β-NANA carboxyl group opposite the arginine pocket, a destabilizing steric interaction between the C2 hydroxyl group of β-NANA and side chain of Y409 would result.

The most puzzling observation in this study was the ten-fold reduction in the ePANA inhibition level for the N9 neuraminidase. Many viral proteins from different virus strains have structural, catalytic, or regulatory regions whose residues are strictly conserved among all strains and are required for proper viral functioning. Because of the strong conservation of residues in these functional sites among the differing viral strains, they are attractive targets for the design of anti-viral agents, which should be effective against all strains of the virus. A careful analysis of the NA-ePANA complex crystal structures indicates that there are

no detectable differences in the binding mode of ePANA to the N9 strain versus other neuraminidases (Tables 2 and 3). The r.m.s. deviation for ePANA that occurs between the individual NA-ePANA complex structures is comparable to the deviation that exists between (1) the structures of different native NA strains and (2) the structures of NANA complexed to different NA strains. Clearly, the depressed inhibition activity of ePANA for the N9 strain could not be due to alternative ePANA binding modes. The lower inhibition may reflect a difference in the dynamic properties of the N9 strain in solution when compared to the majority of NA strains. Such dynamic processes would not be detected by the time-averaged crystallography experiments at equilibrium conditions reported in this paper. Although the active site structure of N9 NA determined by X-ray crystallography may be the same as other NA strains, the dynamic mobility of N9 NA in solution may differ from other NA strain and influence the on/off rate of ePANA binding. Some aspects of N9 NA reactivity have been shown to differ from the typical influenza neuraminidase strain. For example, N9 NA has a much higher reaction rate for the hydration of DANA, one of the side reactions observed with neuraminidase, when compared to other NA strains even though the N9 strain has a similar K_m and turnover number for glycosidic hydrolysis as compared to other NA strains (Janakiraman *et al.*, 1994). It should be noted that the influenza virus inhibitor 4-guanidino DANA has been shown to display a ten-fold variation between type A and type B NA inhibition levels (von Itzstein *et al.*, 1993).

Axial phosphonate binding

As predicted, the axial phosphonate, which corresponds to α-NANA, binds to the NA active site with its sugar ring in a boat-like ($B_{2,5}$) conformation (Figure 5). The boat-like conformation places the phosphonoyl group of aPANA in a pseudo-equatorial position, which is favorable for interacting with the active site arginine pocket. Modeling had indicated that the $^2C_5$ conformation of the axial phosphonate could not bind in the NA active site because the phosphonoyl group would protrude into the floor of the active site pocket. The active site geometry in the N2 NA-aPANA complex is nearly identical to the active site structure observed in the N2 NA-ePANA complex (Table 4).

Owing to the aPANA binding in a $B_{2,5}$-like conformation and ePANA binding in a $^2C_5$ conformation, the C1, C2, and O5 atoms of the inhibitor sugar ring show the largest positional differences between the two PANA complexes (Table 5). However, this variation in the ring atoms does not result in a major positional difference between the aPANA and ePANA phosphonate groups. Therefore, aPANA in the N2 NA-aPANA complex makes the same inhibitor protein interactions as ePANA does in the three NA-ePANA complexes. The crystal structure of the N2 NA-aPANA complex does not reflect the observation that aPANA has a much lower inhibitory activity than ePANA in the solution assays. Presumably, the lower inhibition activity of aPANA versus ePANA results from two additional steps that are required for aPANA to effectively bind NA. First, the free aPANA must convert from a $^2C_5$ conformation to a boat-like conformation for binding, similar to NANA, and this transition is

Table 4

r.m.s. differences (Å) of active site residues for N2 neuraminidase aPANA and ePANA complexes after superposition by active site backbone atoms

Group	N2 NA-aPANA *versus* N2 NA-ePANA
Active site backbone atoms	0.107
Active site side-chain atoms	0.169
R116 side-chain	0.184
E117 side-chain	0.132
D149 side-chain	0.165
R 150 side-chain	0.116
W177 side-chain	0.068
I221 side-chain	0.163
R223 side-chain	0.220
E275 side-chain	0.110
R292 side-chain	0.131
R374 side-chain	0.302
Y409 side-chain	0.296

†B/Lee/40 NA residue numbering

Table 5

r.m.s differences (Å) of inhibitor functional groups for N2 neuraminidase aPANA and ePANA complexes after superposition by inhibitor atoms (P, ring atoms, O-3, N-4 and C-6)

Group	N2 NA-aPANA *versus* N2 NA-ePANA
Superposition atoms	0.312
P atoms	0.169
Ring atoms:	
C-1†	0.683
C-2, O-5	0.438
C-3, C-5, C-6	0.101
O-3 hydroxyl atom	0.198
Acetamido group	0.265
Glycerol group	0.301

†PANA atom numbering

energetically unfavorable. In contrast, the ePANA inhibitor assumes the $^2C_5$ conformation both in solution and when bound to NA. Second, a weak intramolecular hydrogen bonding network may occur between the glycerol O7 and O8 hydroxyls and one of the phosphonoyl oxygen atoms of the $^2C_5$ conformer of aPANA, which dominates in solution and in the absence of NA, thereby increasing the energy required for transition to the NA bound boat-like conformation of aPANA. No analogous intramolecular hydrogen bonding network is possible for the $^2C_5$ conformation of ePANA due to the phosphonoyl group being in an equatorial position. We can not speculate on the magnitude of these additional potential entropic and enthalpic energy costs required for aPANA binding to NA, but they may be significant.

Elements affecting inhibitor binding

As mentioned, the active site of neuraminidase does not change its structure when it is complexed with either NANA, DANA, or PANA. Therefore, it is possible that the contrasting inhibition levels observed for the different inhibitor compounds are related to the differences in binding of each inhibitor with respect to the neuraminidase active site. A closer look at the refined structure of these inhibitors in the complex may reveal the important elements that affect the binding of these compounds to NA.

The results from this report and previous studies indicate that the contributions of each of the inhibitor functional groups are not equal for active site binding (Meindl *et al.*, 1974; Flashner *et al.*, 1983; Chong *et al.*, 1991; Varghese *et al.*, 1992; Holzer *et al.*, 1993; Woods *et al.*, 1993). The most important inhibitor functional group

is the acidic carboxyl or phosphonoyl group, which interacts with the active site arginine pocket through charge-charge interactions. In the B/Lee/40 NA-ePANA complex, the distance from the phosphonoyl P atom to the central arginine (R374) CZ atom of the arginine pocket is 4.34Å, while analogous distance in the B/Lee/40 NA-DANA complex, carboxylate C1 atom to CZ atom of R374, is 4.56 Å (Table 1) (Janakiraman *et al.*, 1994). The lack of change in the acidic group-arginine distance for the NA-ePANA complex is the result of the slightly longer C-P bond (1.86 Å) present in the PANA inhibitor versus the C-C bond distance in DANA (1.39 Å) and is not due to any significant movement of the R374 position in the ePANA complex (Figure 5).

Comparison of the bound inhibitors in the aPANA and ePANA N2 NA complexes stresses the importance and specificity of the position of the phosphonoyl group in maintaining the electrostatic attraction to the arginine pocket. The distance from the phosphonoyl P atom to the central arginine CZ atom of the arginine pocket in the aPANA complex shows only a slight increase of 0.10 Å versus the same distance in the ePANA complex structure.

The inhibitor pyranosidic ring also plays an important role in inhibitor binding. If the inhibitor acid group is a carboxylate, the optimal conformation of the inhibitor ring is the half-chair conformation of DANA, a transition state analog, which correctly places the carboxylate in the most favorable position for interacting with the arginine active site pocket. On the other hand, if the inhibitor acid group is not a carboxylate, as is the case for the PANA inhibitors, the pyranosidic ring is free to assume the conformation

which will optimize the new acid group-arginine pocket interactions and still maintain the other inhibitor functional group interactions in the NA active site. The inhibitor ring itself is not required to always assume the half-chair conformation of DANA, but instead the pyranosidic ring conformation is dictated by the nature of the inhibitor functional group interactions with the NA active site. The inhibitor pyranosidic ring acts only as a scaffolding to correctly orientate the attached inhibitor functional groups in the NA active site and does not directly interact with the active site. The limited role of the inhibitor ring, as a scaffolding for inhibitor functional groups, should benefit the design of new, novel influenza virus NA inhibitors. New inhibitors with novel chemical moieties substituted for the pyranosidic ring of NANA, which also result in the correct constellation of inhibitor functional groups.

DANA has a double bond between C2 and C3, which fixes the ring into a half chair conformation in solution and when bound to NA. The half-chair conformation results in the strongest interaction between the carboxyl group and the arginine pocket and requires no energetically unfavorable alterations in the ring conformation for binding. Like DANA, the solution form of ePANA, $^{2}C_{5}$, is not required to undergo any changes in ring conformation for binding to NA. Nevertheless, slight deviations from the ideal ePANA solution conformation required for efficient NA binding, which result in higher ring strain or the restriction of vibrational and rotational degrees of freedom, may increase in the energy barrier associated with NA binding for ePANA when compared to DANA.

Unlike DANA and ePANA, which do not require a major change in their ring conformation for binding NA and are much better NA inhibitors, both aPANA and NANA undergo substantial conformational change when they bind NA. In addition, the dihedral angles of the pyranosidic ring in NA-bound NANA are slightly distorted from ideal $B_{2,5}$ values, which allows the carboxyl group of NANA to be positioned for the strongest interaction with the arginine pocket (Table 6; Burmeister *et al.*, 1992; Janakiraman *et al.*, 1994). Unlike NANA, distortion of the ring in the ePANA or aPANA NA complexes to place the acidic group in a more favorable equatorial position opposite the arginine pocket may not be possible due to the larger bulk of the phosphonate group, which may prevent ring flattening due to steric clashes with residues in the active site wall.

The contribution of the remaining side groups (the hydroxyl, acetamido, and glycerol moieties) to inhibitor binding can not be assessed because their chemical structures were invariant in the inhibitor complexes examined in this study. This is not to imply that the nature of these side groups is not important. It has been shown that the substitution of different functional groups in the ring side chains can have very pronounced effects upon inhibition levels (Holzer *et al.*, 1993; von Itzstein *et al.*, 1993; Woods *et al.*, 1993).

Conclusions

In conclusion, our results indicate that the strong charge-charge group in NANA (α-sialic acid), and the arginine pocket of the active site is a dominant force in determining the inhibitor binding mode.

Table 6

Comparison of the inhibitor sugar ring dihedral angles (°) for different neuraminidase inhibitor complexes

Dihedral angle	B/Lee/40 NA-ePANA	B/Lee/40 NA-NANA	B/Lee/40 NA-DANA	N2 NA-aPANA
$C_{(2)}$-$C_{(3)}$-$C_{(4)}$-$C_{(5)}$† $C_{(1)}$-$C_{(2)}$-$C_{(3)}$-$C_{(5)}$	50.34	12.61	21.98	6.99
$C_{(3)}$-$C_{(4)}$-$C_{(5)}$-$C_{(6)}$ $C_{(2)}$-$C_{(3)}$-$C_{(4)}$-$C_{(5)}$	-51.27	-56.17	-38.31	-49.07
$C_{(4)}$-$C_{(5)}$-$C_{(6)}$-$O_{(6)}$ $C_{(3)}$-$C_{(4)}$-$C_{(5)}$-$O_{(5)}$	56.81	45.58	60.41	43.80
$C_{(5)}$-$C_{(6)}$-$O_{(6)}$-$C_{(2)}$ $C_{(4)}$-$C_{(5)}$-$O_{(5)}$-$C_{(1)}$	-68.55	12.37	-75.88	4.78
$C_{(6)}$-$O_{(6)}$-$C_{(2)}$-$C_{(3)}$ $C_{(5)}$-$O_{(5)}$-$C_{(1)}$-$C_{(2)}$	67.32	-57.15	55.48	-49.54
$O_{(6)}$-$C_{(2)}$-$C_{(3)}$-$C_{(4)}$ $O_{(5)}$-$C_{(1)}$-$C_{(2)}$-$C_{(3)}$	-54.82	39.52	-25.60	40.78

†NANA/DANA atom numbering followed by equivalent PANA atom numbering in parentheses.

We can also conclude that the ring conformation of the bound inhibitor is driven by the need to properly position the inhibitor acidic group and side-chain functional groups to conserve the NANA (substrate) active site interactions. In addition, the conformational flexibility of the inhibitor pyranosidic ring can severely affect tight binding by increasing the energy costs associated with transferring the inhibitor from solution to its NA-bound form and those inhibitors that have decreased degrees of ring freedom, like DANA, do display higher inhibition activities. A direct comparison of aPANA to NANA (α-sialic acid) is difficult, due to the anomerization of NANA and the low proportion of the α-anomer of NANA in solution. That aPANA is at all bound to NA, and acts as an inhibitor, is presumably the effect of the relatively easy conformational change of the pyranosyl ring containing an ionized phosphonoyl group, as compared to a carboxylate group, to adopt a equatorial orientation (Hirsch, 1967; Thiem *et al.*, 1978). The strong interaction of the phosphonoyl group with the arginine pocket in the active site should also favor the equatorial orientation. The inhibition by aPANA constitutes strong evidence for a similar conformation change in the binding to NA and hydrolysis of NANA α-glycosides. A direct comparison of ePANA to NANA is impractical given the change in ring conformation required for NA binding. The results of the NA-ePANA complex analysis do highlight the important role that the inhibitor acid group-arginine pocket charge-charge interaction plays in orientating and stabilizing the inhibitor in the NA active site.

Materials and Methods

Phosphonate inhibition and IC_{50} assays

The neuraminidase-inhibition test recommended by the World Health Organization was used to measure the neuraminidase inhibition activity of both the ePANA and aPANA (Aymard-Henry *et al.*, 1973). The ePANA IC_{50} values, which is the concentration of inhibitor that causes 50% inhibition, were determined using a standard fluorometric assay (Potier *et al.*, 1979). Using purified influenza virions as the neuraminidase source, dilutions of the inhibitor were incubated with 0.1mM 4-Me-umbelliferyl-*N*-acetylneuraminic acid as the substrate. The purified viruses used to measure the IC_{50} values were the type A N9 subtype (A/tern/Australia/G70c/75) and type B (B/Memphis/3/89) neuraminidase strains.

Crystallization and inhibitor soaking conditions

The native neuraminidase heads were released by proteolytic treatment of whole virus propagated in embryonic eggs and purified from the allantoic fluid. The native proteins were crystallized by the hanging drop method. The B/Lee/40 native protein was crystallized from 0.01 M Hepes buffer, pH 7.4, containing 2 M $NaNO_3$, 5 mM Ca^{2+}, and 15% (w/v) polyethylene glycol (PEG) 3350. The N2 neuraminidase native protein was crystallized from 0.1 M phosphate buffer, pH 7.2, containing 0.15 M NaCl and 12.5% (w/v) polyethylene glycol (PEG) 3350. The N9 native protein was crystallized from 1.7 M potassium phosphate buffer, pH 6.6.

Crystals of the B/Lee/40 NA-ePANA complex were prepared by soaking the native B/Lee/40 crystals in the native buffer solution containing 10 mM ePANA inhibitor for approximately one day. The N2 NA-ePANA complex crystals were prepared by soaking the native N2 crystals in the native N2 buffer solution containing 10 mM ePANA for approximately three days at room temperature. The N2 NA-aPANA complex crystals were prepared by soaking the native N2 crystals in the native N2 buffer containing 10 mM aPANA for approximately three days at room temperature. Finally, the N9 NA-ePANA complex crystals were prepared by soaking native N9 crystals in the native N9 buffer solution containing 10 mM ePANA for approximately three days at room temperature.

Data collection and processing

Data were collected on a Siemens area detector mounted on a Rigaku rotating anode generator operating at 100mA and 40kV at 22°C. Oscillation diffraction data were collected at a crystal-to-detector distance of 16.0 cm, a θ detector angle of 20°, an oscillation range of 0.25°, and an exposure period of 300 seconds per frame. Data indexing, reduction, scaling, and structure factor tabulation were accomplished using the XENGEN computer package (1987). From the data statistics, it is clear the N9 NA-ePANA and N2-aPANA data sets are not as high quality as the other two ePANA data sets. This may be due to crystal aging in the case of the N9 NA-ePANA data set and poor aPANA binding in the N2 NA-aPANA data set (Tables 7 and 8).

Table 7

Crystallographic parameters for neuraminidase PANA complexes

Data set	Space group	*a* (Å)	*b* (Å)	*c* (Å)
B/Lee/40 NA-ePANA	$P42_12$	124.73	124.73	71.88
N2 NA-ePANA	$C222_1$	120.42	139.83	140.07
N9 NA-ePANA	$I432$	184.86	184.86	184.86
N2 NA-aPANA	$C222_1$	122.08	141.67	141.87

Table 8

Data statistics for neuraminidase PANA complexes

Data set		∞-2.4Å			3.0 - 2.4Å		
	$d_{min.}$ (Å)	% Complete	Average redundancy	R_3	% Complete	Average redundancy	R_3
B/Lee/40 NA-ePANA	2.38	72.3	2.23	9.67	61.5	1.87	17.52
N2 NA-ePANA	2.38	74.1	1.87	8.01	67.2	1.58	16.16
N9 NA-ePANA	2.38	75.9	3.97	16.57	91.9	3.18	42.43
N2 NA-aPANA	2.42	76.0	1.45	7.38	66.8	1.27	40.41

R_3, unweighted absolute-value R-factor on intensity x 100 (XENGEN).

Structure determination and refinement

The native coordinates of B/Lee/40 neuraminidase were obtained from this laboratory (Janakiraman *et al.*, 1994). The refined coordinates of N9 neuraminidase were obtained from the Brookhaven protein data bank (Tulip *et al.*, 1991). The native coordinates of N2 NA in an unreported crystalline form ($C222_1$) were also obtained from this laboratory (Jedrzejas *et al.*, manuscript in preparation). Initial modeling of the inhibitors into the neuraminidase active site was accomplished using $F_{complex}$-$F_{native\ calculated}$ electron difference density maps calculated at 3.0 Å using native phases. In all the equatorial phosphonate complexes, the initial difference density clearly favored modeling of the inhibitor compound with its sugar ring in the chair conformation. The initial difference density for the axial phosphonate complex was also very defined and strongly favored the modeling of the axial compound with its sugar ring in the boat conformation. All modeling was performed using FRODO on an Evans and Sutherland ESV graphics workstation (Jones, 1985). X-PLOR topology and parameter files were constructed for both the equatorial and axial phosphonate compounds (Brunger, 1988, 1992). The sialic acid topology and parameter files found in the X-PLOR system library were used as the templates. The exact bond distances for the phosphonate group were determined using the Alchemy program and the calculated distances used in both phosphonate parameter files are C_2-P_1: 1.84 Å, P_1-O: 1.50 Å, P_1-OH_1: 1.53 Å, and OH_1-H: 0.98 Å. During X-PLOR refinement of the ePANA and aPANA NA complexes, the energy restraint terms for the C2 position were relaxed to allow for the potential distortion of the C2

geometry. Topology and parameter file terms that could not be measured were approximated from similar structures found in the X-PLOR library.

The refinement of the equatorial and axial phosphonate complexes was carried out using the X-PLOR simulated annealing protocol and slowcooling option from 3000 K to 300 K. Diffraction data in the 8.0 to 2.4Å resolution range with a 2σ cutoff on F_{obs} were used for the X-PLOR simulated annealing refinement. When alternating cycles of simulated annealing and $|2|F_{obs}|-|F_{calc}||$ map interpretation produced a model with a *R*-factor below 21%, structural water molecules were placed into the model using $|2|F_{obs}|-|F_{calc}||$ and $||F_{obs}|-|F_{calc}||$ maps contoured at 2σ. Initial water molecules whose position were not stable in further rounds of simulated annealing were deleted before the beginning the next round. Following the simulated annealing refinement, two rounds of *B*-factor/occupancy refinement and one final round of individual *B*-factor refinement were sufficient for convergence. Before each round of occupancy refinement, those atoms whose occupancy was greater than one were reset to one. After the second round of occupancy refinement, any water molecule that consistently had a very high or negligible occupancy was deleted from the model. After the last round of individual *B*-factor refinement, any water molecule that consistently had a *B*-factor greater than 70 $Å^2$ was deleted from the final model. In the N2 NA-ePANA and N2 NA-aPANA inhibitor complexes, only those water molecules that were conserved in both of the independently solved phosphonate complexes were retained in the final models (Tables 9 and 10). A similar lack of connecting density as that between the C4

Table 9

Refinement statistics (8.0-2.4 Å) for neuraminidase PANA complexes

	B/Lee/40 NA-ePANA	N2 NA-ePANA	N9 NA-ePANA	N2 NA-aPANA
Non-hydrogen waters	3040	3226	3257	3022
Defined water molecules	117	79	55	79
Protein $\langle B \rangle$ Å^2†	13.13	9.28	10.16	12.79
Calcium $\langle B \rangle$ Å^2	16.12	11.37	12.38	11.37
Inhibitor $\langle B \rangle$ Å^2	18.87	7.79	12.37	17.68
Water $\langle B \rangle$ Å^2	14.31	11.24	14.43	14.21
R-factor‡	0.154	0.179	0.187	0.206
Estimated coordinate error, Å§	0.22	0.28	0.31	0.40

†$\langle B \rangle$ = average *B*-factor.

‡*R*-factor = $R_{crystallographic} = \Sigma||F_o|-|F_c||/\Sigma|F_o|$.

§Estimated coordinate error, derived from Luzatti plot (R-factor *versus* resolution).

Table 10

Geometry r.m.s. differences (r.m.s.d.) from ideality for refined neuraminidase PANA complexes

Data Set	Bond r.m.s.d. (Å)	Angle r.m.s.d. (°)	Dihedral r.m.s.d. (°)	Improper r.m.s.d. (°)
B/Lee/40 NA-ePANA	0.012	1.77	26.9	1.45
N2 NA-ePANA	0.013	1.94	26.1	1.68
N9 NA-ePANA	0.018	2.11	25.5	1.62
N2 NA-aPANA	0.015	2.06	26.1	1.64

X-PLOR parameter set was used.

and C5 atoms in the N2 NA-aPANA $|2|F_{obs}|-|F_{calc}||$ map (Figure 3) has also been reported for other NA-inhibitor complexes (von Itzstein *et al.*, 1993) and may be the result of inhibitor ring flexibility at those positions. A Luzatti analysis of the four NA-PANA inhibitor complexes shows that all NA-ePANA complexes have an estimated coordinate error between 0.22-0.31 Å, while the N2 NA-aPANA complex shows a higher estimated coordinate error. This observation is consistent with the poor quality of the N2 NA-aPANA data when compared to the three NA-ePANA data sets. The structural data for the four NA-PANA complexes have been deposited into the Brookhaven Protein Data Bank (codes 1INU, 1INV, 1INW, and 1INX).

Acknowledgments

The authors would like to acknowledge A. Dean for expert technical assistance, L. Yang for figure assistance, and M. Jedrzejas for providing the coordinates of the type A N2 NA crystal structure ($C222_1$) and helpful discussions. This work was funded by the NIH grants AI31888 (M.L) and AI26718 (G.M.A).

References

Air, G. M. & Laver, W. G. (1989). The neuraminidase of influenza virus. *Proteins: Struct., Funct., and Genet.* **6**, 341-356.

Air, G. M., Laver, W. G., Luo, M., Stray, S. J., Legrone, G. & Webster, R. G. (1990). Antigenic, sequence, and crystal variation in influenza B neuraminidase. *Virology* **177**, 578-587.

Aymard-Henry, M., Coleman, M. T., Dowdle, W. R., Laver, W. G., Schild, G. C. & Webster, R. G. (1973). Influenza neuraminidase and

neuraminidase-inhibition test procedures. *Bull. WHO*, **48**, 199-202.

Blok, J., Air, G. M., Laver, W. G., Ward, C. W., Lilley, G. G., Woods, E. F., Roxburgh, C. M. & Inglis, A. S. (1982). Studies on the size, chemical composition, and partial sequence of the neuraminidase (NA) from type A influenza viruses show that the N-terminal region of the NA is not processed and serves to anchor the NA in the viral membrane. *Virology* **119**, 109-121.

Bossart-Whitaker, P., Carson, M., Babu, Y. S., Smith, C. D., Laver, W. G. & Air, G. (1993). Three-dimensional structure of influenza A N9 neu .minidase and its complex with the inhibitor 2-deoxy-2,3-dehydro-*N*-acetyl neuraminic acid. *J. Mol. Biol.* **232**, 1069-1083.

Brunger, A. T. (1988). Crystallographic refinement by simulated annealing: application to a 2.8Å resolution structure of aspartate aminotransferase. *J. Mol. Biol.* **203**, 803-816.

Brunger, A. T. (1992). *X-PLOR Version 3.1: A System for X-ray Crystallography and NMR*, Yale University Press, New Haven and London.

Burmeister, W. P., Ruigrok, R. W. H. & Cusack, S. (1992). The 2.2Å resolution crystal structure of influenza B neuraminidase and its complex to sialic acid. *EMBO J.* **11**(1), 49-56.Chong, A. K., Pegg, M. S. & von Itzstein, M. (1991). Characterization of an Ionisable Group Involved in Binding and Catalysis by Sialidase from Influenza Virus. *Biochemistry International* **24**(1), 165-171.

Chong, A. K., Pegg, M. S. & von Itzstein, M. (1991). Characterization of an ionisable group involved in binding and catalysis by sialidase from influenza virus. *Biochem. Int.* **24**(1), 165-171.

Chong, A., K.J., Pegg, M. S., Taylor, N. R. & von Itzstein, M. (1992). Evidence for a sialosyl cation transition-state complex in the reaction of sialidase from influenza virus. *Eur. J. Biochem.* **207**, 335-343.

Colman, P. M., Varghese, J. N. & Laver, W. G. (1983). Structure of the catalytic and antigenic sites in influenza virus neuraminidase. *Nature (London)*, **303**, 41-44.

Flashner, M., Kessler, J. & Tanenbaum, S. W. (1983). The interaction of substrate-related ketals with bacterial and viral neuraminidases. *Arch. Biochem. Biophys.* **221**(1), 188-196.

Gottschalk, A. (1957). Neuraminidase: The specific enzyme of influenza virus and *Vibrio cholerae*. *Biochim. Biophys. Acta* **23**, 645-646.

Gottschalk, A. (1959). The viruses. In *The Viruses* (Burnet, F. M. & Stanley, W. M., eds), vol. 3. pp. 51-61, Academic Press, New York.

Hirsch, J. A. (1967). Table of conformation energies. In *Topics in Stereochemistry* (Allinger, N. L. & Eliel, E. L., eds), vol.1, pp. 199-222, John Wiley & Sons, New York.

Hirst, G. K. (1941). The agglutination of red blood cells by allontoic fluid of chick embryos infected with influenza virus. *Science,* **94**, 22-23.

Holzer, C. T., von Itzstein, M., Jin, B., Pegg, M. S., Stewart, W. P. & Wu, W.-y. (1993). Inhibition of sialidases from viral, bacterial, and mammalian sources by analogues of 2-deoxy-2,3-didehydro-*N*-acetylneuraminic acid modified at the C-4 position. *Glycoconj. J.* **10**, 40-44.

Janakiraman, M. N., White, C. L., Laver, W. G., Air, G. M. & Luo, M. (1994). Structure of influenza virus neuraminidase B/Lee/40 complexed with sialic acid and a dehydro analog at 1.8Å resolution: Implications for the catalytic mechanism. *Biochemistry* , **33**, 8172-8179.

Jones, T. A. (1985). Interactive computer graphics: FRODO. *Methods. Enzymol.* **115**, 157-171.

Laver, W. G. (1978). Crystallization and peptide maps of neuraminidase "Heads" from H2N2 and H3N2 influenza virus strains. *Virology* , **86**, 78-87.

Lentz, M. R., Webster, R. G. & Air, G. M. (1987). Site-directed mutation of the active site of influenza neuraminidase and implications for the catalytic mechanism. *Biochemistry* , **26**, 5351-5358.

Liu, C. & Air, G. M. (1993). Selection and characterization of a neuraminidase-minus mutant of influenza virus and its rescue by cloned neuraminidase genes. *Virology* , **193**, 1-5.

Meindl, P., Bodo, G., Palese, P., Schulman, J. & Tuppy, H. (1974). Inhibition of neuraminidase activity by derivatives of 2-deoxy-2,3-dehydro-*N*-acetylneuraminic acid. *Virology* , **58**, 457-463.

Palese, P. & Schulman, J. L. (1974). Inhibition of influenza and parainfluenza virus replication in tissue culture by 2-deoxy-2,3-dehydro-*N*-trifluoroacetylneuraminic acid (FANA). *Virology*, **59**, 490-498.

Potier, M., Mameli, L., Belisle, M., Dallaire, L. & Melancon, S. B. (1979). Fluorometric assay of neuraminidase with a sodium (4-methylumbelliferyl-α-*D*-*N*-acetylneuraminate) substrate. *Anal. Biochem.* **94**(2), 287-296.

Taylor, N. R. & von Itzstein, M. (1994). Molecular modeling studies of ligand binding to sialidase from influenza virus and the mechanism of catalysis. *J. Med. Chem.* **37**, 616-624.

Thiem, J., Meyer, B. & Paulsen, H. (1978). Untersuchung der hydrierung ungesättigter glycosyl-phosphonate. Anomer effekt und A-wert der dimethylphopshono-gruppe. *Chem. Ber.* **111**, 3325-3335.

Tulip, W. R., Varghese, J. N., Baker, A. T., van Danelaar, A., Laver, W. G., Webster, R. G. & Colman, P. M. (1991). Refined atomic structures of N9 subtype influenza virus neuraminidase and escape mutants. *J. Mol. Biol.* **221**, 487-497.

Varghese, J. N. & Colman, P. M. (1991). Three-dimensional structure of the neuraminidase of influenza virus A/Tokyo/3/67 at 2.2 Å resolution. *J. Mol Biol.* **221**, 473-486.

Varghese, J. N., Laver, W. G. & Colman, P. M. (1983). Structure of the influenza virus glycoprotein antigen neuraminidase at 2.9 Å resolution. *Nature (London)*, **303**, 35-40.

Varghese, J. N., McKimm-Breschkin, J. L., Caldwell, J. B., Kortt, A. A. & Colman, P. M. (1992). The structure of the complex between

influenza virus neuraminidase and sialic acid, the viral receptor. *Proteins: Struct. Func. and Genet.* **14**, 327-332.

Vasella, A., Baudin, G. & Panza, L. (1991). Synthesis of glycosyl phosphonates and related compounds. *Heteroatom Chem.* **2**(1), 151-161.

Vasella, A. & Wyler, R. (1991). Synthesis of a phosphonic acid analog of *N*-acetyl-2,3-didehydro-2-deoxyneuraminic acid, an inhibitor of *Vibrio cholerae* sialidase. *Hel. Chim. Acta* **74**, 451-463.

von Itzstein, M., Wu, W.-Y., Kok, G. B., Pegg, M. S., Dyason, J. C., Jin, B., Van Phan, T., Symthe, M. L., White, H. F., Oliver, S. W., Colman, P. G., Varghese, J. N., Ryan, D. M., Woods, J. M., Bethell, R. C., Hotham, V. J., Cameron, J. M. & Penn, C. R. (1993). Rational design of potent sialidase-based inhibitors of influenza virus replication. *Nature (London)*, **363**, 418-423.

Wallimann, K. & Vasella, A. (1990). Phosphonic-acid analogs of the *N*-acetyl-2-deoxyneuraminic acids: Synthesis and inhibition of *Vibrio cholerae* sialidase. *Hel. Chim. Acta* **73**, 1359-1372.

Woods, J. M., Bethell, R. C., Coates, J. A. V., Healy, N., Hoscox, S. A., Pearson, B. A., Ryan, D. M., Ticehurst, J., Tilling, J., Walcott, S. M. & Penn, C. R. (1993). 4-Guanidino-2,4-dideoxy-2,3-didehydro-*N*-acetylneuraminic acid is a highly effective inhibitor both of the sialidase (neuraminidase) and of growth of a wide range of influenza A and B viruses *in Vitro*. *Antimicrob. Agents and Chemother.* **37**(7), 1473-1479.

XENGEN: A Guide to Macromolecular X-ray Data Reduction Using the XENGEN Package for Nicolet Area Detector Systems. (1987). Nicolet Instrument Co., Madison, WI.

MODELING POTENTIAL INHIBITORS OF BACTERIAL SIALIDASE

CLINTON L. WHITE[1,3] AND MING LUO[2,3,*]

[1]*Department of Biochemistry and Molecular Genetics,*
[2]*Department of Microbiology, and*
[3]*Center for Macromolecular Crystallography,*
University of Alabama at Birmingham,
Birmingham, Alabama 35294, USA

submitted to *Structure*

Keywords: sialidase, structure-based inhibitor design, trans-sialidase

---

*Corresponding Author

Abbreviations: Neu5Ac2en, 2-deoxy-2,3-dehydro-*N*-acetylneuraminic acid; 4-guanidino Neu5Ac2en, 2-deoxy-2,3-dehydro-4-guanidino-*N*-acetylneuraminic acid; HNBA, 4-acetylamino-3-hydroxyl-5-nitro-benzoic acid; GBA, 4-acetylamino-3-guanidino-benzoic acid; MUN, 4-methylumbelliferyl-α-*D*-*N*-acetylneuraminic acid; HBA, 4-acetylamino-3-hydroxyl-benzoic acid; ΔG_{el}, electrostatic contribution to the free energy change; E1, electrostatic energy of inhibitor-protein complex in the presence of protein charges and absence of inhibitor charges; E2, electrostatic energy of inhibitor-protein complex in the presence of inhibitor charges and absence of protein charges; E1, electrostatic energy of inhibitor-protein complex in the presence of both protein charges and inhibitor charges; DMSO, Dimethyl sulfoxide; ε_p, protein dielectric; ε_s, solvent dielectric.

Abstract

Background: Bacterial sialidases play an important role in bacterial host cell adhesion and have been implicated in pathogenicity. The trypanosomal trans-sialidase has been predicted to be quite similar to the bacterial sialidase and is required for human infection (Chagas' disease).

Results: Three new classes of bacterial sialidase specific inhibitors have been constructed using two benzoic acid-based lead compounds. The coordinates of 2-deoxy-2,3-dehydro-*N*-acetylneuraminic acid (Neu5Ac2en) complexed to the *Salmonella typhimurium* LT2 bacterial sialidase (Crennell *et al.*, 1994, *Proc. Nat. Acad. Sci USA 90*: 9852-9856) were used as a template for inhibitor binding. The program GRID was used to identify potentially useful binding sites. The new compounds were ranked using the free energy change of complex formation for the modeled inhibitor-bacterial sialidase complexes. The three classes of potential inhibitors (INSA class I, II, and III) are primarily targeted towards a hydrophobic pocket located near Trp 128 and a strong anionic pocket located between Asp 100 and Glu 231 in the bacterial sialidase active site.

Conclusion: Based on the calculated free energy changes of complex formation, several of the new INSA compounds are predicted to have substantially higher affinity for the bacterial sialidase as compared to the lead inhibitor compounds. Therefore, these compounds should be specific, high affinity inhibitors of bacterial sialidase and the related enzyme, trypanosomal trans-sialidase.

Introduction

Sialidases (i.e., neuraminidases, EC 3.2.1.18) have been isolated, purified, and characterized from several viral, bacterial, and mammalian sources [1-14]. Sialidases catalyze the cleavage of terminal sialic acid residues from sialoglycoconjugates. In the influenza virus, the virally encoded sialidase plays a critical role in releasing newly produced progeny virus particles from a host cell during infection [15]. The postulated biological role of the bacterial sialidase is to enhance adherence *in vivo* and provide an alternate carbon energy source for metabolism. A sialidase related enzyme, trans-sialidase, has been characterized in the organism *Trypanosome cruzi* and shares many sequence characteristics and structural motifs with bacterial sialidases [16-18]. The trypanosomal trans-sialidase transfers a terminal sialic acid moiety from a host donor sialoglycoconjugate to the Ssp-3 protein located on the trypanosomal surface. The trypanosomal trans-sialidase will also display hydrolase activity using water as an acceptor, but only in the absence of a suitable protein acceptor. The coating of the trypanosomal surface with sialic acid allows the parasite to escape recognition and destruction by the host's alternate complement pathway and may be required for host cell invasion, though the mechanism is still undefined [17, 19, 20].

Although all sialidases catalyze the same reaction, .i.e., hydrolysis of a terminal sialic acid, the enzymes can be divided into two classes based on their amino acid homology and the quaternary structure. The first class is comprised of the influenza virus

enzymes, and the second class represents the bacterial sialidases and trypanosomal trans-sialidase. The influenza virus sialidase is a tetramer composed of identical subunits (52 kDa). Each subunit contains six, four-stranded antiparallel β-sheets arranged as in a left-handed propeller. In both types A and B influenza virus strains, each subunit contains several intra-strand and intra-sheet disulfide bonds. In contrast, the bacterial sialidase (*S. typhimurium*) is a monomer (41 kDa), but it also shares the same β-propeller motif. The bacterial sialidase monomer also differs in that it contains only one disulfide bond.

Despite the similarity in tertiary structure, the viral and bacterial sialidases differ in their enzymatic activities [1, 21-33]. In general, the bacterial sialidases have a broader substrate specificity for α2→3, α2→6 or α2→8 linked sialic acids, though both the influenza virus and *S. typhimurium* sialidases prefer the α2→3 linked terminal sialic acids. The influenza sialidases bind two Ca^{2+} ions, one of which is required for activity. The bacterial *S. typhimurium* sialidase does not bind any metal ions and its activity is not dependent on metal ion concentration [7, 34]. In addition, the bacterial sialidases have a dramatically higher turnover number of ~2700 s^{-1} than that of the influenza virus sialidases (10 s^{-1}) [7].

The influenza virus sialidase has been targeted for the rational design of inhibitors, which may be potential anti-influenza drugs. Several classes of potential inhibitors have been developed through X-ray crystallographic analysis of the native and inhibitor-bound sialidase structures [35-41]. One of the influenza sialidase inhibitors, 2-deoxy-2,3-dehydro-4-guanidino-*N*-acetylneuraminic

acid (4-guanidino-Neu5Ac2en), has shown encouraging clinical results [42].

The recently reported crystal structure of the complex between the bacterial sialidase from Salmonella *typhimurium* LT2 and the inhibitor Neu5Ac2en now allows, for the first time, the development of specific inhibitors of bacterial sialidases and the related trypanosomal trans-sialidase using structure-based design [34]. Potent inhibitors of bacterial sialidase and trypanosomal trans-sialidase will have direct application to the clinical treatment of bacterial and trypanosomal infections in humans and feedstock. In many bacterial infections, the production of bacterial sialidases has been correlated with efficient colonization of the host infection site. Thus, bacterial sialidase inhibitors may decrease the magnitude of bacterial infection. Inhibitors of trypanosomal trans-sialidase should be an effective treatment for Chagas' disease and potentially African sleeping sickness, because the parasite requires the trans-sialidase activity for evasion of the alternative complement system and infection of new cells in human infections. They will also be useful in studying the basic mechanisms of metabolism, cell adherence, and immune system evasion present in these organisms [3, 19, 20, 43-55].

Using the coordinates of the *S. typhimurium* sialidase as a template for the bacterial family of homologous enzymes, we have employed a computational-intensive modeling protocol to design novel inhibitor compounds. Beginning with the two simple benzoic acid inhibitors, the program GRID was used to assist in identifying sites for the binding of new constituents in the bacterial sialidase

active site [56, 57]. The program DELPHI was used to assess the improvement of the modified compounds when modeled into the bacterial sialidase active site [58-60]. On the basis of their calculated free energy change upon complex formation, several of the proposed INSA series compounds are predicted to exhibit substantially higher affinity for the bacterial sialidase than the starting lead compounds.

Results

In vitro testing of benzoic acid inhibitors against bacterial sialidase

Aside from their moderate inhibition activity, carbohydrate-based inhibitors of sialidase, such as Neu5Ac2en, suffer as potential therapeutics due to the unfavorable economics and difficulty of manufacturing large scale amounts of the compounds for general use. The advantage of using benzoic acid based sialidase inhibitors is that they are chemically easier and cheaper to synthesize. In addition, there are numerous common synthetic routes available to selectively modify the benzene ring with different chemical functional groups. The substitution of a benzene ring for the sugar ring of Neu5Ac2en should not dramatically affect inhibition activity, because previous studies have shown that the sugar ring of the carbohydrate based inhibitors do not interact directly with the protein active site and only serve as a scaffolding to direct the placement of the inhibitor function groups [41]. The similar geometry and size of a benzene ring to the carbohydrate ring of Neu5Ac2en suggests that a benzene ring could also act as a scaffolding element for inhibitor functional groups and, therefore,

benzoic acid based compounds could inhibit sialidase activity. Recently, a series of benzoic acid derivatives have been synthesized and shown to inhibit influenza virus sialidase [40, 61].

Two benzoic acid derivatives, 4-acetylamino-3-hydroxyl-5-nitro-benzoic acid (HNBA) and 4-acetylamino-3-guanidino-benzoic acid (GBA), which are, respectively, millimolar and micromolar inhibitors of influenza virus sialidase, were tested for inhibition activity against bacterial sialidase (*Micromonospora viridifaciens*) using a fluorescence assay and the substrate 4-methylumbelliferyl-α-*D*-*N*-acetylneuraminic acid (MUN) [22, 62]. The *M. viridifaciens* sialidase amino acid sequence is highly homologous to the sialidases isolated from bacteria *Salmonella typhimurium* and *Clostridium perfringens* [7, 63]. Figure 1 shows the relative inhibition activity for the compounds HNBA and GBA versus Neu5Ac2en (bacterial sialidase $K_i \approx 10^{-6}$ M [26]) determined for *M. viridifaciens* bacterial sialidase. On the basis of the inhibition assay results, HNBA and GBA were selected as lead compounds for the construction of bacterial specific sialidase inhibitors.

Modeling and GRID analysis of inhibitor-bacterial sialidase complexes

The structure of a prototypical bacterial sialidase from *S. typhimurium* complexed with the inhibitor Neu5Ac2en by Crennell *et al.* was used to position the benzoic acid inhibitors HNBA and GBA into the bacterial sialidase active site (Figure 2).

To model the HNBA-bacterial sialidase complex, the C1, O3, and C5 atoms of HNBA were superimposed onto the C2, O4, C6 atoms of Neu5Ac2en using a least-squares approach. The superposition aligns

Figure 1. Inhibition activity of benzoic acid lead compounds. The percent inhibition of the compounds 4-acetylamino-3-hydroxyl-5-nitro-benzoic acid (HNBA), 4-acetylamino-3-guanidino-benzoic acid (GBA) and Neu5Ac2en against bacterial sialidase (*Micromonospora viridifaciens*) were determined using a fluorescence assay and the substrate 4-methylumbelliferyl-α-*D*-*N*-acetylneuraminic acid (MUN) [22, 40, 62]. The inhibition activity of Neu5Ac2en was standardized against the water control, which contains no Neu5Ac2en. Due to the requirement that the benzoic acid compounds be dissolved into dimethyl sulfoxide (DMSO), the inhibition activity of the benzoic acid compounds were standardized against a DMSO control, which contains only DMSO and no benzoic acid inhibitors. Both of the benzoic acid compounds show inhibition activity comparable to Neu5Ac2en, which has an approximate K_i equal to 1 $x10^{-6}$ M for other bacterial sialidases [26, 34]. The structures of the benzoic acid based compounds and the inhibitor Neu5Ac2en are shown above the graph.

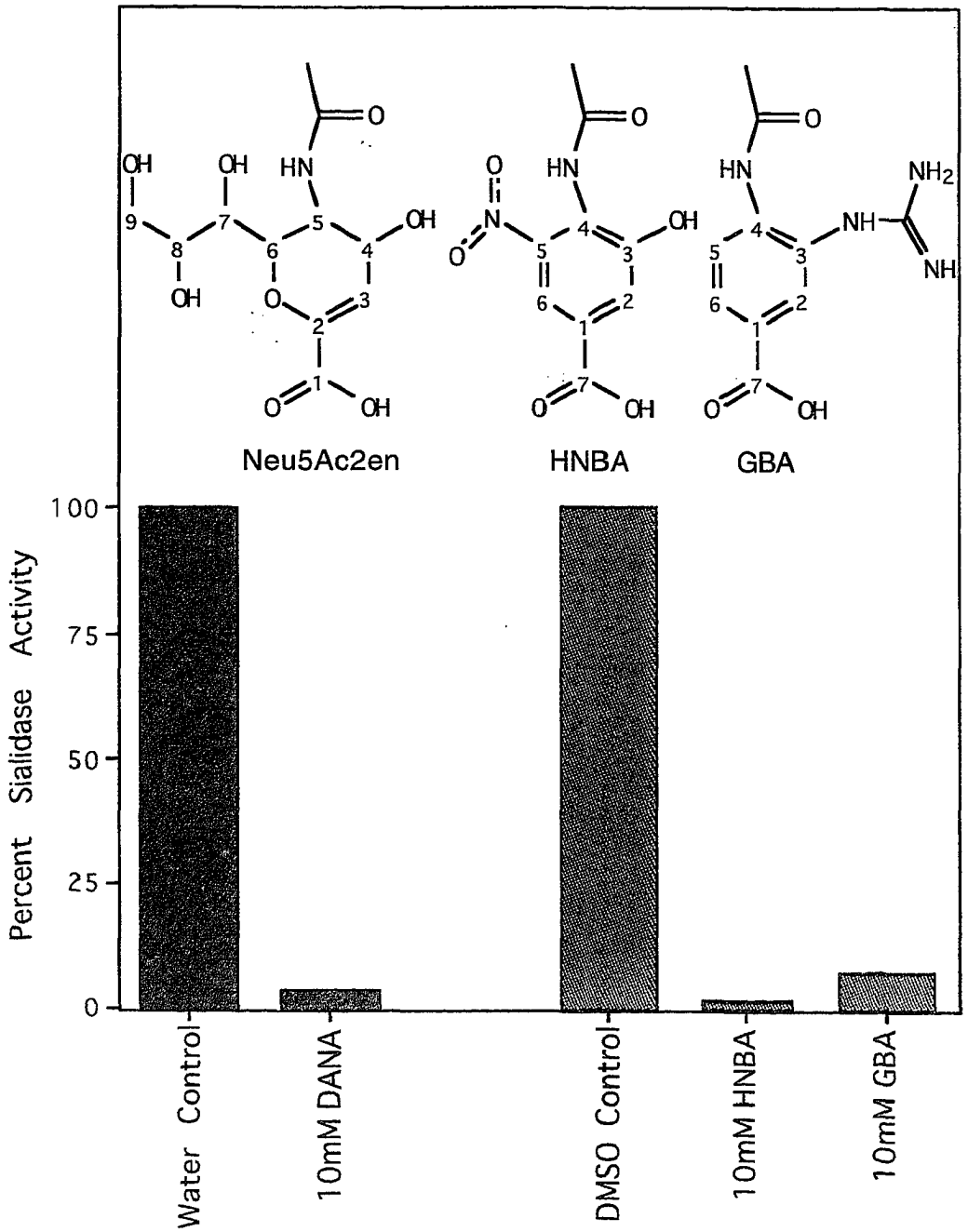

Figure 2. Stereoview of the modeled benzoic acid-bacterial sialidase complexes. (a) Structure of the energy minimized **HNBA**-bacterial sialidase. Prior to energy minimization, the 4-acetylamino-3-hydroxyl-5-nitro-benzoic acid (HNBA) C1, O3, and C5 atoms were least squares superimposed onto the position of the *Salmonella typhimurium* complexed Neu5Ac2en C2, O4, and C6 atoms to preserve the carboxylate, hydroxyl and acetylamino group orientation in the bacterial sialidase active site. (b) Structure of the energy minimized **GBA**-bacterial sialidase complex. The 4-acetylamino-3-guanidino-benzoic acid (GBA) C1, N3, and C5 atoms were initially least squares superimposed onto the position of the *S. typhimurium* complexed Neu5Ac2en C2, C7, and C4 atoms to preserve the carboxylate, acetylamino orientation in the bacterial sialidase active site, while aligning the benzoic acid guanidino group to the Neu5Ac2en glycerol group, but the **N3**$^+$ GRID map results suggest that the GBA guanidino sidechain should be placed into the **N3**$^+$ binding site **A**. Energy minimization of the GBA-bacterial sialidase complex resulted in the GBA ring tilting toward site **A**, which allows the guanidino sidechain to reach deeper into the **N3**$^+$ binding site. Atoms are colored according to the atom type: carbon, green; nitrogen, blue; oxygen, red; sulfur, yellow; and water molecule oxygens, orange. This figure was generated using the program MOLSCRIPT [65].

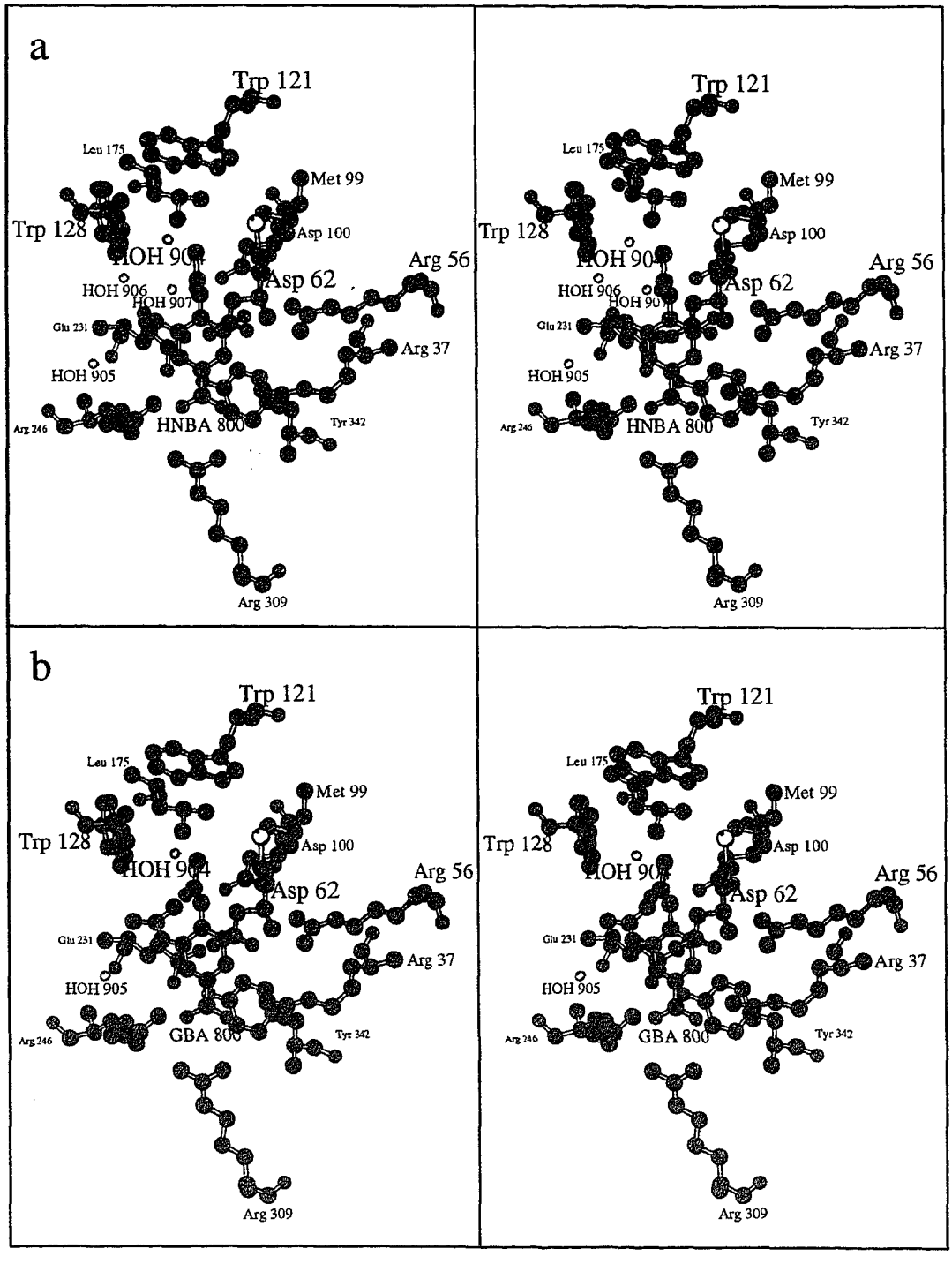

the C1 carboxylate, C3 hydroxyl, and C4 acetylamino groups of HNBA with the C2 carboxylate, O4 hydroxyl, and C5 acetylamino groups of Neu5Ac2en and preserves the important interactions of these groups with the bacterial sialidase active site residues in the HNBA-bacterial sialidase modeled complex.

The GBA-bacterial sialidase complex was modeled by a least-squares superposition of the C1, N3, and C5 atoms of GBA onto the C2, C7, and C4 atoms of Neu5Ac2en. The superposition aligns the GBA guanidinium group to the Neu5Ac2en glycerol group in the bacterial sialidase active site. This orientation corresponds to the binding mode observed in the GBA influenza virus type A N2 sialidase complex [40]. Following the initial least squares superposition, the guanidinium sidegroup of GBA was manually rotated into the **N3+** binding site **A** identified in the GRID map analysis (see below) on a graphics display using the program FRODO [64].

All of the water molecules identified in the Neu5Ac2en-bacterial sialidase crystal structure were included in the HNBA-bacterial sialidase model. The criteria for retaining the waters in the HNBA-bacterial sialidase complex was that none of the water molecules were sterically excluded by the presence of the HNBA inhibitor and all of the water molecules possessed potential hydrogen bonding partners. In the GBA-bacterial sialidase, two of the water molecules in the Neu5Ac2en-bacterial complex, HOH 906 and HOH 907, were excluded due to steric overlap with the GBA guanidino group.

The HNBA and GBA bacterial sialidase complexes were energy minimized using a conjugate gradient protocol within the program X-

PLOR to relieve steric conflicts that may have resulted from the Neu5Ac2en superposition. A harmonic constraint of 500 kcal/mol was placed on atoms more than 10 Å distant from the benzoic acid compound, while those atoms within a 10 Å radius of the benzoic acid compound had no harmonic constraints. The active site geometry in the energy minimized benzoic acid-bacterial sialidase complexes was almost identical to that observed in the energy minimized Neu5Ac2en-bacterial sialidase complex. Energy minimization of the HNBA-bacterial sialidase complex did not significantly alter the orientation of HNBA in the bacterial sialidase active site. Surprisingly, energy minimization of the GBA-bacterial sialidase complex changed the orientation of GBA in the bacterial sialidase active site when compared to the starting position (Neu5Ac2en least-squares superposition). In the energy minimized GBA-bacterial sialidase complex, the benzene ring of GBA is rotated ~20° around the inhibitor carboxylate-acetylamino axis. The rotation places the GBA guanidino group closer to the **N3**$^{+}$ binding site and tilts the benzene ring C5 and C6 atoms away from the active site floor. Despite the tilt in the GBA benzene ring, no change in orientation was observed for the GBA carboxylate and *N*-acetylamino groups in the energy minimized GBA-bacterial sialidase complex when compared to the energy minimized HNBA-bacterial sialidase complex. In addition, the active site residues in both of the energy minimized benzoic acid-bacterial sialidase complexes adopt conformations, which are analogous to the active site residues of the energy minimized Neu5Ac2en-bacterial sialidase. The root-mean-square (r.m.s.) deviation for sialidase atoms within the 10 Å

radius between the energy minimized Neu5Ac2en and HNBA-bacterial sialidase complexes is 0.05 Å, and between the minimized Neu5Ac2en and GBA-bacterial sialidase complexes, 0.07 Å.

GRID maps were calculated to identify favorable probe binding sites in the *S. typhimurium* bacterial sialidase active site for the purpose of improving the activity of the lead compounds. GRID determines the interaction energy between a given probe and a protein target site as the probe is placed at each point within a three-dimensional lattice centered at the target site [56]. By displaying GRID maps contoured at specific interaction energies on a graphics system, potential binding sites for the selected probes can be identified. Probe functionalities, which display favorable interaction energies, can then be incorporated into the lead compound to create new ligands with potentially higher affinities for the target site [57].

The GRID calculations were performed using the HNBA-bacterial sialidase complex modified by the deletion of the C5 nitro group coordinates (i.e., 4-acetylamino-3-hydroxyl-benzoic acid = HBA). Removal of the C5 nitro group allows a larger region of the active site to be included in the GRID search. Two sets of GRID maps were calculated using the coordinates of the HBA-bacterial sialidase complex: (1) either in the presence of waters or (2) in the total absence of waters. Five probe types were selected for the GRID calculations: (1) **C3** ($-CH_3$), a hydrophobic probe; (2) **N3+** (NH_3^+), a cationic probe; (3) F^-, an anionic probe; (4) **O::** (carboxylate C=O), a polar hydrogen bond donor probe; and (5) **OH2** (water), a hydrogen bond donor/acceptor probe. No changes were made to the chemical

default parameters for each probe type. The lattice used in our GRID calculations was defined as a box with edges roughly 10 Å greater than the maximum dimensions of HNBA in the HNBA-bacterial sialidase complex. The GRID box size results in a GRID search step size of 0.126 Å along the x-axis, 0.117 Å along the y-axis, and 0.141 Å along the z-axis.

In the present study, an internal calibration of favorable interaction energy levels was provided by the **OH2** GRID map calculated for the HBA-bacterial sialidase complex model without waters. In this GRID map, the binding sites of several water molecules observed in the active site of the Neu5Ac2en-bacterial sialidase crystal structure were successfully predicted by the **OH2** probe. Therefore, probe binding sites were considered significant if they had an interaction energy less than the average interaction energy exhibited by the crystallographic water molecules, i.e., energies less than approximately -5 kcal/mol.

For the first set of GRID calculations, which used the HBA-bacterial sialidase coordinates in the absence of water molecules, only the **N3**$^{+}$ and **OH2** probes produced maps that contained highly favorable probe binding sites in the active site. The GRID maps generated using the **F**$^{-}$ and **O**:: probes did not produce any significant probe binding sites in the active site region. The **C3** GRID map gave a good indication of the accessible volume, which preferred van der Waals interactions. These **C3** sites had high interaction energies (greater than -2 kcal/mol) and were reproducible to a large extent with the remaining probe types. The hydrophobic binding pocket near Trp 128, which accommodates the hydrophobic C9 methyl group of

Neu5Ac2en, was the most prominent site defined by the **C3** probe. Binding sites for the **C3** probe were also found in the active site pocket responsible for binding the Neu5Ac2en glycerol group.

The major feature of the **N3+** GRID map, calculated using the HBA-bacterial sialidase complex in the absence of the water molecules, was binding site **A**, which overlapped the HOH 906 and HOH 907 binding sites (Figure 3). This binding site favors a positive charge due to the presence of the neighboring acidic residues Asp 100 and Glu 231. Of all the GRID maps calculated using the five probe types, this site in the **N3+** map had the most significant interaction energy (-29 kcal/mol).

The **OH2** GRID map, calculated using the HBA-bacterial sialidase complex coordinates in the absence of the water molecules, predicted several areas within the active site that should favor hydrogen bonding (Figure 3). The first favorable binding site for a water probe is site **A**, which is also the highly favorable **N3+** probe binding site. The second water probe binding site is **B**, which slightly overlaps site **A**. Sites **A** and **B** roughly correspond to the binding sites of HOH 906 and HOH 907 and both sites have a maximum water probe interaction energy of approximately -7.5 kcal/mol. A third favorable site for **OH2** binding in the glycerol active site pocket is site **C**. Site **C** does not correspond to any crystallographic water binding site and has a maximum interaction energy of approximately -9 kcal/mol. Finally, using the **OH2** probe, the three discrete binding sites **D**, **E** and **F** were observed, which form a long hydration channel in the active site. Binding site **D** corresponds to the position of HOH 904 and has a maximum

Figure 3. GRID maps generated by **N3+** and **OH2** probes. Interaction energy contour maps were calculated using the program GRID, the **N3+** ($-NH_3^+$) and **OH2** (water) probes, and the coordinates of the HBA-bacterial sialidase complex in the absence of water molecules. The yellow density is the **N3+** probe GRID map contoured at -18 kcal/mol. The blue density is the **OH2** probe GRID map contoured at -5 kcal/mol. The *Salmonella typhimurium* bacterial sialidase active site residues are colored red and the HBA coordinates are colored green. The prominent probe binding sites have been labeled. Site **A** is a very favorable **N3+** binding site located near water molecules HOH 906 and HOH 907. Site **B** is a **OH2** binding site located near water molecule HOH 905. Site **C** is another **OH2** binding site in the glycerol pocket, but it does not contain any water molecule binding sites. Sites **D**, **E**, and **F** are **OH2** binding sites, which form a curve hydration channel leading away from the active site. Site **D** includes the binding site of the water molecule HOH 904, while sites **E** and **F** do not contain any crystallographic water binding sites.

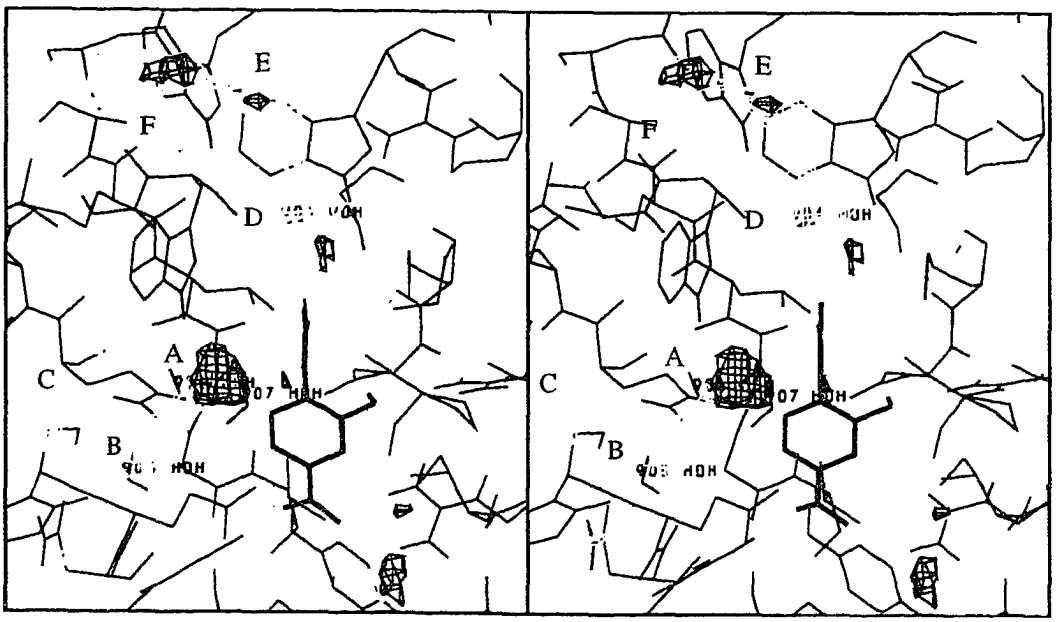

interaction energy of -9 kcal/mol. The more distal binding sites **E** and **F** have maximum interaction energies of -10 and -9 kcal/mol and do not contain any crystallographically determined water binding sites.

The coordinates of the HBA-bacterial sialidase complex in the presence of the water molecules were used to calculate the second set of GRID maps utilizing the **C3, N3+, F-, O::**, and **OH2** probe types. No new probe binding sites in the sialidase active site were identified for the second set of GRID maps, which were not present in the first set of GRID maps calculated in the absence of water residues.

Construction of new inhibitors specific for bacterial sialidase

A new series of novel compounds (INSA series) were composed which take advantage of the favorable binding sites predicted from the GRID map analysis, while still retaining the favorable inhibitor-protein interactions of the C1 carboxylate, C3 hydroxyl and C4 acetylamino groups. Using the HBA-bacterial sialidase coordinates as a template, the new compounds were constructed on a graphics display running the program FRODO. Three classes of novel, potential bacterial-sialidase inhibitors were composed and designated as INSA classes I, II, and III.

The class I compounds (INSA I-1, I-2, I-3, and I-4) were constructed to fill the mostly hydrophobic pocket formed by Trp 121, Trp 128 and Leu 175 (Figure 4a). Because of the lack of strong hydrogen bonds to the benzoic acid O8 atom, it was deemed feasible to cyclize the acetyl group into either a furan ring (compounds I-1, I-

Figure 4. Structure of the INSA classes I, II, and III compounds. (a) The INSA class I compounds constructed to fill the active site hydrophobic pocket formed by Trp 121, Trp 128 and Leu 175. Compound I-4 also places a hydroxyl group in the **OH2** binding site **D**. (b) The INSA class II compounds, which contain an amino sidegroup to fill the **N3+** binding site **A** and hydroxyl sidegroups to fill the **OH2** binding sites **B**. (c) The INSA class III compounds, which also contain a amino sidegroup to fill the **N3+** binding site **A** and hydroxyl sidegroups to fill the **OH2** binding site **B**.

a)

INSA Class I

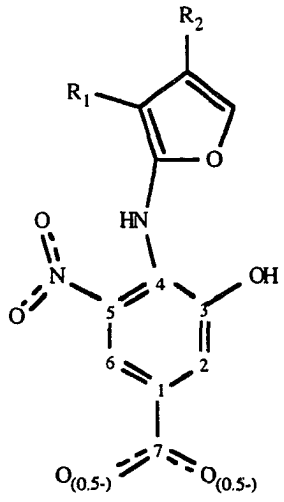

I-1: R1=H, R2=H
I-2: R1=CH3, R2=H
I-3: R1=H, R2=CH3

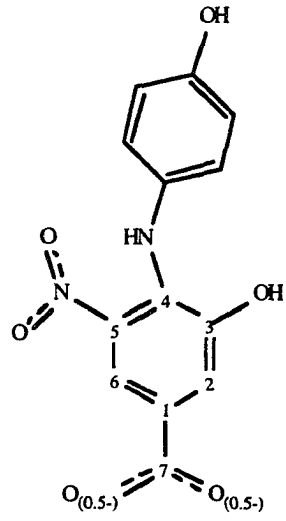

I-4

b)

INSA Class II

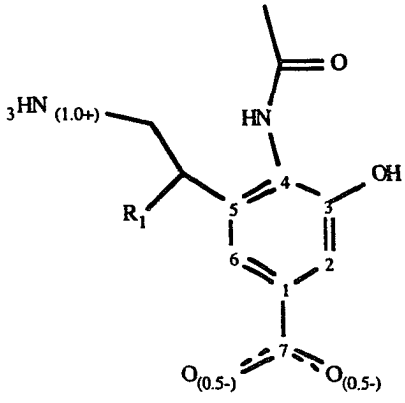

II-1: R1=OH
II-2: R1=CH2OH
II-3: R1=CH2OHCH2OH

c)

INSA Class III

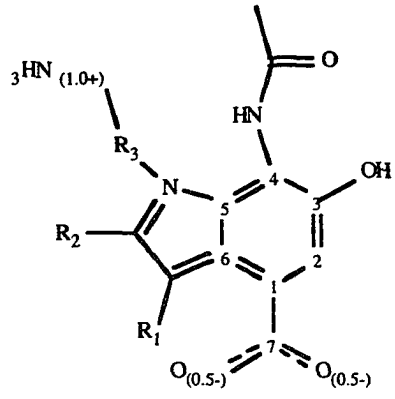

III-1: R1=OH, R2=OH, R3=CH2
III-2: R1=H, R2=OH, R3=CH2
III-3: R1=H, R2=CH2(CH2OH)2, R3=CH2
III-4: R1=H, R2=C(CH2OH)3, R3=CH2
III-5: R1=H, R2=OH, R3=CH2CH2

2, and I-3) or benzene ring (I-4). In the compounds I-1, I-2, and I-3, the furanyl ring has a suitable size to fill the hydrophobic pocket and should pack favorably against the Trp 128 indole ring. To completely fill the hydrophobic pocket, methyl groups were added to the furanyl ring of compounds I-2 and I-3. The C9 and the C10 position in compounds I-2 or I-3 were equally favored for methyl group addition.

The *N*-phenylamino group present in the I-4 compound has two favorable qualities. First, the *N*-acetyl benzene ring of I-4, analogous to the other class I compounds, is good hydrophobic moiety and should fill the hydrophobic pocket formed by Trp 121, Trp 128, and Leu 175. Second, use of a *N*-acetyl benzene ring allows the placement of a hydroxyl group into site **D**, the favorable **OH2** binding site determined from the GRID calculations. Because the **OH2** interaction energy for site **D** is significant, the addition of a phenol hydroxyl group in site **D** should substantially contribute to the binding energy of compound I-4. The placement of a suitable hydrogen bond donor/acceptor moiety in pocket **D** in the INSA I-1, I-2, and I-3 compounds is not possible due to the geometry of the furan ring.

The class II compounds (INSA II-1, II-2, and II-3) were built to take advantage of site **A**, the very favorable **N3+** probe binding site (Figure 4b). The ethylamino sidechains of the class II compounds were modeled into the **N3+** pocket where they should make strong electrostatic interactions with the neighboring acidic sidegroups. The R_1 groups in the class II series were included to increase the

potential interaction energy of the inhibitors by placing hydrogen bonding moieties in pocket **B**, a favorable **OH2** probe binding site.

The class III compounds (INSA III-1, III-2, III-3, III-4, and III-5) were also constructed to reach site **A**, the very favorable **N3+** binding site (Figure 4c). The indole ring system in the class III compounds should provide a rigid scaffolding for extending amino sidegroups into site **A**, as well as hydrogen bonding groups into site **B** and possibly site **C**. The inclusion of a rigid ring system in the class III compounds should lower the entropic cost for inhibitor binding associated reducing conformational degrees of freedom in the bound inhibitor.

Each INSA compound was built using the program QUANTA and modeled into the *S. typhimurium* sialidase active site in a manner similar to HNBA [66]. Water molecules present in the Neu5Ac2en-bacterial sialidase complex were included in each modeled INSA-bacterial sialidase complex if they were not sterically excluded by the INSA compound.

DELPHI calculation of free energy change upon complex formation for the modeled INSA-bacterial sialidase complexes

The ability to determine the relative binding affinity of a newly designed compound, or series of compounds, without having to wait on costly and lengthy synthesis, is of utmost value. Several methods have been developed to predict binding affinities, both qualitatively and quantitatively, for modeled inhibitor-protein complexes [67-70]. The program DELPHI has been developed to calculate the electrostatic potential of macromolecular systems using a finite difference solution to the non-linear Poisson-Boltzmann equation

[59]. For a given macromolecular inhibitor-protein complex, DELPHI can be used to calculate the total electrostatic energy of the system [58, 59, 71]. For the modeled INSA-bacterial sialidase complexes, the electrostatic contribution to the free energy change upon complex formation, ΔG_{el}, can be derived from the total electrostatic energies of three inhibitor complexes: E_1, the electrostatic energy of the complex when charges are present only on the protein residues; E_2, the electrostatic energy of the complex when charges are present only on the inhibitor residues; and E_3, the electrostatic energy of the complex when charges are present on both the protein and inhibitor residues (Figure 5). The free energy change resulting from electrostatic interactions is therefore equal to $E_1 - (E_2 + E_3)$. Because the binding of inhibitors to the bacterial active site is dominated by electrostatic interactions and due the inherent complexity of hydrophobic interactions, the contribution of the hydrophobic effect was not explicitly included in the DELPHI calculation. However, the contribution of the hydrophobic effect to the free energy of complex formation for compounds within a single INSA class, which have a similar functional groups and chemical properties, should be roughly on the same order of magnitude. Therefore, exclusion of the hydrophobic contribution to the calculated free energy of complex formation should not change the relative ranking of a series of compounds within a single class.

For each of the modeled INSA-bacterial sialidase complexes, the electrostatic contribution to the change in free energy of complex formation was calculated using a protein/inhibitor dielectric constant of 4, a solvent dielectric constant of 80, an ionic strength

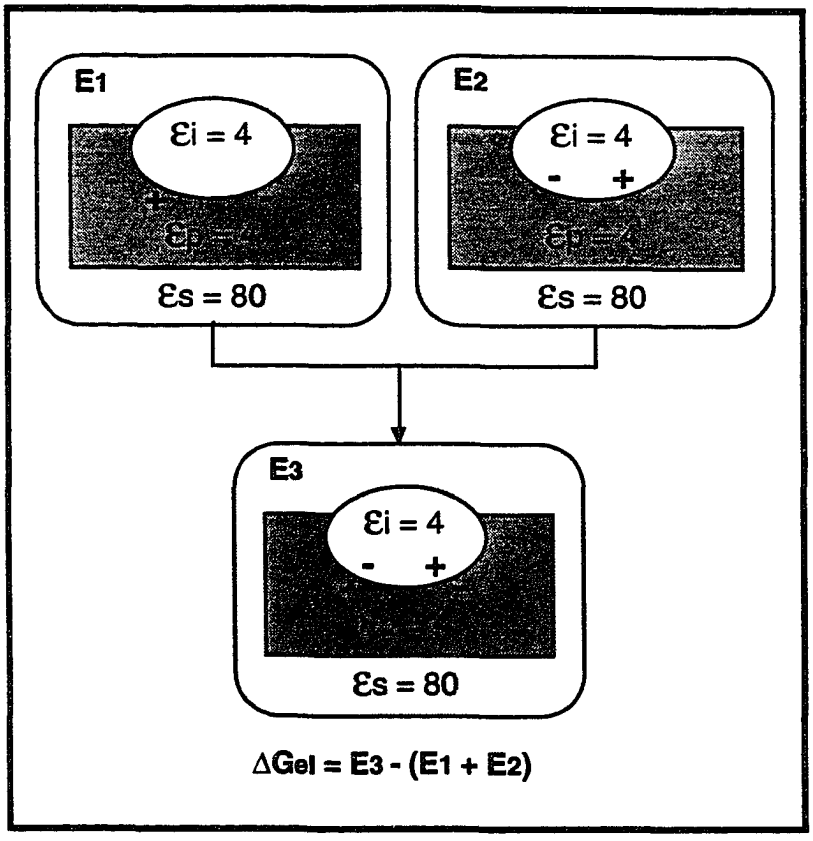

Figure 5. DELPHI free energy of complex formation protocol. The electrostatic contribution to the change in free energy upon complex formation as determined by DELPHI program [60]. The change in free energy of complex formation, ΔG_{el}, is derived from calculating total electrostatic energies of three inhibitor complexes: E_1, the energy of the complex when charges are present only on the protein residues; E_2, the energy of the complex when charges are present only on the inhibitor residues; and E_3, the energy of the complex when charges are present on both the protein and inhibitor residues. Therefore, $\Delta G_{el} = E_3 - (E_1 + E_2)$.

of 0.145 M, and a focusing protocol of 30→90% fill. Table 1 presents the calculated free energies of complex formation for the proposed INSA-bacterial sialidase complexes, as well as the calculated free energies of complex formation for the benzoic acid-bacterial sialidase complexes. The compounds have been ranked in Table 1 within each separate class according to their $\Delta(\Delta G)$ values. The $\Delta(\Delta G)$ values are defined as the ΔG_{el} of a particular INSA-bacterial sialidase complex minus the ΔG_{el} of the HNBA-bacterial sialidase complex, which is the starting lead compound. A positive $\Delta(\Delta G)$ indicates that the predicted INSA-bacterial sialidase complex is energetically less favorable than the starting HNBA-bacterial sialidase complex. Conversely, a negative $\Delta(\Delta G)$ indicates that the predicted INSA-bacterial sialidase complex is energetically more favorable than the starting HNBA-bacterial sialidase complex and, therefore, that INSA compound should exhibit a higher binding affinity for the bacterial sialidase active site.

Discussion

Comparison of influenza virus and bacterial sialidase active sites

As in the influenza virus sialidases, the bacterial sialidase active site from *S. typhimurium* also contains an arginine triad (Arg 37, Arg 246, and Arg 309), which binds the carboxylate moiety of sialic acid; a hydrophobic pocket, which accommodates the methyl group of the substrate *N*-acetylamino moiety; and a tyrosine residue (Tyr 342) located beneath the substrate pocket (Figure 6). Though functionally similar, the residues that compose the hydrophobic pocket differ between the bacterial and viral active sites. The

Table 1. DELPHI electrostatic energies of complex formation for HNBA, GBA, and the INSA series of inhibitors when complexed to bacterial sialidase from *Salmonella typhimurium*. Compounds have been ranked within structural classes according to their calculated $\Delta(\Delta G)$ values†.

Data Set	E_1 (kT)	E_2 (kT)	E_3 (kT)	ΔG_{el} (kT)	ΔG_{el} (kcal/mol)	$\Delta(\Delta G)$ (kcal/mol)
HNBA	29438.42	107.24	29514.95	-30.71	-18.21	0.00
GBA	29341.89	99.49	29388.96	-52.42	-31.09	-12.87
INSA I-2	29393.17	104.17	29473.08	-24.26	-14.39	3.82
INSA I-3	29379.15	106.03	29455.7	-29.48	-17.48	0.73
INSA I-1	29370.14	96.82	29436.5	-30.46	-18.06	0.15
INSA I-4	29362.41	111.02	29441.14	-32.29	-19.15	-0.94
INSA II-2	29400.59	117.71	29463.3	-55.00	-32.62	-14.40
INSA II-1	29373.78	125.47	29442.27	-56.98	-33.79	-15.58
INSA II-3	29322.68	129.49	29393.28	-58.89	-34.92	-16.71
INSA III-4	29266.96	123.37	29353.29	-37.04	-21.96	-3.75
INSA III-1	29337.47	119.73	29416.36	-40.84	-24.22	-6.01
INSA III-2	29349.77	121.58	29427.53	-43.82	-25.99	-7.77
INSA III-3	29303.24	138.17	29392.56	-48.85	-28.97	-10.76
INSA III-5	29391.85	126.96	29462.2	-56.61	-33.57	-15.36

†$\Delta(\Delta G) = \Delta G_{el}(i) - \Delta G_{el}(\text{HNBA})$, where i is any inhibitor. A negative $\Delta(\Delta G)$ values indicates that the selected compound is predicted to have a higher binding affinity for bacterial sialidase as compared to the HNBA compound.

Figure 6. Stereoview of modeled INSA-bacterial sialidase complexes. One representative compound from each of the proposed series of INSA inhibitors is shown modeled into the *Salmonella typhimurium* bacterial sialidase active site. The INSA class I series is represented by compound I-4, the INSA class II series is represented by compound II-1, and the INSA class III series is represented by compound III-5. Based on the free energy calculations, each of the representative compounds were predicted to show increase binding affinity for bacterial sialidase For comparison purposes, the Neu5Ac2en-*Salmonella typhimurium* bacterial sialidase complex has also been included [34]. Atoms are colored according to the atom type: carbon, green; nitrogen, blue; oxygen, red; sulfur, yellow; and water molecule oxygens, orange. This figure was generated using the program MOLSCRIPT [65]. (a) Neu5Ac2en complexed to *S. typhimurium* sialidase. The significant features of the active site are the arginine triad (Arg 37, Arg 246, Arg 307), which binds the Neu5Ac2en carboxylate group; the charged residues (Arg 56 and Asp 100), which form a hydrogen bonding network with the Neu5Ac2en O4 hydroxyl; the hydrophobic pocket (Met 99, Trp 121, Trp 128, and Leu 175), which binds the Neu5Ac2en C9 methyl group; and the wide pocket, which binds the Neu5Ac2en glycerol group. The structurally defined water molecules located in the active site are HOH 904, HOH 905, HOH 906, and HOH 907. (b) INSA I-4 complexed to *S. typhimurium* bacterial sialidase. This compound contains a phenol moiety, which favors binding in the active site hydrophobic pocket and excludes the presence of HOH 904. (c) INSA II-1 complexed to *S. typhimurium* bacterial sialidase. This compound contains a ethylamino sidegroup, which favors binding in the NH3+ binding site **A** and therefore sterically prohibits the modeling of HOH 906 and HOH 907. (d) INSA III-5 complexed to *S. typhimurium* bacterial sialidase. This indole ring-based compound also contains an amino sidegroup in the NH3+ binding site **A**. Hence, HOH 906 and HOH 907 have not been included in the modeled complex.

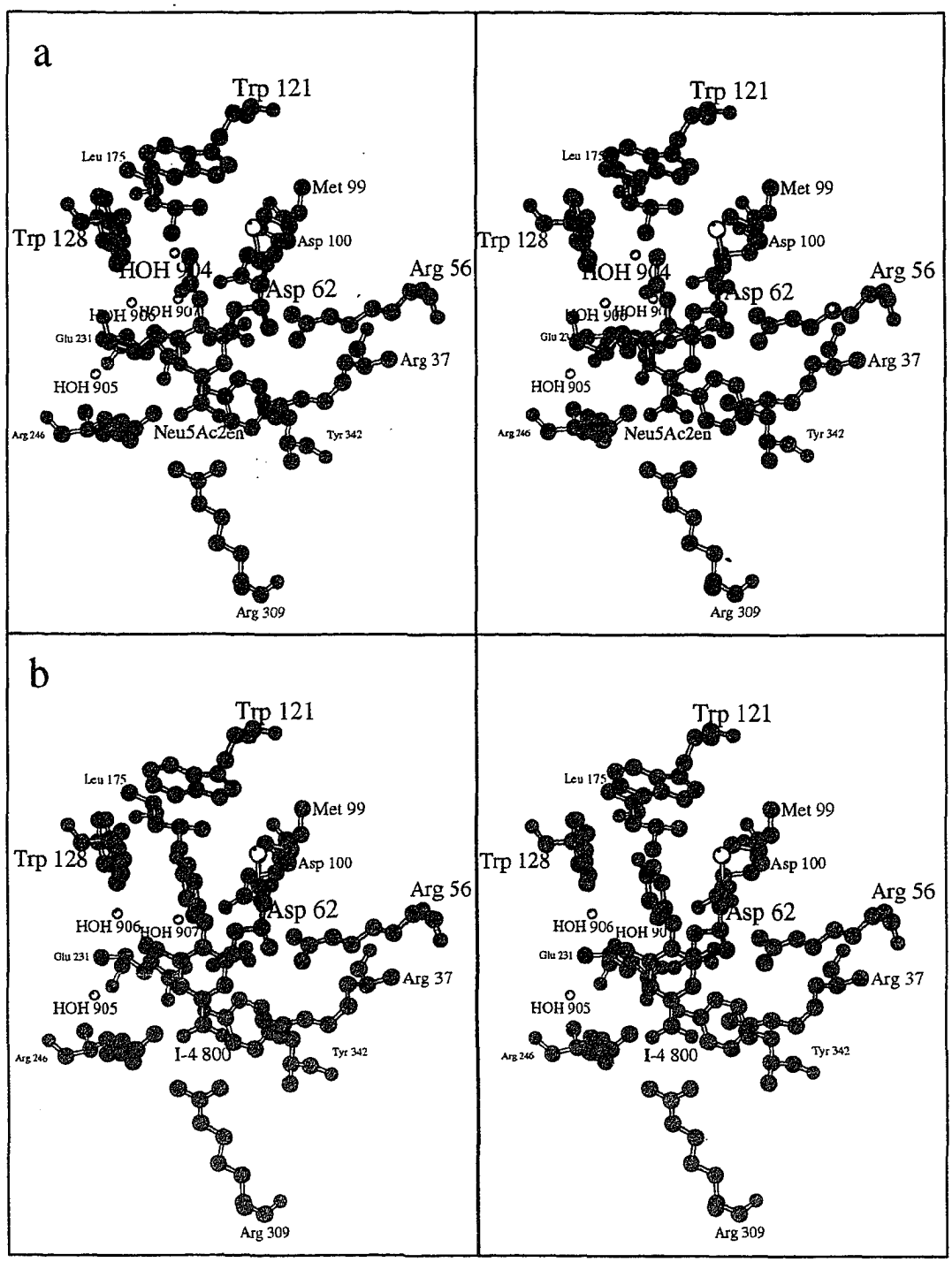

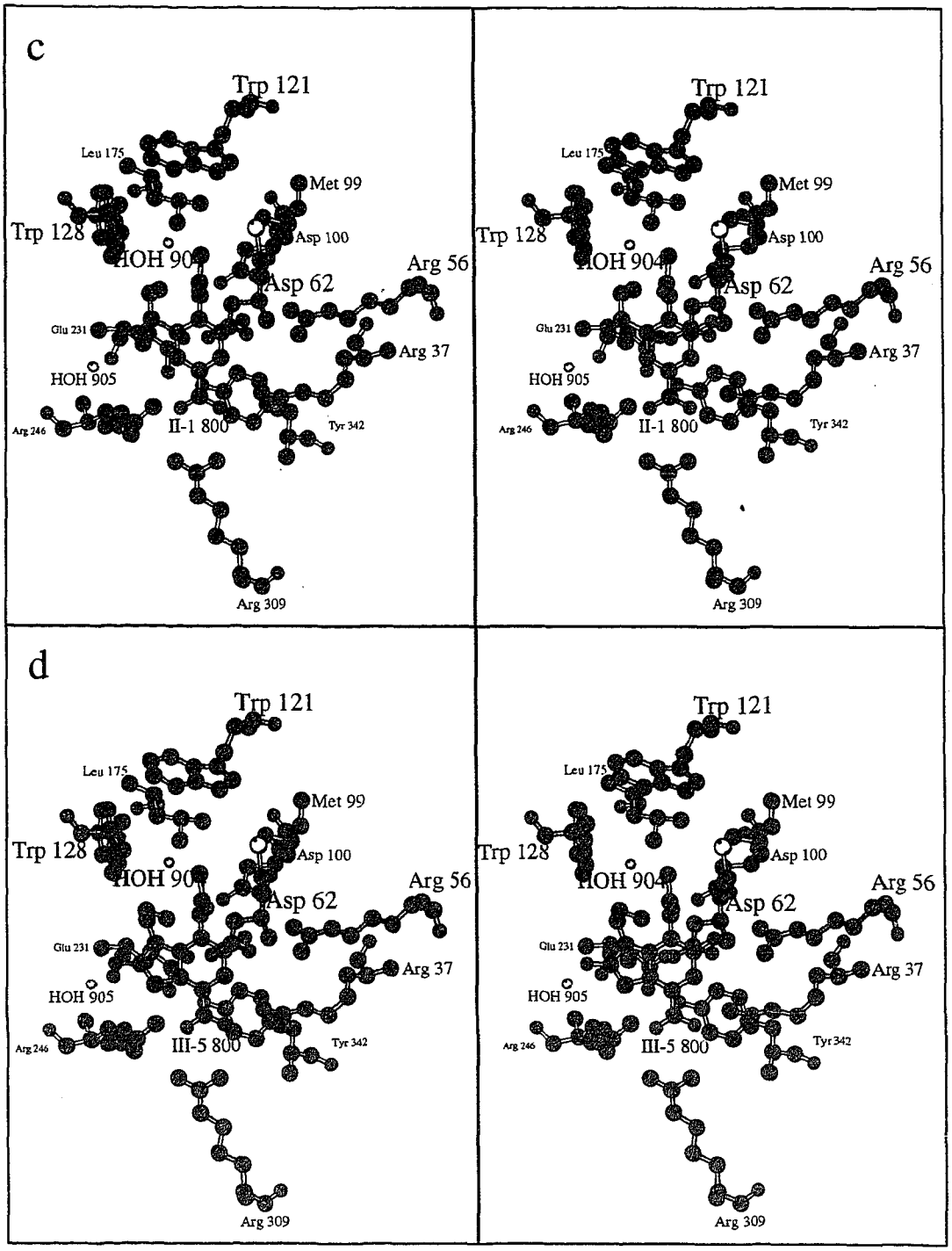

bacterial hydrophobic binding site is composed of two tryptophans (Trp 121, Trp 128), one methionine (Met 99), and one leucine (Leu 175), whereas the viral hydrophobic pocket contains just one tyrosine (which is analogous in position to Trp 128 of *S. typhimurium*), one isoleucine, and one arginine sidechain. In addition, several other features can be used to distinguish the *S. typhimurium* bacterial active site from its counterpart in the influenza virus sialidase. For example, there are several significant differences in the active site residues that form the binding pockets for the O4 hydroxyl and glycerol groups of sialic acid. In the bacterial enzyme, an arginine and an aspartic acid residue (Arg 56 and Asp 100 in *S. typhimurium*), which the viral sialidase does not contain, formstrong hydrogen bonds to the O4 atom of the bound sialic acid. The presence of these residues in the bacterial active site also prevents binding of sialic acid analogs modified at the O4 position with large, bulky groups [26]. At the glycerol binding pocket, the bacterial enzyme is lacking a glutamic residue (Glu 275) found in the influenza virus enzyme, which provides two hydrogen bonds to the glycerol O8 and O9 atoms of the bound sialic acid. In addition, the glycerol pocket found in the bacterial sialidase is much larger and broader than the glycerol pocket of influenza virus sialidase due to the alternate orientation of a loop in the bacterial sialidase. In the bacterial enzyme, the loop, comprised of residues 196-205, points away from the active site to create a wide, shallow glycerol binding pocket. The analogous loop in the influenza virus sialidase points toward the active site and effectively limits the size of the pocket to inhibitor sidegroups no longer than glycerol.

Modeling of inhibitors into bacterial sialidase

The lead compounds, HNBA and GBA, used in this study are potent inhibitors of both type A and B influenza virus sialidases. The IC_{50} value, defined as the concentration required to produce 50% inhibition, for HNBA inhibition of influenza virus sialidase is equal to ~10 μM, which is similar to the Neu5Ac2en IC_{50} value for influenza virus sialidase inhibition [40]. Based on the inhibition assay results reported in this study, HNBA and GBA also seem to inhibit bacterial sialidase with efficiencies similar to Neu5Ac2en.

Initial modeling of the benzoic acid lead compounds into the bacterial sialidase was guided by the crystal structure of the Neu5Ac2en-bacterial sialidase complex. The placement of the benzoic acid inhibitors into the bacterial active site by superposition onto the Neu5Ac2en position did not disturb the overall geometry of the active site, as evidenced by the low root-mean-square deviation between the energy minimized benzoic acid and Neu5Ac2en bacterial sialidase complexes.

In the bacterial sialidase, superposition of GBA to align its guanidinium group to the Neu5Ac2en O4 hydroxyl group, which will mimic the 4-guanidino-Neu5Ac2en binding mode, is not possible due to steric conflicts with residues Arg 56 and Asp 100 in bacterial sialidase. This steric interference in the Neu5Ac2en O4 pocket also explains the inhibition selectivity of 4-guanidino-Neu5Ac2en for influenza virus sialidase versus bacterial sialidases [39]. A comparison of the HNBA and GBA structures suggests that the rotation of the GBA ring, which resulted from energy minimization,

may be due to the lack of a hydroxyl group at the C5 position in GBA, which would bind in the Neu5Ac2en O4 hydroxyl site.

Targeting of active site regions for exploitation by potential inhibitors

The three new classes of bacterial sialidase specific inhibitor compounds that are proposed were primarily targeted against site **A**, the **N3+** binding site identified from the GRID analysis, and the active site hydrophobic pocket formed by Trp 121, Trp 128 and Leu 175. These regions of the active site were selected for exploitation on the basis of the relative interaction energies of the GRID probe binding sites, the structural differences between the bacterial and viral sialidases in these regions, and the chemical intuition of the authors.

The GRID map analysis was helpful in identifying the sites with substantial interaction energies in the bacterial sialidase active site. Site **A** was observed to be a very favorable anionic binding site for the **N3+** probe. Site **A** also includes the binding sites of the crystallographic water molecules HOH 906 and HOH 907. The hydrophilic binding site **B** was defined by the **OH2** probe and includes the binding site for the crystallographic water molecule HOH 905. Site **C** is another hydrophilic binding site defined by the **OH2** map, but this site does not contain any crystallographic water molecule binding sites. Sites **D**, **E**, and **F** were observed in the **OH2** map and these hydrophilic binding sites form a long hydration channel leading away from the active site. Site **D** contains the binding site of HOH 904, while sites **E** and **F** do not include any crystallographic water molecules. The **C3** hydrophobic probe was

helpful in identifying the regions of the active site, which favored van der Waals interactions. The bacterial sialidase residues, which surround the probe binding sites **A** through **F**, are not conserved in the influenza virus sialidase. Therefore, modification of the lead compounds to include functional groups that chemically mimic the GRID probes and, hence, should strongly interact with the active site residues that form the favorable probe binding sites, should result in inhibitors specific for bacterial sialidase and the related trypanosomal trans-sialidase.

Rational for inhibitor construction

The hydrophobic substitutions in the INSA class I compounds were targeted towards binding the active site hydrophobic pocket formed by Trp 121, Trp 128 and Leu 175. The orientation of the Trp 128 indole ring suggested that the substitution of an aromatic ring for the acetyl group of the lead compound could lead to favorable π-π ring stacking interactions. Based on this assumption, the acetyl group of the lead compound was cyclized to create the furan ring present in the I-1, I-2, and I-3 compounds. The furan ring is a conservative substitution in that it still maintains a O atom at the O8 position of the acetyl group. Because an analysis of Neu5Ac2en bound to bacterial sialidase does not indicate that the acetyl O8 atom is involved in any important hydrogen bonding, a benzene ring was substituted for the acetyl group in the I-4 compound. The potential to place a hydroxyl group in the **OH2** binding site **D**, which results in compound I-4 being a *N*-phenylamino modified inhibitor,

also strongly suggested the benzene ring addition at the inhibitor C4 amino position.

The INSA class II and III compounds were constructed to place a positively charged amino group in the anionic site **A** located by the **N3+** probe. An extension of the lead compound into site **A** from the N4 atom of the acetylamino group was considered, but was discarded due to a potentially difficult synthesis and the possibility that such an extension would disturb the hydrogen bonding of N4 to Asp 100. The addition of a flexible amino sidegroup required to reach site **A** in the class II compounds could decrease the binding affinity of this compound series due to higher entropic costs upon binding. Therefore, an indole ring was used in the class III compound series to minimize the conformational flexibility of the ligand while still allowing binding of an amino group in site **A**.

Analysis of free energy of complex formation

The sole use of the calculated free energy change of complex formation for the proposed compounds in this study was to rank the proposed compounds according to their modifications. The calculated values for the free energy of complex formation are clearly overestimated, because the contribution of hydrophobic, entropic, and desolvation terms were excluded from the free energy calculations. Hence, the reported free energy changes can not be used to give meaningful binding affinity constants for the proposed compounds. What is important is the order of relative binding preference for the proposed compounds that is predicted by this method. The relative binding preference of the proposed inhibitors

should help in the selection of the compounds that should be synthesized first. The effectiveness of using the calculated free energy of complex formation based protocol present in this paper as a predictive tool still awaits experimental confirmation. The generation of experimental derived binding affinities for several of the proposed compounds would allow a greater appreciation of which parts of the current protocol are required for predictive analysis and/or which parts should be modified to reduce sources of error. Hence, the chemical synthesis of several INSA compounds is being pursued.

The calculated free energy changes of complex formation for the proposed INSA classes I, II and III compounds indicate that strong potential inhibitors of bacterial sialidase should result when inhibitor constituents establish interactions in the favorable GRID probe binding sites identified in the enzyme active site. The largest contribution to the binding energy is clearly the presence of a positive charge in site **A**, the anionic **N3+** binding site formed by the negatively charged Asp 100 and Glu 231 residues. Since a **NH3+** probe was used to locate site **A**, an amino containing sidegroup was the logical choice for incorporation into the lead inhibitor to interact with site **A**. However, the high inhibition activity of GBA in the inhibition assay would suggest that a guanidino group may also be a suitable candidate for binding in site **A**. The classes II and III compounds, which all contain a positively charged amino group, have a substantial increase in calculated binding affinity when compared to the lead compound, HNBA. As a whole, the class II INSA compounds, which have flexible ethylamino sidegroup, displayed a

higher binding affinity for bacterial sialidase than the more rigid indole-based class III compounds. The presence of a flexible linker to connect the amino group to the body of the inhibitor seems to be critical for positioning the amino group effectively in the **N3**+ binding site **A**. This may explain the higher than average binding affinity of the INSA III-5 compound versus the other class III compounds. In contrast to the other class III compounds, which all have a methylamino group at the indole branch point, the III-5 compound has an ethylamino group, which offers more conformational flexibility to reach into the anionic **N3**+ binding site.

The substitution of a hydrophobic aromatic ring moiety in the class I compounds for the acetyl group present in the lead compounds also improved the calculated free energy change of complex formation. The small increase in the predicted binding affinity of the class I compounds versus the lead benzoic acid compounds is probably due to the fact that the class I furanyl and phenyl constituents make a hydrophobic contribution to inhibitor binding and hydrophobic effects were not included in the free energy calculations. For the similar reasons, compound I-4 has the highest predicted binding affinity of all the class I compounds due to the significant electrostatic contribution that results from placing the phenol hydroxyl group in the favorable **OH2** binding site **B**. The binding affinity of compound I-4 should also increase in comparison to the Neu5Ac2en due to the displacement of HOH 904 in the modeled I-4 bacterial sialidase complex. The release of bound waters has been estimated to contribute at least -1.8 kJ/mol to the total energy of the system [72].

Surprisingly, the predicted binding affinities of the class II and III potential inhibitors were not significantly increased by the placement of hydrogen bonding moieties in binding site **B**, which was located using an **OH2** grid probe. Theoretically, the placement of a hydroxyl group in site **B** should provide a highly favorable interaction, which should lower the free energy change associated with complex formation. The minimal contribution to the binding affinity of a hydroxyl group placed in site **B** versus an amino group placed in site **A** may reflect the smaller **OH2** probe interaction energy for site **B** versus the quite large **NH3+** probe interaction energy for site **A**. In addition, the displacement of HOH 905 in several of the class II and III inhibitor-bacterial sialidase complexes should also make a favorable contribution to inhibitor binding affinity when compared to Neu5Ac2en.

Biological Significance

Bacterial and trypanosomal infections of humans and livestock can result in serious medical complications and economic loss. Though antibiotics are available for the treatment of bacterial infections, inhibitors of bacterial sialidase may be medically useful where sialidase activity has been correlated with severe bacterial infection pathology, including streptococcal infection, middle ear effusions, bacterial vaginosis, and arteritis [47, 48, 73-78]. Currently, no effective treatment is available for trypanosomal infection, but it has been shown that the trans-sialidase activity is required for trypanosomal infection in mammals [17, 52]. Because the structure of the trans-sialidase enzyme is not known, the

structure-based design of trans-sialidase specific inhibitors is not presently possible. However, the amino acid sequence of the trypanosomal enzyme is highly homologous to the bacterial sialidases [16]. Therefore, the structure of the *Salmonella typhimurium* sialidase was used in the present study as a template for constructing new compounds which should be specific, tight binding inhibitors of both bacterial sialidase and trypanosomal trans-sialidase [34]. The coordinates of the bacterial sialidase inhibitor complex, two benzoic acid lead compounds, and the program GRID were used to construct the new series of inhibitors (INSA compounds). The electrostatic contribution to the free energy change of complex formation was also calculated for each proposed INSA-bacterial sialidase complex using the program DELPHI. Predicting the relative binding affinity of the proposed compounds helps to guide the selection of compounds that should be synthesized first. Based on the free energy calculations, several of the proposed INSA compounds have the potential to be specific, high affinity inhibitors of bacterial sialidase and, therefore, trypanosomal trans-sialidase.

Materials and Methods

Testing of benzoic acid compounds against bacterial sialidase

Several benzoic acid compounds were screened for inhibition activity against the bacterial sialidase isolated from *Micromonospora viridifaciens*, which was kindly provided by Dr. G. Air courtesy of Drs. T. Uwajima and K. Aisaka, Kyowa Hakko Kogya Company, Tokyo, Japan. The inhibition activities were determined

using a modified standard fluorometric assay employing 4-methylumbelliferyl-α-*D*-*N*-acetylneuraminic acid (MUN) as the substrate [22, 62]. Because the benzoic acid compounds have a low solubility in water, a 100 mM stock solution of the benzoic acid compounds was prepared in the organic solvent dimethyl sulfoxide (DMSO). An appropriate amount of the DMSO stock solution was added to the reaction mixture, which contained a final concentration of 10 mM inhibitor, 0.1 mM MUN, 50 mM NaAc (pH 6.0), 0.075 mM $CaCl_2$, 0.240 mM $MgCl_2$, 0.045 mM NaCl, and bacterial sialidase (diluted to give a linear response range in the fluorometer). Following addition of MUN, the sample was incubated at 37°C for 15 minutes. The reaction was stopped by the addition of 25 mM HEPES (pH 8.0). The amount of fluorescent product generated in the reaction was measured using an excitement wavelength of 365 nm and emission wavelength of 450 nm.

The inhibition activity of Neu5Ac2en was standardized against a background control containing only water and no Neu5Ac2en. Likewise, the inhibition activity of the benzoic acid compounds was standardized against a control containing only DMSO to negate the potential inhibition effects of DMSO on bacterial sialidase. Due to standardization, the inhibition activities of Neu5Ac2en and the benzoic acid inhibitors are reported as percent inhibition values. The percent inhibition of Neu5Ac2en serves as a positive control for inhibition by the benzoic acid compounds.

Initial modeling of the benzoic-acid compounds into the bacterial sialidase

The coordinates for the native and Neu5Ac2en complexed *Salmonella typhimurium* LT2 bacterial sialidase were kindly provided by Dr. Garry Taylor and his colleges [34]. The coordinates of the HNBA and GBA were extracted from the N2 influenza virus neuraminidase complexes of HNBA and GBA [40]. The HNBA compound C1, O3, and C5 atom positions were least-squares fitted to the Neu5Ac2en C2, O4, and C6 atoms in the Neu5Ac2en-bacterial sialidase complex. The GBA compound was superimposed onto the *S. typhimurium* complexed Neu5Ac2en by least-square fitting of the GBA C1, N3, and C5 atoms to the Neu5Ac2en C2, C7, and C4 atoms. After superposition, the GBA guanidino group was aligned with the Neu5Ac2en glycerol group which is the configuration observed in the N2 influenza virus neuraminidase GBA complex. The GBA guanidino group was then manually manipulated on a graphics display running FRODO to optimize the chemical and steric contacts with the bacterial sialidase active site residues. The orientation of the benzoic acid compound carboxylate and *N*-acetylamino groups was manually manipulated to match their Neu5Ac2en counterparts. All of the crystallographic water molecules identified in the Neu5Ac2en-*Salmonella typhimurium* sialidase complex were included in the HNBA-bacterial sialidase complex. The crystallographic water molecules, HOH 906 and HOH 907, were removed from the GBA-bacterial sialidase complex due to steric interference with the GBA guanidino group. In both of the modeled benzoic acid-bacterial sialidase complexes, the water molecules,

which were not sterically excluded by the inhibitor, still maintained reasonable hydrogen bonding partners.

Mapping of bacterial active site using GRID program

The program GRID, which calculates the interaction energy of a selected probe over discrete GRID steps, was used to map the areas of favorable probe interaction that occur in the active site of the *Salmonella typhimurium* bacterial sialidase [56, 57]. The HBA-bacterial sialidase coordinates were used in the GRID calculation. Five probe types were used for the GRID calculation: **C3** (methyl), **N3+** (NH_3^+ cation), **F-** (fluoride anion), **O::** (carboxylate C=O), and **OH2** (water). Using the HBA-bacterial sialidase coordinates and the five probe types, two sets of GRID maps were calculated using: (1) modified coordinates containing all of the crystallographically identified waters in the modeled complex and (2) modified coordinates containing no waters.

The GRID search was performed using a lattice box with dimensions of 10 Å greater than the maximum/minimum dimensions of the HNBA in the HNBA-bacterial sialidase complex. The selected lattice box produced a GRID search step size of 0.126 Å along the x-axis, 0.117 Å along the y-axis, and 0.141 Å along the z-axis. The GRID-generated contour map KONT files were then converted to the FRODO DSN6 format and displayed using FRODO [64]. Unless specified, all other input parameters used in the GRID calculations were set to the GRID default values.

Modeling and energy minimization of INSA compounds

The program QUANTA was used to build the coordinates of the proposed inhibitor compounds and the program X-PLOR was used to energy minimize the coordinates using partial charges derived from the QUANTA template method, which uses the CHARMm parameter set. The X-PLOR topology and parameter files for the INSA compounds were preferably generated from geometric information retrieved from the Cambridge Crystallographic Database or by comparison to analogous structures present in the X-PLOR topology and parameter libraries [79].

The first round of X-PLOR energy minimization consisted of 500 cycles of the conjugate gradient minimization on the free inhibitor coordinates. During this round of minimization, the carboxylate O71-C7-C1-C2 dihedral was restricted to 0.0° and *N*-acetylamino C3-C4-N4-C8 dihedral was restricted to 90.0°. No other geometric parameters were constrained. The restricted dihedral values are close to the values of the analogous dihedrals angles observed in the Neu5Ac2en-*Salmonella typhimurium* sialidase complex and provide a standardized geometry for modeling the INSA compounds into the bacterial sialidase active site.

For each energy minimized INSA inhibitor compound, the C1, O3, and C5 atoms were least-squares fitted to the HNBA C1, O3, and C5 atoms in the HNBA-bacterial sialidase complex. For each INSA-bacterial sialidase complex, water molecules present in the Neu5Ac2en-*Salmonella typhimurium* bacterial sialidase complex, which did not sterically conflict with the modeled INSA compound, were included in the inhibitor complex.

To relieve potentially bad contacts resulting from the initial superposition of the INSA compounds in the *S. typhimurium* active site, the INSA compound-bacterial sialidase complexes were energy minimized for 100 cycles using the Powell method using the program X-PLOR. A harmonic restraint of 500 kcal/mol was placed on all atoms more than 10 Å distant from the INSA compound, while no harmonic constraints were applied to atoms within 10 Å of the INSA compound. No geometric restrictions were applied to the INSA compounds during the energy refinement of the modeled INSA *S. typhimurium* complexes. Also, the partial charges assigned to the aspartic acid, glutamic acid, lysine, and arginine protein sidechains, as well as the INSA amino group when present, were set to zero during the energy minimization of the modeled INSA *S. typhimurium* complexes.

DELPHI calculation of the electrostatic free energy of complex formation

The electrostatic energy of complex formation was determined using the energy minimized coordinates of each INSA compound-bacterial sialidase complex. The partial charges assigned to the INSA compounds in the DELPHI calculation were determined using the semiemperical program MOPAC v6.0 and the coordinates of the final energy minimized inhibitor compound when complexed to the *S. typhimurium* sialidase. The DELPHI electrostatic energies were calculated using a focusing protocol comprised of three stages of the percent fill: 30%, 90%, and 90%. Using 90% fill in the final stage gave a step size of 1.04 Å. The following parameters were used for all DELPHI calculations: protein dielectric, $\varepsilon_p = 4$; solvent dielectric,

ε_s = 80; ionic strength = 0.145; linear iterations = 1000; and non-linear iterations = 3000. Unless otherwise stated, the DELPHI default values were used for all other parameters in the electrostatic free energy calculations.

Acknowledgments

The authors would like to thank Dr. G. Taylor and colleges for the coordinates of the Neu5Ac2en-*Salmonella typhimurium* bacterial sialidase complex and Dr. G. Air for her gift of *Micromonospora viridifaciens* bacterial sialidase courtesy of Drs. T. Uwajima and K. Aisaka, Kyowa Hakko Kogya Company, Tokyo, Japan. The authors would also like to thank Dr. S. C. Harvey for computational resources and access to the programs DELPHI and QUANTA, Drs. W. Brouillette and S. Singh for synthesis of the HNBA and GBA compounds, Dr. M. Jedrzejas for discussions, and the Alabama Supercomputer Network for computational resources and access to the program MOPAC. Funding for this project was provided by the National Institutes of Health, grant AI31888 (M.L).

References

1. Gottschalk, A. (1957). Neuraminidase: The specific enzyme of influenza virus and *Vibrio cholerae*. *Biochim. Biophys. Acta* **23**, 645-646.

2. Drzeniek, R. (1972). Viral and bacterial neuraminidases. *Curr. Top. Microbiol. Immunol.* **59**, 35-74.

3. Corfield, T. (1992). Bacterial sialidases--roles in pathogenicity and nutrition. *Glycobiology* **2**, 509-521.

4. Fraser (1978). Neuraminidase production by clostridia. *J. Med. Microbiol.* **11**, 269-280.

5. Fraser, A.G. & Brown, R. (1981). Neuraminidase production by Bacteroidaceae. *J. Med. Microbiol.* **14**, 63-76.

6. Berg, J.O., Lindqvist, L., Andersson, G. & Nord, C.E. (1983). Neuraminidase in *Bacteroides fragilis*. *Appl. Environ. Microbiol.* **46**, 75-80.

7. Hoyer, L.L., Roggentin, P., Schauer, R. & Vimr, E.R. (1991). Purification and properties of cloned *Salmonella typhimurium* LT2 sialidase with virus-typical kinetic preference for sialyl alpha 2→3 linkages. *J. Biochem.* **110**, 462-467.

8. Srivastava, P.N. & Abou-Issa, H. (1977). Purification and properties of rabbit spermatozoal acrosomal neuraminidase. *Biochem. J.* **161**, 193-200.

9. Mutton, T., Resnick, M.I. & Boyce, W.H. (1978). Human renal neuraminidase. *Invest. Urol.* **15**, 419-421.

10. Meyer, D.M., Lemonnier, M. & Bourrillon, R. (1981). Human liver neuraminidase. *Biochem. Biophys. Res. Commun.* **103**, 1302-1309.

11. Marchesini, S., Cestaro, B., Lombardo, A., Sciorelli, G. & Preti, A. (1984). Human blood cells sialidases. *Biochem. Int.* **8**, 151-158.

12. Hiraiwa, M., Uda, Y., Nishizawa, M. & Miyatake, T. (1987). Human placental sialidase: partial purification and characterization. *J. Biochem.* **101**, 1273-1279.

13. Warner, T.G., *et al.*, & Sliwkowski, M. B. (1993). Isolation and properties of a soluble sialidase from the culture fluid of Chinese hamster ovary cells. *Glycobiology* **3**, 455-463.

14. Venerando, B., *et al.*, & Tettamanti, G. (1994). Cytosolic sialidase from pig brain: a 'protein complex' containing catalytic and protective units. *Biochim. Biophy. Acta* **1208**, 229-237.

15. Liu, C. & Air, G.M. (1993). Selection and characterization of a neuraminidase-minus mutant of influenza virus and its rescue by cloned neuraminidase genes. *Virology* **194**, 403-407.

16. Pereira, M.E., Mejia, J.S., Ortega-Barria, E., Matzilevich, D. & Prioli, R.P. (1991). The *Trypanosoma cruzi* neuraminidase contains sequences similar to bacterial neuraminidases, YWTD repeats of the low density lipoprotein receptor, and type III modules of fibronectin. *J. Exp. Med.* **174**, 179-91.

17. Schenkman, S., Jiang, M.S., Hart, G.W. & Nussenzweig, V. (1991). A novel cell surface trans-sialidase of *Trypanosoma cruzi* generates a stage-specific epitope required for invasion of mammalian cells. *Cell* **65**, 1117-1125.

18. Schenkman, S., Pontes de Carvalho, L. & Nussenzweig, V. (1992). *Trypanosoma cruzi* trans-sialidase and neuraminidase activities can be mediated by the same enzymes. *J. Exp. Med.* **175**, 567-575.

19. Hall, B.F., Webster, P., Ma, A.K., Joiner, K.A. & Andrews, N.W. (1992). Desialylation of lysosomal membrane glycoproteins by *Trypanosoma cruzi*: A role for the surface neuraminidase in facilitating parasite entry into the host cell cytoplasm. *J. Exp. Med.* **176**, 313-325.

20. Ming, M., Chuenkova, M., Ortega-Barria, E. & Pereira, M.E. (1993). Mediation of *Trypanosoma cruzi* invasion by sialic acid on the host cell and trans-sialidase on the trypanosome. *Mol. Biochem. Parasitol.* **59**, 243-252.

21. Sander-Wewer, M., Schauer, R. & Corfield, A.P. (1982). Substrate specificity of viral, bacterial and mammalian sialidases with regard to different N,O-acetylated sialic acids and GM1. *Adv. Exp. Med. Biol.* **152**, 215-222.

22. Lentz, M.R., Webster, R.G. & Air, G.M. (1987). Site-directed mutation of the active site of influenza neuraminidase and implications for the catalytic mechanism. *Biochemistry* **26**, 5351-558.

23. Chong, A.K., Pegg, M.S. & von Itzstein, M. (1991). Characterisation of an ionisable group involved in binding and catalysis by sialidase from influenza virus. *Biochem. Int.* **24**, 165-171.

24. Chong, A.K., Pegg, M.S. & von Itzstein, M. (1991). Influenza virus sialidase: Effect of calcium on steady-state kinetic parameters. *Biochim. Biophys. Acta* **1077**, 65-71.

25. Chong, A.K., Pegg, M.S., Taylor, N.R. & von Itzstein, M. (1992). Evidence for a sialosyl cation transition-state complex in the reaction of sialidase from influenza virus. *Eur. J. Biochem.* **207**, 335-343.

26. Holzer, C.T., *et al.*, & Wu, W.Y. (1993). Inhibition of sialidases from viral, bacterial and mammalian sources by analogues of 2-deoxy-2,3-didehydro-N-acetylneuraminic acid modified at the C-4 position. *Glycoconj. J.* **10**, 40-44.

27. Finne, E. (1978). Specificity of action of neuraminidase, according to its bacteriological origin. *Endokinol.* **72**, 363-364.

28. Venerando, B., *et al.*, & Tettamanti, G. (1982). Kinetics of *Vibrio cholerae* sialidase action on gangliosidic substrates at different supramolecular-organizational levels. *Biochem. J.* **203**, 735-742.

29. Corfield, A.P., Higa, H., Paulson, J.C. & Schauer, R. (1983). The specificity of viral and bacterial sialidases for alpha(2-3)- and alpha(2-6)-linked sialic acids in glycoproteins. *Biochim. Biophy. Acta* **744**, 121-126.

30. Flashner, M., Kessler, J. & Tanenbaum, S.W. (1983). The interaction of substrate-related ketals with bacterial and viral neuraminidases. *Arch. Biochem. Biophys* **221**, 188-196.

31. Schreiner, E., Zbiral, E., Kleineidam, R.G. & Schauer, R. (1991). 2,3-Didehydro-2-deoxysialic acids structurally varied at C-5 and their behaviour towards the sialidase from *Vibrio cholerae*. *Carbohydr. Res.* **216**, 61-66.

32. Warner, T.G., Harris, R., McDowell, R. & Vimr, E.R. (1992). Photolabelling of *Salmonella typhimurium* LT2 sialidase. Identification of a peptide with a predicted structural similarity to the active sites of influenza-virus sialidases. *Biochem. J.* **285**, 957-964.

33. Guo, X. & Sinnott, M.L. (1993). *Salmonella typhimurium* neuraminidase acts with inversion of configuration. *Biochem. J.* **296**, 291-292.

34. Crennell, S.J., Garman, E.F., Laver, W.G., Vimr, E.R. & Taylor, G.L. (1993). Crystal structure of a bacterial sialidase (from *Salmonella typhimurium* LT2) shows the same fold as an influenza virus neuraminidase. *Proc. Nat. Acad. Sci. USA* **90**, 9852-9856.

35. Varghese, J.N., Laver, W.G. & Colman, P.M. (1983). Structure of the influenza virus glycoprotein antigen neuraminidase at 2.9 A resolution. *Nature (London)* **303**, 35-40.

36. Burmeister, W.P., Ruigrok, R.W. & Cusack, S. (1992). The 2.2 A resolution crystal structure of influenza B neuraminidase and its complex with sialic acid. *EMBO J.* **11**, 49-56.

37. Bossart-Whitaker, P., *et al.*, & (1993). Three-dimensional structure of influenza A N9 neuraminidase and its complex with the inhibitor 2-deoxy 2,3-dehydro-N-acetyl neuraminic acid. *J. Mol. Biol.* **232**, 1069-1083.

38. Janakiraman, M.N., White, C.L., Laver, W.G., Air, G.M. & Luo, M. (1994). Structure of influenza virus neuraminidase B/Lee/40 complexed with sialic acid and a dehydro analog at 1.8-A resolution: implications for the catalytic mechanism. *Biochemistry* **33**, 8172-8179.

39. von Itzstein, M., *et al.*, & Penn, C. R. (1993). Rational design of potent sialidase-based inhibitors of influenza virus replication [see comments]. *Nature (London)* **363**, 418-423.

40. Jedrzejas, M.J., *et al.*, & Luo, M. (1995). Structures of aromatic inhibitors of influenza virus neuraminidase. *Biochemistry* **34**, 3144-3151.

41. White, C.L., *et al.*, & Luo, M. (1995). A sialic acid-derived phosphonate analog inhibits different strains of influenza virus neuraminidase with different efficiencies. *J. Mol. Biol.* **254**, 623-634.

42. Hayden, F.G. (1994). Anti-influenza virus activity of the novel neuraminidase inhibitor 4-guanidino-Neu5Ac2en. Proceedings of the *Second Annual Antivirals Conference*. Washington, D.C., International Business Communications USA Conferences.

43. Durham, D.L., Mattingly, S.J., Doran, T.I., Milligan, T.W. & Straus, D.C. (1981). Correlation between the production of extracellular substances by type III group B streptococcal strains and virulence in a mouse model. *Infect. Immun.* **34**, 448-454.

44. Liljemark, W.F., Bloomquist, C.G., Fenner, L.J., Antonelli, P.J. & Coulter, M.C. (1989). Effect of neuraminidase on the adherence to salivary pellicle of *Streptococcus sanguis* and *Streptococcus mitis*. *Caries Res.* **23**, 141-145.

45. Guzman, C.A., Plate, M. & Pruzzo, C. (1990). Role of neuraminidase-dependent adherence in *Bacteroides fragilis* attachment to human epithelial cells. *FEMS Microbiol. Lett.* **59**, 187-192.

46. Childs, W.D. & Gibbons, R.J. (1990). Selective modulation of bacterial attachment to oral epithelial cells by enzyme activities associated with poor oral hygiene. *J. Period. Res.* **25**, 172-178.

47. Briselden, A.M., Moncla, B.J., Stevens, C.E. & Hillier, S.L. (1992). Sialidases (neuraminidases) in bacterial vaginosis and bacterial vaginosis-associated microflora. *J. Clin. Microbiol.* **30**, 663-666.

48. McGregor, J.A., *et al.*, & (1994). Bacterial vaginosis is associated with prematurity and vaginal fluid mucinase and sialidase: results of a controlled trial of topical clindamycin cream. *Am. J. Obstet. Gynecol.* **170**, 1048-1059.

49. Namavar, F., Van der Bijl, M.W., Appelmelk, B.J., De Graaff, J. & MacLaren, D.M. (1994). The role of neuraminidase in haemagglutination and adherence to colon WiDr cells by *Bacteroides fragilis*. *J. Med. Microbiol.* **40**, 393-396.

50. Kipnis, T.L., David, J.R., Alper, C.A., Sher, A. & da Silva, W.D. (1981). Enzymatic treatment transforms trypomastigotes of

Trypanosoma cruzi into activators of alternative complement pathway and potentiates their uptake by macrophages. *Proc. Nat. Acad. Sci. USA* **78**, 602-605.

51. Libby, P., Alroy, J. & Pereira, M.E. (1986). A neuraminidase from *Trypanosoma cruzi* removes sialic acid from the surface of mammalian myocardial and endothelial cells. *J. Clin. Invest.* **77**, 127-135.

52. de Titto, E.H. & Araujo, F.G. (1987). Mechanism of cell invasion by *Trypanosoma cruzi*: importance of sialidase activity. *Acta Trop. (Basel)* **44**, 273-282.

53. Prioli, R.P., Mejia, J.S. & Pereira, M.E. (1991). On the interaction of *Trypanosoma cruzi* neuraminidase and human lipoproteins. *Eur. J. Epidemiol.* **7**, 344-348.

54. Ferrero-Garcia, M.A., *et al.*, & Parodi, A. J. (1993). The action of *Trypanosoma cruzi* trans-sialidase on glycolipids and glycoproteins. *Eur. J. Biochem.* **213**, 765-771.

55. Frasch, A.C. (1994). Trans-sialidase, SAPA amino acid repeats and the relationship between *Trypanosoma cruzi* and the mammalian host. *Parasitology* **108**, S37-44.

56. Goodford, P.J. (1985). A computational procedure for determining energetically favourable binding sites on biologically important macromolecules. *J. Med. Chem.* **28**, 849-875.

57. Reynolds, C.A., Wade, R.C. & Goodford, P.J. (1989). Identifying targets for bioreductive agents: using GRID to predict selective binding regions of proteins. *J. Mol. Graph.* **7**, 103-108.

58. Gilson, M.K., Rashin, A., Fine, R. & Honig, B. (1985). On the calculation of electrostatic interactions in proteins. *J. Mol. Biol.* **184**, 503-516.

59. Gilson, M.K. & Honig, B. (1988). Calculation of the total electrostatic energy of a macromolecular system: solvation energies, binding energies, and conformational analysis. *Proteins* **4**, 7-18.

60. Sharp, K. & Honig, B. (1990). Electrostatic interactions in macromolecules: theory and applications. *Annu. Rev. Biophys. Biophys. Chem.* **19**, 301-332.

61. Singh, S., Jedrzejas, M., Air, G.M., Luo, M., Laver, W.G. & Brouillette, W. (1994). Structure-based inhibitors of influenza virus sialidase. A benzoic acid lead with novel interaction. *J. Med. Chem.*, in press.

62. Potier, M., Mameli, L., Belisle, M., Dallaire, L. & Melancon, S.B. (1979). Fluorometric assay of neuraminidase with a sodium (4-methylumbelliferyl-α-*D*-*N*-acetylneuraminate) substrate. *Anal. Biochem.* **94**, 287-296.

63. Sakurada, K., Ohta, T. & Hasegawa, M. (1992). Cloning, expression, and characterization of the *Micromonospora viridifaciens* neuraminidase gene in . *J. Bacteriol.* **174**, 6896-6903.

64. Jones, T.A. (1985). Interactive computer graphics: FRODO. *Methods Enzymol.* **115**, 157-171.

65. Kraulis, P.J. (1991). MOLSCRIPT: a program to produce both detailed and schematic plots of protein structures. *J. Appl. Crystallogr.* **24**, 946-950.

66. (1994). *QUANTA: Generating and Displaying Molecules* . (4.0), Molecular Simulations Inc., Burlington, Massachuets.

67. Cummings, P.L. & Gready, J.E. (1993). Computer-aided drug design: A free energy pertubation study on the binding of methyl-substituted pterins and N5-deazapterins to dihrofolate reductase. *J. Comput. Aided Mol. Des.* **7**, 535-555.

68. Wendolosk, J.J., Shen, J., Oliva, M.T. & Weber, P.C. (1993). Biophysical tools for structure-based drug design. *Pharmol. Ther.* **60**, 169-183.

69. Aqvist, J., Medina, C. & Samuelsson, J.-E. (1994). A new method for predicting binding affinity in computer-aided drug design. *Protein Eng.* **7**, 385-391.

70. Wang, S., *et al.*, & Blumberg, P.M. (1994). Protein kinase C. Modeling of the binding site and prediction of binding constants. *J. Med. Chem.* **37**, 1326-1338.

71. Klapper, I., Hagstrom, R., Fine, R., Sharp, K. & Honig, B. (1986). Focusing of electric fields in the active site of Cu-Zn superoxide dismutase. *Proteins* **1**, 47-59.

72. Vriend, G., *et al.*, & Eijink, V.G.H. (1991). Stabilization of the neutral protease of *Bacillus stearothermophilus* by removal of a buried water molecule. *Protein Eng.* **4**, 941-945.

73. Mosquera, J. & Rodriguez-Iturbe, B. (1984). Extracellular neuraminidase production of streptococci associated with acute nephritis. *Clin. Nephrol.* **21**, 21-28.

74. LaMarco, K.L., Diven, W.F. & Glew, R.H. (1986). Experimental alteration of chinchilla middle ear mucosae by bacterial neuraminidase. *Ann. Otol. Rhinol. Laryngol.* **95**, 304-308.

75. Nakato, H., Shinomiya, K. & Mikawa, H. (1986). Possible role of neuraminidase in the pathogenesis of arteritis and thrombocytopenia induced in rats by *Erysipelothrix rhusiopathiae*. *Pathol. Res. Pract.* **181**, 311-319.

76. Udezulu, I.A. & Leitch, G.J. (1987). A membrane-associated neuraminidase in *Entamoeba histolytica* trophozoites. *Infect. Immun.* **55**, 181-186.

77. Corfield, T. (1992). Bacterial sialidases-roles in pathogenicity and nutrition. *Glycobiology* **2**, 509-521.

78. Galen, J.E., *et al.*, & Kaper, J. B. (1992). Role of *Vibrio cholerae* neuraminidase in the function of cholera toxin. *Infect. Immun.* **60**, 406-415.

79. Allen, F.H., *et al.*, & Watson, D.G. (1991). The development of versions 3 and 4 of the Cambridge Structural Database system. *J. Chem. Inf. Comp. Sci.* **31**, 187-204.

SUMMARY

The work presented here represents just one step in the process of understanding sialidase structure and function. Using X-ray crystallography, we can now begin to understand the fine details of influenza sialidase activity and substrate-active site interaction. By studying the ability of several different sialidase inhibitors, we have been able to discern some of the properties that characterize "good" influenza sialidase inhibitors. We have then expanded this knowledge base by investigating the bacterial sialidase family of enzymes. The results indicate that though the influenza virus sialidase and bacterial sialidase share many common features, it should be possible to construct inhibitors that are specific for either the bacterial or influenza virus sialidase.

The early studies of the B/Lee/40 influenza sialidase and its complex with Neu5Ac2en were instrumental to deciphering the driving force of substrate binding and cleavage. Our work strongly suggests that upon binding, the substrate Neu5Ac must be distorted to a half-chair conformation. The half-chair conformation of Neu5Ac is stabilized by the many charged electrostatic interactions and hydrogen bonds that occur between the bound substrate and the 11 strictly conserved active site residues. The B/Lee/40 studies also indicate that the conversion of Neu5Ac (NANA) to Neu5Ac2en (DANA) by the influenza virus sialidase is at best a very minor side

reaction. Finally, on the basis of the X-ray crystallographic results, we were able to postulate a model for the influenza virus sialidase mechanism which is consistent with the previously published biochemical data. The proposed mechanism is also consistent with the reported turnover number (9 s^{-1}) due to the inefficient nature of substrate binding and cleavage.

The crystallographic analysis of types A and B influenza virus sialidase complexed to two phosphonate inhibitors resulted in a meticulous study of how inhibitor structure relates to influenza sialidase binding. By comparing the crystal structures of Neu5Ac, Neu5Ac2en, ePANA, and aPANA inhibitors complexed to several type A and type B influenza virus sialidase strains, several important conclusions can be drawn. First, the influenza virus active site is very rigid both in the absence and presence of bound substrate/inhibitor. The large hydrogen bonding network that occurs between the 11 active site residues and the surrounding ring of neighboring residues is the most likely reason for the influenza virus active site rigidity. Second, binding of inhibitors to the influenza virus sialidase active site is dictated by (1) the strong charge-charge interaction between the inhibitor acidic group and active site arginine triad and (2) the ability to correctly position the *N*-acetylamino, and to a lesser extent, the O4 hydroxyl group, in the active site to maximize the protein-inhibitor contacts. Third, the substitution of a phosphonyl group for a carboxyl group in the phosphonate inhibitors does not dramatically increase the inhibitor binding affinity. The higher negative charge present on the phosphonyl group should result in a stronger charge-charge

interaction between the PANA inhibitors and the sialidase arginine triad, but the larger size and geometry of the phosphonyl group may counteract the electrostatic benefits. Fourth, the ring of the inhibitor does not directly interact with the active site residues. Its major function is to properly position the inhibitor sidegroups in the active site, and, hence, the conformation of the inhibitor ring is arbitrary as long as the adopted conformation results in the correct sidegroup geometry. Finally, the crystal structures of the ePANA complexed to several influenza sialidases indicate that the lower inhibition of ePANA versus the type A N9 influenza virus sialidase is not due to alternate modes of inhibitors binding or loss of inhibitor-protein interactions.

The structure-based modeling of bacterial sialidase inhibitors provided a chance to apply the lessons learned from the influenza sialidase inhibitor studies to a new system. Like the influenza sialidase active site, the bacterial sialidase active site also contains an arginine triad, which binds the carboxylate of Neu5Ac, as well as a hydrophobic pocket to bind the *N*-acetylamino group of Neu5Ac. Otherwise, the active site residues of the two sialidases significantly differ in their composition and geometry. The bacterial sialidase modeling study also provided an opportunity to implement and evaluate the use of the several computer-intensive methodologies, which hold promise for future drug design efforts.

Thirteen new compounds were constructed to be specific inhibitors of bacterial sialidase using the crystal structure of the *Salmonella typhimurium* sialidase-Neu5Ac2en complex as the template structure and two benzoic acid lead compounds. The

program GRID, which calculates the interaction energy between a probe and the protein as the probe is placed at specific points within the target site of the protein, was instrumental in building the new, proposed compounds. A highly favorable cation binding site (NH_3^+ probe), as well as several hydrophilic sites, which favor hydrogen bonding (OH2 probe), were identified from the GRID analysis of the bacterial sialidase active site. The program DELPHI, which calculates the total electrostatic energy of a system, was used to evaluate the increased binding affinity of the proposed compounds. In comparison to the lead compounds, several of the designer compounds were predicted by DELPHI to exhibit significantly higher binding affinities for the bacterial sialidase. The next phase of synthesis and testing of the designer compounds is in progress and should provide many new exciting results.

DISCUSSION

Future studies of influenza virus sialidase

What is the next step for the analysis of sialidase structure and its application to the structure-based design of new and novel sialidases? I would first like to express my thoughts concerning the influenza virus sialidase studies. The structural work on the influenza virus sialidase performed in the laboratory of Dr. Luo, which this dissertation is a part of, has contributed greatly to the design of new anti-influenza compounds. The benzoic acid based compounds, or BANA inhibitor series, show the most promise as potential therapeutic agents for influenza infection (Jedrzejas *et al.*, 1995; Luo *et al.*, 1994). The use of structure-based design has been the key to the rapid development of the benzoic acid compounds, from the inception stage to the potential drug stage. On the basis of the X-ray crystal structure results, it was decided that a benzene ring spacer could be substituted for the sugar ring present in the carbohydrate-based inhibitors. The previous crystallographic work on influenza virus sialidase also implied that the presence of a carboxylate and *N*-acetylamino sidegroup was sufficient to direct inhibitor binding in the correct orientation. Currently, more advanced benzoic acid-based compounds have been designed to target specific regions of the active site identified using the structure of

the influenza virus sialidase. The new compounds have been synthesized and the crystal structure of the influenza virus sialidase complexes determined. As is the hallmark of structure-based methodologies, the crystal structures of the previously synthesized benzoic acid-influenza sialidase complexes have driven the design of new, or altered, benzoic acid-based inhibitors. The current benzoic acid compounds display inhibition activities on the order of Neu5Ac2en, but the multitude of common chemical methodologies, which can be used to easily modify the benzoate benzene ring, hold the promise of future benzoic acid-based compounds with significantly increased inhibition activities.

Given the success of the benzoic acid-based compounds, are there alternatives for designing influenza sialidase inhibitors? Definitely, the answer is yes. If anything the success of the benzoic acid-based series would suggest that inhibitors based on the compounds shown in Figure 1 may also exhibit inhibition activity. As long as the alternative compounds correctly placed the carboxylate and *N*-acetylamino groups, or homologues thereof, in the appropriate active site pocket, they should exhibit inhibition activity. The small ring structures of these compounds could prove beneficial by exposing the bottom of the active site pocket as a potential target region. The varying geometry of the alternative ring-based compounds would also allow for the placement of inhibitor sidegroups in active site pockets, which are favorable, but inaccessible, to the BANA compounds due to the larger size and geometry of the benzene ring. Again, the development of the alternative ring-based compounds as effective influenza virus

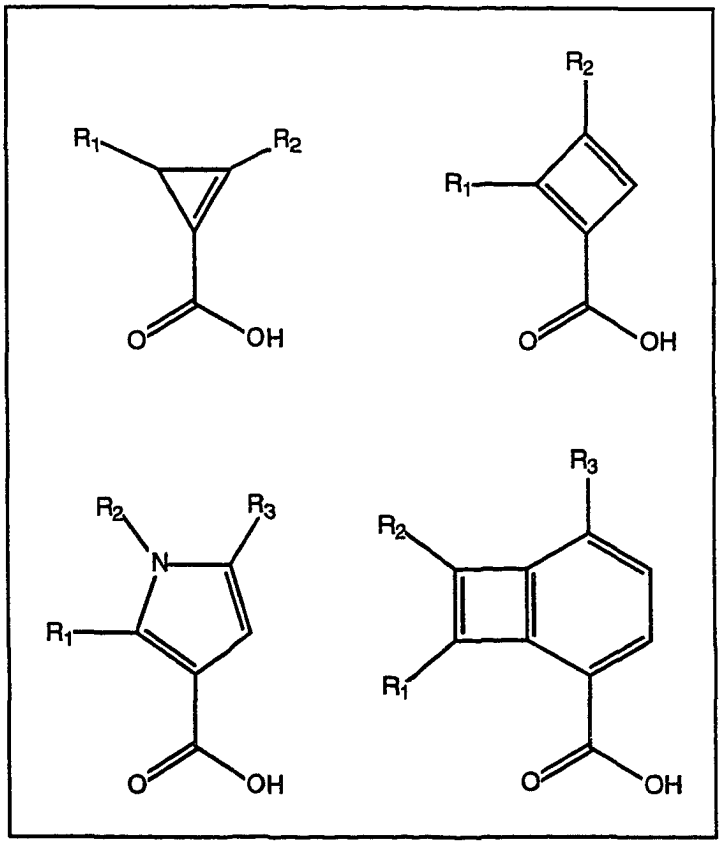

Figure 1. New proposed inhibitor motifs.

sialidase specific inhibitors would depend on the crystallographic analysis of the alternative compound-sialidase complexes. In addition, several of the alternative compounds may face chemical synthesis obstacles.

Future studies of bacterial sialidase

What is the next step for the bacterial sialidase studies? First and foremost, crystals of a bacterial sialidase are required. I have attempted to crystallize the bacterial sialidase purified from *Clostridium perfringens*, but to no avail. The *C. perfringens* sialidase, due to large degree of homology to the *Salmonella typhimurium* sialidase, would be a good target for further bacterial specific sialidase inhibitors. In the event that X-ray diffraction quality crystals of *S. typhimurium, C. perfringens*, or another bacterial sialidase become available, the crystal structure of the native protein could be solved using molecular replacement and the coordinates of the *Salmonella typhimurium* sialidase (Crennell *et al.*, 1993). It may also be possible to use the coordinates of the *Vibrio cholerae* as the molecular replacement model (Crennell *et al.*, 1994).

Based on the advantages cited above for the design of influenza sialidase inhibitors, benzoic acid-based compounds are also the prime lead compounds for the design bacterial specific sialidase inhibitors. Several of the compounds that resulted from the bacterial sialidase modeling studies have been selected for synthesis. When the compounds become available, the next step would be to soak the inhibitors into native crystals of a bacterial sialidase and solve the crystal structures of the complexes using

molecular replacement and difference Fourier techniques. Based on my chemical intuition, I predict that some, if not all, of the proposed compounds will show some inhibition activity against bacterial sialidase. Concurrent to the crystallographic studies, *in vitro* inhibition testing of the synthesized compounds against several bacterial sialidases would also be performed. The results of the crystallographic and *in vitro* studies would then be used to guide the selection of chemical substituants to be included in the next generation of bacterial sialidase specific inhibitors.

In addition to the binding sites determined using the NH_3^+ and OH_2 GRID probes, several other regions of the bacterial sialidase active site may prove to be useful for drug design. In particular, the GRID map analysis identified a long hydration channel leading away from the hydrophobic pocket in the bacterial sialidase. This unique feature is not present in the influenza virus sialidase and therefore may be exploited for bacterial specificity. The pocket could be easily filled using a glycerol-like extension from the *N*-acetylamino moiety (or homologue) of a bacterial sialidase inhibitor.

The glycerol binding pocket of the bacterial sialidase contains several functional groups that are also not present in the influenza virus sialidase glycerol binding pocket. The wide valley characteristic of the bacterial glycerol pocket may also allow for the use of larger inhibitor ring systems.

Future studies of trypanosomal trans-sialidase

Given the high sequence homology between the N-terminal domain of the trypanosomal trans-sialidase and the bacterial

sialidase, it is our hope that the inhibitors designed against the bacterial sialidase active site will also prove to be effective against the trypanosomal enzyme. The homology modeling of the trypanosomal trans-sialidase active site was encouraging, but without a crystal structure, some aspects of the trans-sialidase structure remain questionable. For example, only two of the three conserved arginines, which form the carboxylate binding pocket, could be identified in the trypanosomal enzyme by sequence alignment to bacterial sialidases. Of the arginine triad residues, only the central arginine and the arginine located on the same side of the active site as the glycerol pocket were identified. The arginine, which should be found on the same side as the O4 hydroxyl binding pocket, cannot be located in the trypanosomal sequence. One implication of the "missing" arginine may reflect the substrate requirements of trans-sialidase, which recognizes the terminal sialic acid residue of a donor molecule, as well as the terminal galactose residue of the acceptor molecule. Could it be possible that the arginine is "missing" due to the presence of a galactose binding site? Based on modeling of sialylactose, Neu5Ac-($\alpha 2 \rightarrow 3$)-galactose-$\beta(1 \rightarrow 4)$-glucose, into the active site of the trans-sialidase homology model, the "missing" arginine location would be ideal for galactose binding pocket. A slight rotation of the sialic acid residue in the trans-sialidase active site along the carboxylate axis-acetylamino axis towards the "missing arginine" would direct the galactose residue into a slight depression created in the absence of the "missing arginine." Note, one should view these results with a healthy dose of skepticism due to the inherent error involved in the

homology modeling, but the potential of a galactose binding site does give rise to many exciting implications. It may be possible to target both the acceptor and donor binding sites for structure-based drug design. To accurately and correctly locate the acceptor and/or donor molecule binding site, the crystal structure of the trypanosomal trans-sialidase complexed to a non-cleavable thio-substrate or similar competitive inhibitor must be solved. In order to solve the crystal structure, large amounts of the trans-sialidase protein are required for crystallization experiments. My colleague, Mr. Qui, and I have been working to solve this problem by subcloning and expressing the N-terminal domain of the trypanosomal trans-sialidase in *E. coli* using the full-length trans-sialidase clone provided by Dr. M. E. Pereira, Tufts University School of Medicine. The full-length trans-sialidase clone when expressed in *E. coli* does exhibit native enzymatic specificity and activity. Using the N-terminal trans-sialidase domain subclone, several *E. coli* expression protocols have all resulted in the formation of inclusion bodies containing the over expressed trans-sialidase domain. Currently, the work is focused on developing a protocol to refold denatured trans-sialidase, which has been purified from the inclusion bodies. We have several potential assays at out disposal to measure both the sialidase activity and trans-sialidase activity. In the trans-sialidase enzyme, the sialidase activity is apparent only in the absence of a suitable acceptor protein.

The studies of the trans-sialidase offer an exciting opportunity to understand the mechanism of a new sialidase, which has great medical importance. Successful expression, purification,

crystallization, and X-ray diffraction analysis of the trypanosomal trans-sialidase should make possible the structure-based design of trans-sialidase specific inhibitors. In addition, the design of trans-sialidase inhibitors should benefit greatly from the work presently conducted on the bacterial sialidase system. Due to predicted structural similarity of the enzyme active sites, several of the bacterial sialidase inhibitors should be excellent lead compounds for developing the trans-sialidase inhibitors. If we are lucky, some of the bacterial-based sialidase inhibitors will show substantial affinity for the trypanosomal trans-sialidase. The new trans-sialidase inhibitor compounds would be useful as anti-trypanosomal agents in the treatment of Chagas' disease in humans, as well as trypanosome-related infections in other mammals.

Future studies on mammalian sialidases

To further complement the structural studies on the viral, bacterial, and trypanosomal trans-sialidase, the crystal structure of a mammalian sialidase should be solved. Several mammalian sialidases have been identified and/or isolated from the liver, brain, blood, skin, and placental tissues (Chen *et al.*, 1994; Hiraiwa *et al.*, 1991; Marchesini et al., 1984; Meyer *et al.*, 1981; Michalski *et al.*, 1986; Mier *et al.*, 1982; Miyagi & Tsuiki, 1984; Saito & Yu, 1986; Usuki *et al.*, 1988; Venerando *et al.*, 1994). At present, no mammalian sialidase structure has been solved by X-ray crystallography. The crystal structure of a mammalian sialidase would be useful in the design of non-mammalian sialidase inhibitors, because the sites that are not present in the mammalian

sialidase structure could be used to build inhibitor compounds specific for the viral, bacterial, or trypanosomal enzymes. Hence, the new compounds would be less likely to inhibit the mammalian sialidases and, therefore, less likely to result in potentially harmful side-effects.

The mammalian sialidase crystal structure could also lead to the design of mammalian-specific sialidase inhibitors for the medical treatment of disease states caused by excessive endogenous sialidase activity.

Future developments in structure-based drug design

For structure-based drug techniques to continue to prosper, advances in the fields of protein crystallization, predicting protein flexibility, molecular graphics, and computational chemistry must be realized.

Currently, the crystallization of hydrophobic or membrane-bound proteins is a hit-or-miss venture. The arrival of new detergents and other solubilizing agents, as well as the current systematic studies of protein crystallization being conducted at UAB and other universities, should provide some help for this problem. In the absence of improvements in crystallization, many medically important hydrophobic proteins will be eliminated as potential targets for structure-based drug design.

The development of tight binding ligands can be difficult if the active site of the target molecule is flexible. One must know which geometry (or geometries) should be the basis for the structure-based design of inhibitors. Flexibility in the molecular target, such

as ordering/disordering of an active site loop caused by ligand binding, may not be apparent if only the crystal structure of the bound or unbound target molecule is known. Though flexibility in the target crystal structure can be inferred by high temperature factors, the motions of movement are not always obvious. Predicting conformational flexibility using molecular dynamics techniques is also risky, but the increase in computational power should help in some cases. Furthermore, the binding of slightly different ligands into a target molecule active site can produce energetically significant changes in the active site structure. To fully comprehend and appreciate the role of flexibility in the design of inhibitors usually requires solving several inhibitor-target molecule complexes, which span the full spectra of possible conformations. Fortunately, the bacterial and viral sialidases target sites are extremely rigid.

In the area of molecular graphics, new programs need to be implemented to take advantage of the increased raw computing power of the current and future generations of computers. I would like to see the features of QUANTA, which are used in small molecule studies (such as charge calculations, chemical building routines, etc.), implemented inside a large-scale molecular graphics environment as used by the programs FRODO or O. Also, it would be very useful if the Cambridge Crystallographic Database entries were available from the main program level. Such an integrated program would prove very beneficial to structure-based design teams. In addition, I believe the program would increase the time spent actually designing new inhibitors and decrease the wasted time

spent shuttling information and potential structures between different computer platforms and program formats.

In my opinion, the field of computational chemistry is now the limiting factor in successful structure-based inhibitor design. The current methods of predicting binding affinity produce only produce qualitative results. Molecular mechanics, molecular dynamic, and free energy perturbation techniques produce more accurate results for small atom systems, but are either too computationally involved or too expensive for use with large atom systems. Predictive binding affinity methods are also limited by the algorithms available to correctly predict the polarization state of the ligand and active site residues in the bound complex. Because the binding of a ligand often induces polarization of the molecule that is required for tight binding, efficient and accurate methods to determining the polarization state of the system are vital to structure-based drug design.

In conclusion, the field of structure-based drug design is an important and powerful tool for constructing high affinity inhibitors of target molecules in a relatively short time period. As the power of computer systems continues to increase, the design steps involving molecular graphics, chemical modeling, and computation of binding affinities should increase in efficiency and accuracy. But persistent problems remain, which will not be resolved by more computational resources. How should hydrophobic terms be treated when calculating binding affinities? Is it necessary to determine the dielectric environment of the active site? What are the best methods to predict protein flexibility and modes of movement?

These and other questions will require new insights, better methods, and novel approaches--the seeds of which have already been planted.

LIST OF REFERENCES

Beveridge, W. I. B. (1978). *Influenza: The Last Great Plague*, Neale Watson Academic Publications, Inc., New York, NY.

Blok, J., Air, G. M., Laver, W. G., Ward, C. W., Lilley, G. G., Woods, E. F., Roxburgh, C. M. & Inglis, A. S. (1982). Studies on the size, chemical composition, and partial sequence of the neuraminidase (NA) from type A influenza viruses show that the N-terminal region of the NA is not processed and serves to anchor the NA in the viral membrane. *Virology,* **119**, 109-121.

Blundell, T. L. & Johnson, L. N. (1976). *Protein Crystallography*, Academic Press Inc., San Diego, CA.

Bohm, H. J. (1992). The computer program LUDI: a new method for the de novo design of enzyme inhibitors. *J. Comput. Chem.* **6**(1), 61-78.

Briselden, A. M., Moncla, B. J., Stevens, C. E. & Hillier, S. L. (1992). Sialidases (neuraminidases) in bacterial vaginosis and bacterial vaginosis-associated microflora. *J. Clin. Microbiol.* **30**(3), 663-666.

Brunger, A. T. (1988). Crystallographic refinement by simulated annealing: Application to a 2.8 Å resolution structure of aspartate aminotransferase. *J. Mol. Biol.* **203**, 803-816.

Burmeister, W. P., Ruigrok, R. W. & Cusack, S. (1992). The 2.2 A resolution crystal structure of influenza B neuraminidase and its complex with sialic acid. *EMBO J.* **11**(1), 49-56.

Camara, M., Boulnois, G. J., Andrew, P. W. & Mitchell, T. J. (1994). A neuraminidase from *Streptococcus pneumoniae* has the features of a surface protein. *Infect. Immun.* **62**(9), 3688-3695.

Chen, X. G., Nagai, T. & Yamada, H. (1994). Sialidase in rabbit blood. Characterization of sialidase purified from rabbit erythrocyte membrane. *Eur. J. Biochem.* **221**(2), 655-664.

Chong, A. K., Pegg, M. S. & von Itzstein, M. (1991a). Characterisation of an ionisable group involved in binding and catalysis by sialidase from influenza virus. *Biochem. Int.* **24**(1), 165-171.

Chong, A. K., Pegg, M. S. & von Itzstein, M. (1991b). Influenza virus sialidase: Effect of calcium on steady-state kinetic parameters. *Biochim. Biophys. Acta,* **1077**(1), 65-71.

Colli, W. (1993). Trans-sialidase: A unique enzyme activity discovered in the protozoan *Trypanosoma cruzi. FASEB J.* **7**(13), 1257-1264.

Crennell, S., Garman, E., Laver, G., Vimr, E. & Taylor, G. (1994). Crystal structure of *Vibrio cholerae* neuraminidase reveals dual lectin-like domains in addition to the catalytic domain. *Structure,* **2**(6), 535-544.

Crennell, S. J., Garman, E. F., Laver, W. G., Vimr, E. R. & Taylor, G. L. (1993). Crystal structure of a bacterial sialidase (from *Salmonella typhimurium* LT2) shows the same fold as an influenza virus neuraminidase. *Proc. Nat. Acad. Sci. USA,* **90**(21), 9852-9856.

Cross, G. A. M. & Takle, G. B. (1993). The surface *trans*-sialidase family of *Trypanosoma cruzi. Ann. Rev. Microbiol.* **47**, 385-411.

Crowther, R. A. & Blow, D. M. (1967). A method for positioning a known molecule in an unknown crystal structure. *Acta Crystallogr.* **23**, 544-48.

Cummings, P. L. & Gready, J. E. (1993). Computer-aided drug design: A free energy pertubation study on the binding of methyl-substituted pterins and N5-deazapterins to dihrofolate reductase. *J. Comput. Aided Mol. Des.* **7**, 535-555.

de Titto, E. H. & Araujo, F. G. (1987). Mechanism of cell invasion by *Trypanosoma cruzi*: Importance of sialidase activity. *Acta Trop. (Basel),* **44**(3), 273-282.

DiMasi, J. A., Hansen, R. W., Grabowski, H. G. & Lasagna, L. (1991). Cost of innovation in the pharmaceutical industry. *J. Health Econ.* **10**, 107-142.

Duff, K. C., Gilchrist, P. J., Saxena, A. M. & Bradshaw, J. P. (1994). Neutron diffraction reveals the site of amantadine blockade in the influenza A M2 ion channel. *Virology,* **202**(1), 287-293.

Ealick, S. E., Babu, Y. S., Bugg, C. E., Erion, M. D., Guida, W. C., Montgomery, J. A. & Secrist III, J. A. (1991). Application of crystallogrpahic and modeling methods in the design of purine nucleoside phosphorylase inhibitors. *Proc. Nat. Acad. Sci. USA,* **88**, 11540-11544.

Ganguly, S., Sarkar, D. & Ghosh, J. J. (1976). Sialic acid and sialidase activity in human endometrial tissue, uterine fluid and plasma under different conditions of uterine dysfunction. *Acta Endocrinol.* **81**(3), 574-579.

Gillet, V. J., Newell, W., Mata, P., Myatt, G., Sike, S., Zsoldos, Z. & Johnson, A. P. (1994). SPROUT: Recent developments in the de novo design of molecules. *J. Cell. Biochem. Suppl.* **34**(1), 207-217.

Gilson, M. K. & Honig, B. (1988). Calculation of the total electrostatic energy of a macromolecular system: Solvation energies, binding energies, and conformational analysis. *Proteins: Struct. Func. Genet.* **4**, 7-18.

Goodford, P. J. (1985). A computational procedure for determining energetically favourable binding sites on biologically important macromolecules. *J. Med. Chem.* **28**, 849-875.

Gottschalk, A. (1957). Neuraminidase: the specific enzyme of influenza virus and *Vibrio cholerae*. *Biochim. Biophys. Acta,* **23**, 645-646.

Greer, J., Erickson, J. W., Baldwin, J. J. & Varney, M. D. (1994). Application of the three-dimensional structures of protein target molecules in structure-based drug design. *J. Med. Virol.* **37**(8), 1035-54.

Hiraiwa, M., Uda, Y., Tsuji, S., Miyatake, T., Martin, B. M., Tayama, M., O'Brien, J. S. & Kishimoto, Y. (1991). Human placental sialidase complex: Characterization of the 60 kDa protein that cross-reacts with anti-saposin antibodies. *Biochem. Biophys. Res. Commun.* **177**(3), 1211-1216.

Hirst, G. K. (1941). The agglutination of red blood cells by allontoic fluid of chick embryos infected with influenza virus. *Science,* **94**, 22-23.

Hoffler, U., Gloor, M. & von Nicolai, H. (1981). Neuraminidase production by *Propionibacterium acnes*-strains isolated from patients with acne vulgaris, seborrheic eczema and healthy subjects. *Z. Bakteriol. Mikrobiol. Hygiene,* **250**(1-2), 122-126.

Hogue, B. G. & Nayak, D. P. (1992). Synthesis and processing of the influenza virus neuraminidase, a type II transmembrane glycoprotein. *Virology,,* **188**(2), 510-517.

Hoyer, L. L., Hamilton, A. C., Steenbergen, S. M. & Vimr, E. R. (1992). Cloning, sequencing and distribution of the *Salmonella typhimurium* LT2 sialidase gene, nanH, provides evidence for interspecies gene transfer. *Mol. Microbiol.* **6**(7), 873-884.

Hoyer, L. L., Roggentin, P., Schauer, R. & Vimr, E. R. (1991). Purification and properties of cloned *Salmonella typhimurium* LT2 sialidase with virus-typical kinetic preference for sialyl alpha 2→3 linkages. *J. Biochem.* **110**(3), 462-467.

Jedrzejas, M. J., Singh, S., Brouillette, W. J., Laver, W. G., Air, G. M. & Luo, M. (1995). Structures of aromatic inhibitors of influenza virus neuraminidase. *Biochemistry,* **34**, 3144-3151.

Jones, T. A. (1985). Interactive Computer Graphics: FRODO. *Methods Enzymol.* **115**, 157-71.Kabayo, J. P. & Hutchinson, D. W. (1977). Studies on a neuraminidase from *Streptomyces griseus. FEBS Lett.* **78**(2), 221-224.

Kabayo, J. P. & Hutchinson, D. W. (1977). Studies on a neuraminidase from *Streptomyces griseus. FEBS Lett.* **78**(2), 221-224.

Kilbourne, E. D. (1987). *Influenza*. First edition, Plenum Publishing Corporation, New York, NY.

Kinabo, L. D. B. (1993). Pharmacology of existing drugs for animal trypanosomiasis. *Acta Trop. (Basel),* **54**, 169-183.

Kopitz, J., von Reitzenstein, C., Muhl, C. & Cantz, M. (1994). Role of plasma membrane ganglioside sialidase of human neuroblastoma cells in growth control and differentiation. *Biochem. Biophys. Res. Commun.* **199**(3), 1188-1193.

LaMarco, K. L., Diven, W. F., Glew, R. H., Doyle, W. J. & Cantekin, E. I. (1984). Neuraminidase activity in middle ear effusions. *Ann. Otol. Rhinol. Laryngol.* **93**(1), 76-84.

Laver, W. G. (1978). Crystallization and peptide maps of neuraminidase "heads" from H2N2 and H3N2 influenza virus strains. *Virology,* **86**, 78-87.

Lin, Y., Luo, M., Laver, W. G., Air, G. M., Smith, C. D. & Webster, R. G. (1990). New crystalline forms of neuraminidase of type B human influenza virus. *J. Mol. Biol.* **214**, 639-640.

Liu, C. & Air, G. M. (1993). Selection and characterization of a neuraminidase-minus mutant of influenza virus and its rescue by cloned neuraminidase genes. *Virology,* **194**(1), 403-407.

Liu, C., Eichelberger, M. C., Compans, R. W. & Air, G. M. (1995). Influenza type A virus neuraminidase does not play a role in viral entry, replication, assembly or budding. *J. Virol.* **69**(2), 1099-1106.

Luo, M., Jedrzejas, M. J., Singh, S., White, C. L., Brouillette, W. J., Air, G. M. & Laver, W. G. (1994). Benzoic acid inhibitors of influenza virus neuraminidase. *Acta Crystallogr. D,* in press.

Marchesini, S., Cestaro, B., Lombardo, A., Sciorelli, G. & Preti, A. (1984). Human blood cells sialidases. *Biochem. Int.* **8**(1), 151-158.

Markoff, L., Lin, B. C., Sveda, M. M. & Lai, C. J. (1984). Glycosylation and surface expression of the influenza virus neuraminidase requires the N-terminal hydrophobic region. *Mol. Cell Biol.* **4**(1), 8-16.

Mast, E. E., Harmon, M. W., Gravenstein, S., Wu, S. P., Arden, N. H., Circo, R., Tyszka, G., Kendal, A. P. & Davis, J. P. (1991). Emergence and possible transmission of amantadine-resistant viruses during nursing home outbreaks of influenza A (H3N2). *Am. J. Epidemiol.* **134**(9), 988-997.

Meyer, D. M., Lemonnier, M. & Bourrillon, R. (1981). Human liver neuraminidase. *Biochem. Biophys. Res. Commun.* **103**(4), 1302-1309.

Michalski, J. C., Corfield, A. P. & Schauer, R. (1986). Properties of human liver lysosomal sialidase. *Biol. Chem. Hoppe-Seyler,* **367**(8), 715-722.

Mier, P. D., van Rennes, H., van Erp, P. E. & Roelfzema, H. (1982). Cutaneous sialidase. *J. Invest. Dermatol.* **78**(4), 267-269.

Milligan, T. W., Baker, C. J., Straus, D. C. & Mattingly, S. J. (1978). Association of elevated levels of extracellular neuraminidase with clinical isolates of type III group B *streptococci. Infect. Immun.* **21**(3), 738-746.

Ming, M., Chuenkova, M., Ortega-Barria, E. & Pereira, M. E. (1993). Mediation of *Trypanosoma cruzi* invasion by sialic acid on the host cell and trans-sialidase on the trypanosome. *Mol. Biochem. Parasitol.* **59**(2), 243-252.

Miyagi, T., Hata, K., Konno, K. & Tsuiki, S. (1992). Multiple forms of mammalian sialidase: Altered expression in carcinogenesis. *Tohoko J. Exp. Med.* **168**(2), 223-229.

Miyagi, T., Sagawa, J., Kuroki, T., Matsuya, Y. & Tsuiki, S. (1990). Tumor-promoting phorbol ester induces alterations of sialidase and sialyltransferase activities of JB6 cells. *Jap. J. Cancer Res.* **81**(12), 1286-1292.

Miyagi, T. & Tsuiki, S. (1984). Rat-liver lysosomal sialidase. Solubilization, substrate specificity and comparison with the cytosolic sialidase. *Eur. J. Biochem.* **141**(1), 75-81.

Monto, A. S. & Arden, N. H. (1992). Implications of viral resistance to amantadine in control of influenza A. *Clin. Infect. Disease,* **15**(2), 362-367.

Nakato, H., Shinomiya, K. & Mikawa, H. (1986). Possible role of neuraminidase in the pathogenesis of arteritis and thrombocytopenia induced in rats by *Erysipelothrix rhusiopathiae*. *Pathol. Res. Pract.* **181**(3), 311-319.

Pereira, M. E., Mejia, J. S., Ortega-Barria, E., Matzilevich, D. & Prioli, R. P. (1991). The *Trypanosoma cruzi* neuraminidase contains sequences similar to bacterial neuraminidases, YWTD repeats of the low density lipoprotein receptor, and type III modules of fibronectin. *J. Exp. Med.* **174**(1), 179-191.

Pilatte, Y., Bignon, J. & Lambre, C. R. (1993). Sialic acids as important molecules in the regulation of the immune system: pathophysiological implications of sialidases in immunity. *Glycobiology,* **3**(3), 210-218.

Prioli, R. P., Mejia, J. S. & Pereira, M. E. (1991). On the interaction of *Trypanosoma cruzi* neuraminidase and human lipoproteins. *Eur. J. Epidemiol.* **7**(4), 344-348.

Ramachandran, G. N. & Sasisekharan, V. (1968). Conformation of polypeptides and proteins. *Adv. Protein Chem.* **23**, 283-437.

Rogers, R., Newbrun, E. & Tatevossian, A. (1979). Neuraminidase activity in human dental plaque fluid. *Arch. Oral. Biol.* **24**(9), 703-705.

Roggentin, P., Rothe, B., Kaper, J., Galen, J., Lawrisuk, L., Vimr, E. & Schauer, R. (1989). Conserved sequences in bacterial and viral sialidases. *Glycoconj. J.* **6**(3), 349-353.

Rossmann, M. G. & Blow, D. M. (1962). The detection of sub-units within a crystallographic asymmetric unit. *Acta Crystallogr.* **15**(24), 24-31.

Saito, M. & Yu, R. K. (1986). Further characterization of a myelin-associated neuraminidase: Properties and substrate specificity. *J. Neurochem.* **47**(2), 632-641.

Saito, M. & Yu, R. K. (1992). Role of myelin-associated neuraminidase in the ganglioside metabolism of rat brain myelin. *J. Neurochem.* **58**(1), 83-87.

Shoichet, B. K. & Kuntz, I. D. (1993). Matching chemistry and shape in molecular docking. *Prog. Med. Chem.* **6**(7), 723-732.

Straus, D. C., Unbehagen, P. J. & Purdy, C. W. (1993b). Neuraminidase production by a *Pasteurella haemolytica* A1 strain associated with bovine pneumonia. *Infect. Immun.* **61**(1), 253-259.

Sun, T. (1982). *Pathology and Clinical Features of Parasitic Diseases.* Masson Publishing USA, Inc., New York, NY.

Sweeley, C. C. (1993). Extracellular sialidases. *Adv. Lipid Res.* **26**, 235-252.

Tomlinson, S., Pontes de Carvalho, L., Vandekerckhove, F. & Nussenzweig, V. (1992). Resialylation of sialidase-treated sheep and human erythrocytes by *Trypanosoma cruzi* trans-sialidase: restoration of complement resistance of desialylated sheep erythrocytes. *Glycobiology,* **2**(6), 549-551.

Usuki, S., Lyu, S. C. & Sweeley, C. C. (1988). Sialidase activities of cultured human fibroblasts and the metabolism of GM3 ganglioside. *J. Biol. Chem.* **263**(14), 6847-6853.

Venerando, B., Fiorilli, A., Di Francesco, L., Chiarini, A., Monti, E., Zizioli, D. & Tettamanti, G. (1994). Cytosolic sialidase from pig brain: A 'protein complex' containing catalytic and protective units. *Biochim. Biophy. Acta,* **1208**(2), 229-237.

Webster, R. G., Reay, P. A. & Laver, W. G. (1988). Protection against lethal influenza with neuraminidase. *Virology,* **164**(1), 230-237.

Wharton, S. A., Belshe, R. B., Skehel, J. J. & Hay, A. J. (1994). Role of virion M2 protein in influenza virus uncoating: specific reduction in the rate of membrane fusion between virus and liposomes by amantadine. *J. Gen. Virol.* **75**(Pt 4), 945-948.

Wlodawer, A. & Erickson, J. W. (1993). Structure-based inhibitors of HIV-1 protease. *Annu. Rev. Biochem.* **62**, 543-585.

Program Manual for the Wisconsin Package, Version 8 (1994), Genetics Computer Group, Madison, WI.

XENGEN: A Guide to Macromolecular X-ray Data Reduction Using the XENGEN Package for Nicolet Area Detector Systems (1987), Nicolet Instrument Co., Madison, WI.

APPENDIX A

Summary of known sialidases

Table A

Summary of known sialidases

Source	M.W. (Da)	linkage[a]	pH	K_m (M) for NANL	Location[b]	Notes	Reference
[a] presented in decreasing order of affinity			[b] MB: membrane-bound; EC: extracellular				
Viral Sources:							
Orthomyxoviridae							
Influenza virus, type A	240,000	α2→3, α2→6	5.0-9.0	2.0×10^{-4}	MB	• Ca^{2+} activated • Neu5Ac: Ki = 5×10^{-3} • Neu5Ac2en: Ki = 5×10^{-6} • X-ray structure solved	(Air & Laver, 1989; Drzeniek, 1972; Gottschalk, 1957)
Influenza virus, type B	240,000	α2→3, α2→6	5.0-9.0	2.0×10^{-4}		• Ca^{2+} activated • Neu5Ac Ki ≈ 1×10^{-6} • X-ray structure solved	(Drzeniek, 1972)
Influenza virus, type C						• HN (Hemaglutinin-sialidase)	(Drzeniek, 1972)
Paramyxoviridae							
Newcastle Disease virus							(Corfield *et al.*, 1981)
Mumps virus		α2→3, α2→8			MB	• HN (Hemaglutinin-sialidase) • also called Sendai virus	(Sokol *et al.*, 1961; Waxham & Aronowski, 1988)
Parainfluenza virus, type 1					MB	• HN (Hemaglutinin-sialidase)	(Sokol *et al.*, 1961)

Source	M.W. (Da)	linkage[a]	pH	K_m (M) for NANL	Location[b]	Notes	Reference
[a] presented in decreasing order of affinity			[b] MB: membrane-bound; EC: extracellular				
Parainfluenza virus, type 2			4.5		MB	• HN (Hemaglutinin-sialidase)	(Drzeniek & Gauhe, 1970; Holzer *et al.*, 1993)
Parainfluenza virus, type 3							(Dawson & Patterson, 1967)
Bacterial Sources:							
Actinomyces							
A. israelii						• 63% of isolates produce sialidase	(Moncla & Braham, 1989)
A. meyeri						• 73% of isolates produce sialidase	(Moncla & Braham, 1989)
A. naeslundii						• 85% of isolates produce sialidase • dental pathogen	(Moncla & Braham, 1989; Saunders & Miller, 1983)
A. odontolyticus						• 73% of isolates produce sialidase	(Moncla & Braham, 1989)
A. viscosus	100,000, 113,000, 150,000	α2→6, α2→3, α2→8			MB (?)	• 100% of isolates produce sialidase • gene cloned (2x) • monomeric	(Henningsen *et al.*, 1991; Moncla & Braham, 1989; Teufel *et al.*, 1989; Yeung & Fernandez, 1991)
Arthrobacteridae							
A. aurescens							(Uchida *et al.*, 1977)
A. oxydans							(Uchida *et al.*, 1977)

Source	M.W. (Da)	linkage[a]	pH	K_m (M) for NANL	Location[b]	Notes	Reference
[a] presented in decreasing order of affinity				[b] MB: membrane-bound; EC: extracellular			
A. *sialophilus*	88,000	α2→3, α2→6, α2→8		7.8×10^{-4} 3.3×10^{-3}		• monomeric • Ca^{2+} independent	(Flashner *et al.*, 1977; Miller *et al.*, 1978; Wang *et al.*, 1978)
A. ureaficiens I	51,000	α2→3, α2→6, α2→8	5.0[c]			• potentially oligomeric • pH optimum 5.0-5.5 • Ca^{2+} independent	(Saito *et al.*, 1979; Uchida *et al.*, 1977; Uchida *et al.*, 1979)
A. ureaficiens II	39,000	α2→6, α2→3, α2→8	5.5[d]			• Sulfhydryl groups seemed to be involved in its active site and only sialidase so far reported to cleave the lipid substrate in the presence of bile salts. • pH optimum 5.0-5.5 • Ca^{2+} independent	(Corfield *et al.*, 1983; Uchida *et al.*, 1979)
Bacteroides							

[c] substrate: NANL

[d] substrate: bovine mucin

Source	M.W. (Da)	linkage[a]	pH	K_m (M) for NANL	Location[b]	Notes	Reference
[a] presented in decreasing order of affinity					[b] MB: membrane-bound; EC: extracellular		
B. loescheii	87,000	α2→3, α2→6, α2→8	4.8		EC	• 100% of isolates produce sialidase	(Moncla *et al.*, 1990; Takeshita *et al.*, 1991)
B. bivius						• 98% of isolates produce sialidase	(Fraser & Brown, 1981; Moncla *et al.*, 1990)
B. buccalis						• 100% of isolates produce sialidase	(Moncla *et al.*, 1990)
B. capillosus						• 100% of isolates produce sialidase	(Moncla *et al.*, 1990)
B. denticola						• 100% of isolates produce sialidase	(Moncla *et al.*, 1990)
B. disiens						• 79% of isolates produce sialidase	(Moncla *et al.*, 1990)
B. distasonis							(Fraser & Brown, 1981)
B. forsythus						• 100% of isolates produce sialidase	(Moncla *et al.*, 1990)

Source	M.W. (Da)	linkage[a]	pH	K_m (M) for NANL	Location[b]	Notes	Reference
[a] presented in decreasing order of affinity				[b] MB: membrane-bound; EC: extracellular			
B. fragilis	55,000 monomer, 165,000 trimer	α2→8, α2→3, α2→6	6.4, 4.5	1×10^{-3}M		• 94% of isolates produce sialidase • gene cloned • trimeric • maybe a risk factor for preterm birth • sialidase activity may be for carbon source and/or adherence • most virulent species • not homologous to other sialidases • Ca^{2+} independent • cell associated	(Akimoto *et al.*, 1994; Berg *et al.*, 1983; Briselden *et al.*, 1992; Fraser & Brown, 1981; Godoy *et al.*, 1993; Guzman *et al.*, 1990; Hammann *et al.*, 1981; Moncla *et al.*, 1990; *Ono et al.*, 1994; Tanaka *et al.*, 1992; Tanaka *et al.*, 1994)
B. levii						• 100% of isolates produce sialidase	(Moncla *et al.*, 1990)
B. melaninogenicus						• 100% of isolates produce sialidase	(Moncla *et al.*, 1990)
B. ochraceus							(Fraser & Brown, 1981)
B. oralis						• 55% of isolates produce sialidase	(Fraser & Brown, 1981; Hammann *et al.*, 1981; *Moncla et al.*, 1990)
B. ovatus							(Fraser & Brown, 1981)

Source	M.W. (Da)	linkage[a]	pH	K_m (M) for NANL	Location[b]	Notes	Reference
[a] presented in decreasing order of affinity			[b] MB: membrane-bound; EC: extracellular				
B. thetaiotaomicron							(Fraser & Brown, 1981)
B. variabilis							(Fraser & Brown, 1981)
B. vulgatus							(Fraser & Brown, 1981)
Bifidobacteridae							
B. lactentis	38,000	α2→3, α2→6, α2→8	5.0-6.0	7.1 x10^{-3}			(von Nicolai *et al.*, 1981)
Clostridium							
C. beijerinckii	300,000						(Popoff & Dodin, 1985)
C. butyricum							(Popoff & Dodin, 1985)
C. chauvoei	310,000	α2→3			EC	• dimeric • Ca^{2+} dependent • gene cloned	(Fraser, 1978; Heuermann *et al.*, 1991)
C. difficile	105,000						(Popoff & Dodin, 1985)
C. perfringens I	64,000		4.4-5.6				(Rood & Wilkinson, 1976)
C. perfringens II	66,000						(Bouwstra *et al.*, 1987; Rood & Wilkinson, 1976)
C. perfringens III	125,000	α2→3, α2→6	5.3			• gene cloned	(Rood & Wilkinson, 1976)

Source	M.W. (Da)	linkage[a]	pH	K_m (M) for NANL	Location[b]	Notes	Reference
[a] presented in decreasing order of affinity			[b] MB: membrane-bound; EC: extracellular				
C. septicum	110,000, 125,000 monomer	α2→3, α2→6, α2→8	5.3			• gene cloned • Ca^{2+} independent • exists in monomeric, dimeric, and trimeric forms	(Fraser, 1978; Rothe *et al.*, 1991; Zenz *et al.*, 1993)
C. sordellii							
C. tertium						• Ca^{2+} independent	(Fraser, 1978)
Candidae							
C. albicans							(Royal *et al.*, 1984)
Capnocytophaga ochracea							
C. sputigena						• 100% of isolates produce sialidase	(Moncla *et al.*, 1990)
Corynebacteridae							
C. aquaticum	55,600		5.5	1.3×10^{-4}			(Sondag-Thull *et al.*, 1989)
C. diphtheria	65,000				MB		(Blumberg & Warren, 1961)
C. ulcerans	70,000	α2→3	5.5	5.2×10^{-4}			(Vertiev & Ezepchuk, 1981)
Diplococcus							
D. pneumoniae	70,000				EC		(Heimer & Meyer, 1956)
Erysipelothrix							

Source	M.W. (Da)	linkage[a]	pH	K_m (M) for NANL	Location[b]	Notes	Reference
[a] presented in decreasing order of affinity			[b] MB: membrane-bound; EC: extracellular				
E. rhusiopathiae							(Nakato *et al.*, 1986; von Nicolai *et al.*, 1978)
Gardneralla							
G. vaginalis							(Briselden *et al.*, 1992)
Klebsiella							
K. aerogenes							(Pardoe, 1970)
Micromonosporae							
M. viridifaciens						• gene cloned	(Sakurada *et al.*, 1992)
Pasteurellae							
P. haemolytica A1 subtype	150,000-170,000	α2→3, α2→8	6.5		EC	• etiological agent for bovine pneumonia	(Frank & Tabatabai, 1981; Straus *et al.*, 1993a; Straus *et al.*, 1993b)
P. multicida type 3					MB		(Ifeanyi & Bailie, 1992; Laurell, 1959)
P. pseudotuberculosis							(Laurell, 1959)
Prevotellae							
P. ?							(Briselden *et al.*, 1992)
Porphyromonae							

Source	M.W. (Da)	linkage[a]	pH	K_m (M) for NANL	Location[b]	Notes	Reference
[a] presented in decreasing order of affinity			[b] MB: membrane-bound; EC: extracellular				
P. gingivalis						• 100% of isolates produce sialidase	(Moncla *et al.*, 1990)
Pseudomonae							
P. aeruginosa		α2→3	6.6-7.0		EC	• Ca2+ independent • gene cloned • prevalent in cystic fibrosis patients	(Cacalano *et al.*, 1992; Leprat & Michel-Briand, 1980; Shilo, 1957)
P. fluorescens							(Shilo, 1957)
P. stuzeri							(Shilo, 1957)
Propionibacterium							
P. acnes	33,000	α2→3, α2→6, α2→8	5.0			• 90% of isolates produce sialidase • possible etiological agent for acne vulgaris or seborrheic eczema	(Hoffler *et al.*, 1981; von Nicolai *et al.*, 1980a)
Salmonella							
S. typhimurium	41,300	α2→3	7.0-7.5		EC (all)	• Ca^{2+} independent • X-ray structure solved • mechanism known	(Crennell *et al.*, 1993; Guo & Sinnott, 1993; Hoyer *et al.*, 1992; Hoyer *et al.*, 1991; Milligan *et al.*, 1978; Roggentin *et al.*, 1989)

Source	M.W. (Da)	linkage[a]	pH	K_m (M) for NANL	Location[b]	Notes	Reference
[a] presented in decreasing order of affinity			[b] MB: membrane-bound; EC: extracellular				
Streptococci							
Group A	90,000		5.7	3×10^{-4}M (bovine mucin)		• Ca^{2+} dependent • cleaves only bovine submaxillary mucin, not NANL or colominic acid	(Davis *et al.*, 1979; Hayano & Tanaka, 1969)
Group B							(Hayano & Tanaka, 1969; Milligan *et al.*, 1977)
Group B, type III	106,000-125,000				EC	• cleaves only bovine submaxillary mucin, not NANL or colominic acid • prevalent in neonates	(Brown & Straus, 1987; Mattingly *et al.*, 1980; Milligan *et al.*, 1978; Milligan *et al.*, 1980)
Group C							(Brown & Straus, 1987; Hayano & Tanaka, 1969)
Group F							
Group G							(Hayano & Tanaka, 1969)
Group K							(Hayano & Tanaka, 1967; Hayano & Tanaka, 1968)
Group L							(Hayano & Tanaka, 1969)
Group M							(Hayano & Tanaka, 1969)

Source	M.W. (Da)	linkage[a]	pH	K_m (M) for NANL	Location[b]	Notes	Reference
[a] presented in decreasing order of affinity			[b] MB: membrane-bound; EC: extracellular				
S. intermedius							(Beighton & Whiley, 1990)
S. mitis	42,000				EC	• dental pathogen	(Beighton & Whiley, 1990; Liljemark *et al.*, 1989; Nonaka *et al.*, 1983)
S. oralis							(Beighton & Whiley, 1990)
S. pneumoniae	86,000, 65,000	α2→8, α2→3, α2→3	6.0			• gene cloned • localized to bacteria surface	(Camara *et al.*, 1994; Camara *et al.*, 1991; Lock *et al.*, 1988; Scanlon *et al.*, 1989)
S. sanguis	85,000		6.5		EC	• etiological agent for subacute bacterial endocarditis	(Hayano & Tanaka, 1969; Liljemark *et al.*, 1989; Straus & Portnoy-Duran, 1983)
S. viridans II (I)	42,000						(von Nicolai *et al.*, 1980b)
Streptomyces							
S. griseus							(Kabayo & Hutchinson, 1977)
Vibrio							
V. cholerae		α2→3, α2→6, α2→8	4.0-5.6			• Ca^{2+} activated • gene clone • X-ray structure solved	(Brossmer & Nebelin, 1958; Crennell *et al.*, 1994; Drzeniek, 1972; Venerando *et al.*, 1982)

Source	M.W. (Da)	linkage[a]	pH	K_m (M) for NANL	Location[b]	Notes	Reference
[a] presented in decreasing order of affinity			[b] MB: membrane-bound; EC: extracellular				
Mammalian:							
brain cytosolic sialidase	108,000 complex, 30,000 catalytic, 66,000 subunit 2, 42,000 subunit 3		6.0	4.4×10^{-4}		• porcine • interacts with gangliosides to form inactive complex • trimeric complex containing catalytic subunits and two protective subunits • no beta-galactosidase or carboxypeptidase activity reported for trimer complex	(Breen *et al.*, 1988; Venerando *et al.*, 1994; Venerando *et al.*, 1985)
brain lysosomal sialidase	70,000		4.0-4.3, 5.0			• mice • rat • detergent deactivated	(Fiorilli *et al.*, 1989; Miyagi *et al.*, 1990a; Yohe *et al.*, 1986)
brain plasma-membrane sialidase			5.1			• mice • detergent activated	(Fiorilli *et al.*, 1989)
brain synaptosomal membrane sialidase	70,000		5.0			• rat • prefers ganglioside substrates over sialosaccharides	(Miyagi *et al.*, 1990)

Source	M.W. (Da)	linkage[a]	pH	K_m (M) for NANL	Location[b]	Notes	Reference
[a] presented in decreasing order of affinity			[b] MB: membrane-bound; EC: extracellular				
cerebellar granule cell sialidase			3.9			• human (?) • detergent activates ganglioside activity	(Pitto *et al.*, 1989)
Chinese hamster ovary (CHO) cell extracellular sialidase	43,000	α2→3, α2→6	5.9		EC	• hamster • gene cloned	(Ferrari *et al.*, 1994; Warner *et al.*, 1993)
CNS myelin-associated sialidase			4.0-4.5			• rat brain • active against gangliosides and sialosaccharides • strong preference for GM1 ganglioside	(Moran *et al.*, 1986; Saito & Yu, 1986; Saito & Yu, 1993; Yohe *et al.*, 1986)
erythrocyte plasma membrane sialidase I			4.2		MB	• human • GPI-anchored • prefers ganglioside substrates	(Chiarini *et al.*, 1993; Marchesini *et al.*, 1984)
erythrocyte plasma membrane sialidase II	48,000-54,000		4.6		MB	• human • rat • rabbit • Fe^{2+}, Fe^{3+}, DTT inhibit activity • detergent activated • no GPI-anchor • located in cytosolic face of plasma membrane	(Chen *et al.*, 1994; Marchesini *et al.*, 1984; Sagawa *et al.*, 1990)

Source	M.W. (Da)	linkage[a]	pH	K_m (M) for NANL	Location[b]	Notes	Reference
[a] presented in decreasing order of affinity			[b] MB: membrane-bound; EC: extracellular				
fibroblast lysosomal sialidase		α2→3, α2→6			MB	• human • ganglioside GM3 not a substrate	(Mendla & Cantz, 1984; Zeigler & Bach, 1981)
fibroblast plasma membrane sialidase			4.5		MB	• human • detergent activated • salt activated	(Lieser *et al.*, 1989; Zeigler & Bach, 1981)
fibroblast extracellular sialidase			6.5		EC	• human	(Usuki *et al.*, 1988; Usuki & Sweeley, 1988)
granulocyte sialidase I			4.0			• human	(Marchesini *et al.*, 1984)
granulocyte sialidase II			4.8			• human	(Marchesini *et al.*, 1984)
hepatopancreatic sialidase	32,000		5.0			• shrimp Penaeus japonicus • monomeric • Cu^{2+} or Hg^{2+} inhibits activity • forms complex with beta-galactosidase w/o protective protein carboxypeptidase	(Chuang & Yang, 1990)
kidney lysosomal sialidase		α2→3, α2→8, α2→6	4.4, 4.2	2.8×10^{-4}		• human • rat • Ca^{2+} independent	(Baricos *et al.*, 1986; Cohen-Forterre *et al.*, 1984)
large intestinal sialidase						• rat • human	(Corfield & Clamp, 1984; Den Tandt *et al.*, 1987)

Source	M.W. (Da)	linkage[a]	pH	K_m (M) for NANL	Location[b]	Notes	Reference
[a] presented in decreasing order of affinity			[b] MB: membrane-bound; EC: extracellular				
leukocyte sialidase I	203,000		5.0		MB	• human • oligomeric (?)	(Hong *et al.*, 1980)
leukocyte sialidase II (plasma membrane)	240,000		4.0		MB	• human • oligomeric (?) • prefers gangliosides as substrate • detergent activated • Cu^{2+} inhibited	(Den Tandt & Brossmer, 1984; Hong *et al.*, 1980; Waters *et al.*, 1994)
leukocyte sialidase III (lysosomal membrane ?)	48,500	α2→3, α2→6	4.6			• human • rat • Ca^{2+} activated	(Sagawa *et al.*, 1990; Schauer *et al.*, 1984)
liver cytosolic sialidase (I and/or II)	60,000, 43,000	α2→3, α2→6, α2→8	5.8, 6.0, 6.5, 5.4-5.8			• rat • gangliosides GM1, GM2, bovine submaxillary mucin are not substrate • bile acids required for ganglioside activity	(Michalski *et al.*, 1986; Miyagi *et al.*, 1984; Miyagi & Tsuiki, 1985; Samollow *et al.*, 1990; Spaltro & Alhadeff, 1987)

Source	M.W. (Da)	linkage[a]	pH	K_m (M) for NANL	Location[b]	Notes	Reference
[a] presented in decreasing order of affinity			[b] MB: membrane-bound; EC: extracellular				
liver intralysosomal sialidase	60,000, 70,000	α2→3, α2→6, α2→8	4.0-4.5, 4.6-4.8	1.1×10^{-3}		• human • rat • Ca^{2+} decreases activity • NaCl, LiCl, KCl decrease activity • gangliosides are not a substrate	(Alhadeff & Wolfe, 1981; den Tandt & Scharpe, 1984; Meyer *et al.*, 1981; Michalski *et al.*, 1982; Miyagi *et al.*, 1984; Miyagi & Tsuiki, 1984; Samollow *et al.*, 1990)
liver plasma membrane sialidase		α2→8, α2→3, α2→6,	4.5		MB	• rat	(Sagawa *et al.*, 1988)
lymphocyte sialidase I			4.0			• human	(Marchesini *et al.*, 1984)
lymphocyte sialidase II			4.8			• human	(Marchesini *et al.*, 1984)
macrophage cytosolic sialidase			5.4			• rabbit	(Pilatte *et al.*, 1987)
macrophage lysosomal sialidase			4.2			• rabbit	(Pilatte *et al.*, 1987)

Source	M.W. (Da)	linkage[a]	pH	K_m (M) for NANL	Location[b]	Notes	Reference
[a] presented in decreasing order of affinity			[b] MB: membrane-bound; EC: extracellular				
neuroblastoma lysosomal sialidase						• human • prefers GM3 ganglioside as substrate • regulator of proliferation and differentiation (?) • detergent activated • Cu^{2+} inhibited	(Kopitz *et al.*, 1994)
neuroblastoma plasma membrane sialidase						• human • detergent activated • Cu^{2+} inhibited	(Kopitz *et al.*, 1994)
neutrophil sialidase						• human • transported between granules and plasma-membrane	(Cross & Wright, 1991)
parenchymal cytosolic sialidase			4.6			• porcine • Cu^{2+} inhibits activity • Ca^{2+}, Zn^{2+} increase activity	(Terzidis-Trabelsi *et al.*, 1991)
parenchymal lysosomal sialidase			3.6-3.8			• porcine • Cu^{2+} inhibits activity • Ca^{2+}, Zn^{2+} increase activity	(Terzidis-Trabelsi *et al.*, 1991)

Source	M.W. (Da)	linkage[a]	pH	K_m (M) for NANL	Location[b]	Notes	Reference
[a] presented in decreasing order of affinity			[b] MB: membrane-bound; EC: extracellular				
placental sialidase I	67,000	α2→3, α2→6	4.4	1.0×10^{-4}		• human • will not cleave bovine submaxillary mucin	(Hiraiwa *et al.*, 1988; Hiraiwa *et al.*, 1987; McNamara *et al.*, 1982)
placental sialidase II	63,000		4.4	6.0×10^{-5}		• human • will not cleave fetuin	(McNamara *et al.*, 1982)
placental lysosomal sialidase I	76,000					• human • forms complex with beta-galactosidase and 32 kDa protective protein carboxypeptidase	(Verheijen *et al.*, 1987)
placental lysosomal sialidase II	66,000					• human • forms complex with beta-galactosidase and protective protein carboxypeptidase heterodimer (679 kDa)	(Potier *et al.*, 1990; van der Horst *et al.*, 1989; Verheijen *et al.*, 1987)
platelet sialidase			4.2			• human • rat	(Marchesini *et al.*, 1984; Sagawa *et al.*, 1990)

Source	M.W. (Da)	linkage[a]	pH	K_m (M) for NANL	Location[b]	Notes	Reference
[a] presented in decreasing order of affinity			[b] MB: membrane-bound; EC: extracellular				
retinal rod outer segment sialidase			4.0		MB	• calf • prefers gangliosides (GM1) to glycoprotein substrates	(Dreyfus *et al.*, 1983)
salivary gland lysosomal sialidase			4.0-4.5			• rat	(Sato *et al.*, 1989)
submandibullar/ parotid gland lysosomal sialidase			5.5			• rat	(Sato *et al.*, 1989)
skeletal muscle cytosolic sialidase						• rat • gene cloned	(Dairaku *et al.*, 1986; Miyagi *et al.*, 1993)
spermatazoa sialidase		α2→6	4.3	8.8×10^{-4}	MB	• rabbit • 20mM Ca^{2+} inhibits activity	(Srivastava & Abou-Issa, 1977)
spleen sialidase			3.8		MB	• bovine	(Schengrund *et al.*, 1979)
starfish sialidase	63,000 monomer, 230,000 tetramer	α2→3, α2→6	4.2			• starfish Asterias rubens • tetrameric • Cu^{2+} inhibits activity • salt inhibits activity	(Schauer & Wember, 1989)
thymic sialidase						• calf	(Bieringer & Zoch, 1990)
thymocyte lysosomal sialidase			acidic		MB	• human	(Greffard *et al.*, 1994)

Source	M.W. (Da)	linkage[a]	pH	K_m (M) for NANL	Location[b]	Notes	Reference
[a] presented in decreasing order of affinity				[b] MB: membrane-bound; EC: extracellular			
thyroidal lysosomal membrane sialidase					MB	• bovine • detergent activated	(Van Dessel *et al.*, 1984)
thyroidal plasma membrane sialidase					MB	• bovine • detergent activated	(Van Dessel *et al.*, 1984)
testicular cytosolic sialidase	900,000	α2→3	acidic			• porcine • forms complex with beta-galactosidase	(Yamamoto & Nishimura, 1987)
Parasitic sources:							
Acanthamoeba trophozoites and cyst forms			5.0		MB then EC	• free living amoebae • human pathogen • *colonizes corneal* epithelium	(Pellegrin *et al.*, 1991)
Eimeria *E. tenella*	180,000-190,000					• sialidase activity 10-20x higher in merozoitic versus sporozoitic forms • recognized by antibodies to *T. cruzi* trans-sialidase	(Pellegrin *et al.*, 1993)

Source	M.W. (Da)	linkage[a]	pH	K_m (M) for NANL	Location[b]	Notes	Reference
[a] presented in decreasing order of affinity				[b] MB: membrane-bound; EC: extracellular			
E. maxima						• sialidase activity 10-20x higher in *merozoitic versus* sporozoitic forms	(Pellegrin *et al.*, 1993)
E. necatrix						• sialidase activity 10-20x higher in *merozoitic versus* sporozoitic forms	(Pellegrin *et al.*, 1993)
Endotrypanum trans-sialidase/ sialidase						• kinetics differ from trypanosomal enzyme	(Medina-Acosta *et al.*, 1994a; Medina-Acosta *et al.*, 1994b)
Leishmanae						• no trans-sialidase or sialidase activity found	(Medina-Acosta *et al.*, 1994a; Wyler & Suzuki, 1983)
Plasmodium *P. falciparum*						• human pathogen	(Sharma *et al.*, 1992)
Trichomonae *T. vaginalis* sialidase					EC		(Costa e Silva Filho *et al.*, 1989)

Source	M.W. (Da)	linkage[a]	pH	K_m (M) for NANL	Location[b]	Notes	Reference
[a] presented in decreasing order of affinity			[b] MB: membrane-bound; EC: extracellular				
T. foetus sialidase I	320,000 dimer of tetramers	α2→3, α2→6, α2→8	4.7-5.5		EC	• etiological agent for vaginal infections and sterility/pre-term abortion in bovine • prefers high-molecular weight substrates • Ca^{2+} independent • Cu^{2+}, Hg^{2+} inhibited	(Costa e Silva Filho *et al.*, 1989; Crampen *et al.*, 1979)
T. foetus sialidase II	38,000		4.7-5.5		EC	• etiological agent for vaginal infections and sterility/pre-term abortion in bovine • prefers low-molecular weight substrates • Ca^{2+} independent • Cu^{2+}, Hg^{2+} inhibited	(Crampen *et al.*, 1979)
Trypanosomae							

Source	M.W. (Da)	linkage[a]	pH	K_m (M) for NANL	Location[b]	Notes	Reference
[a] presented in decreasing order of affinity			[b] MB: membrane-bound; EC: extracellular				
T. brucei procyclic form trans-sialidase/ sialidase	67,000	α2→3, α2→6	6.9		MB	• procyclic form found in insect host • mammalian blood stream form did not express sialidase activity • GPI-anchored • divalent metal *ions inhibit* activity	(Engstler *et al.*, 1992; Engstler *et al.*, 1993)
T. cruzi epimastigote form trans-sialidase/ sialidase	90,000	α2→3			MB	• low expression in log phase insect epimastigote form, but high expression in late log-stationary phase insect epimastigote form • may lack tandem repeat domain found in trypomastigote form	(Chaves *et al.*, 1993)

Source	M.W. (Da)	linkage[a]	pH	K_m (M) for NANL	Location[b]	Notes	Reference
[a] presented in decreasing order of affinity			[b] MB: membrane-bound; EC: extracellular				
T. cruzi trypomastigote form trans-sialidase/ sialidase	60,000	α2→3	6.0-6.5, 6.5-7.0		MB	• gene cloned • developmentally regulated expression • high expression in infectious blood stage trypomastigote form • acceptor protein is trypanosomal Ssp-3 protein • etiological agent of Chagas' disease • sialidase/trans-sialidase activity may be responsible for cardiac trauma in infected patients • GPI-anchored	(Colli, 1993; Harth *et al.*, 1987; Libby *et al.*, 1986; Pereira, 1983; Pereira *et al.*, 1991; Schenkman *et al.*, 1991; Schenkman *et al.*, 1992; Scudder *et al.*, 1993)
T. conorhini trans-sialidase/ sialidase							(Medina-Acosta *et al.*, 1994a)
T. leeuwenhoeki sialidase							(Medina-Acosta *et al.*, 1994a)
T. lewisi trans-sialidase/ sialidase							(Medina-Acosta *et al.*, 1994a)

Source	M.W. (Da)	linkage[a]	pH	K_m (M) for NANL	Location[b]	Notes	Reference
[a] presented in decreasing order of affinity			[b] MB: membrane-bound; EC: extracellular				
T. rangeli sialidase	48,000	α2→3, α2→6	5.0			• will not cleave α2→8 link substrates such as submaxillary mucin • no trans-sialidase activity found	(Buschiazzo *et al.*, 1993; Pereira & Moss, 1985; Pontes-de-Carvalho *et al.*, 1993)
T. vivax sialidase							(Esievo, 1979)
Other unique sialidases:							
bacteriophage endosialidase (ϕ 92)	105,000 monomer 328,000 trimer	α2→8				• requires a minimum of 5 sialy residues in poly-sialyl substrate	(*Finne* & Makela, 1985; Hallenbeck *et al.*, 1987)
Macrobdella decora 2,7-anhydro-alpha-N-acetylneuraminic acid sialidase						• leech • only cleaves sialoconjugates, not Neu5Ac-linked substrates	(Li *et al.*, 1990)

Source	M.W. (Da)	linkage[a]	pH	K_m (M) for NANL	Location[b]	Notes	Reference
[a] *presented in decreasing order of affinity*		[b] MB: membrane-bound; EC: extracellular					
KDNase		α2→3, α2→6	4.6			• isolated from loach (fish) • cleaves terminal 3-deoxy-D-glycero-D-galacto-2-nonulosonic acid (KDN) linked substrates	(Li *et al.*, 1994)

APPENDIX B

Homology modeling of trypanosomal trans-sialidase

APPENDIX B. Homology modeling of trypanosomal trans-sialidase

The amino acid sequence for trans-sialidase determined by Pereira *et al.* (1991) was compared to the sialidases isolated from the bacteria *Clostridium perfringens* and *Salmonella typhimurium*. The GenBank data base entries STYNEUR (*S. typhimurium*, 1803 bp ds-DNA) and CFSIALI (*C. perfringens*, 1385 bp ds-DNA) were converted into their corresponding peptide sequences using the GCG package of programs (Computer Genetics Group, 1994; Bilosky & Burks, 1988). The trans-sialidase protein sequence was taken directly from the original paper (Pereira *et al.*, 1991). The GCG package of alignment programs was used to align the three sialidase protein sequences (Figure 1). The inclusion of other bacterial sialidase sequences in addition to the *Salmonella* and *Clostridium* sequences did not improve the overall fit of the bacterial enzymes to the trans-sialidase. The major features of the proposed bacterial sialidase-trypanosomal trans-sialidase sequence alignment are as follows. First, the sequence alignment did not predict a trans-sialidase partner for Arg 37 in *S. typhimurium* sialidase sequence. This residue is part of the arginine triad found in all influenza and bacterial sialidases to date and is required to bind the carboxylate group of the substrate, sialic acid. Second, three cysteine residues in the bacterial sialidase are replaced by non-cysteine residues in the predicted trans-sialidase alignment. The three residues affected

```
                1                                                    50
{S. typh.}      .....MTVEK SVVFKAEGEH FTD.QKGNTI VGSGSGGTTK YFRIPAMCTT
{C. perf.}      MCNKNNTFEK NLDISHKPEP LILFNKDNNI WNS......K YFRIPNIQLL
{T. cruzi}      .......... .......... .......... .......... ..........

               51                                                   100
{S. typh.}      SKGTIVVFAD ARHNTASDQS FIDTAAARST DGGKTWNKKI AIYNDRVNSK
{C. perf.}      NDGTILTFSD IRYNGPDDHA YIDIASARST DFGKTWSYNI AMKNNRIDST
{T. cruzi}      ....MVAIAD ARYETSSENS LIDTVAKYSV DDGETWETQI AIKNSRV.SC

              101                                                   150
{S. typh.}      LSRVMDPTCI VANIQGRETI LVMVGKWNNN DKTWGAYRDK APDTDWDLVL
{C. perf.}      YSRVMDSTTV ITNT...GRI ILIAGSWNTN GN W.AMTTS TRRSDWSVQM
{T. cruzi}      VSRVVDPTVI VKG....NKL YVLVGSYYSS RSYWSSHGDA ...RDWDILL

              151                                                   200
{S. typh.}      YKSTDDGVTF S.KVETNIHD .........I VTKNGTISAM ..LGGVGSGL
{C. perf.}      IYSDDNGLTW SNKIDLTKDS .........S KVKNQPSNTI GWLGGVGSGI
{T. cruzi}      AVGEVTKSTA GGKITASIKW GSPVSLKKFF PAEMEGMHTN QFLGGAGVAI

              201                                                   250
{S. typh.}      QLNDGKLVFP VQMVRTKNIT TVLNTSFIYS TD.GITWSLP SGYCEGFGSE
{C. perf.}      VMDDGTIVMP AQISLRENNE NNYYSLIIYS KDNGETWTMG NKVPNSNTSE
{T. cruzi}      VASNGNLVYP VQVT...NKR KQVFSKIFYS EDDGKTWKFG KGRSDFGCSE

              251                                                   300
{S. typh.}      NNIIEFNASL VNNIR..NSG LRRSFETKDF GKTWTEFPPM DKKV.D....
{C. perf.}      NMVIELDGAL IMSTRYDYSG YRAAYISHDL GTTWEIYEPL NGKILT....
{T. cruzi}      PVALEWEGKL IINTRVDWKR .RLVYESSDM EKPWVEAVGT VSRVWGPSPK

              301                                                   350
{S. typh.}      NRNHGVQGST I.TIPSGNKL VAAHSSAQNK NNDYTRSDIS LYAHNL..YS
{C. perf.}      GKGSGCQGSF IKATTSNGHR IGLISAPKNT KGEYIRDNIA VYMIDFDDLS
{T. cruzi}      SNQPGSQTSF T.AVTIEGMR VMLFTHPLNF KGRCVRDRLN LWLTDNQRIY

              351                                                   400
{S. typh.}      GEVKLIDAFY PKVGNASGAG YSCLSYRKNV DKKHCMLSMK PMEVLSSRTL
{C. perf.}      KGVQEICIPY PEDGNKLGGG YSCLSFKNN. .......... HLGIVYEANG
{T. cruzi}      NVGQVSI... ....GDENSA YSSVLYKDD. ..KLYCLHEI NTDEVYSLVF

              401                                                   450
{S. typh.}      AVIYQ*.... .......... .......... .......... ..........
{C. perf.}      NIEYQDLTPY YSLINKQ*.. .......... .......... ..........
{T. cruzi}      ARLVGELRII KSVLRSWKNW TATCPAFAPL LIQPLRRQRV VVVPLSPRLV

              451                                                   500
{T. cruzi}      LLAFCRQRLP KRMGGSYRCV NASTANAERV RNGLKFAGVG GGALWPVSQQ

              501                                                   550
{T. cruzi}      GQNQRYRFAN HAFTLVASVT IHEAPRAASP LLGA*
```

Figure 1. Alignment of bacterial sialidase to trypanosomal trans-sialidase domain. The active site residues have been highlighted according to their chemical nature: acidic (red); basic (blue); and hydrophobic (green).

are Cys 103, Cys 225, and Cys 344 (*S. typhimurium* numbering). predicted to be cysteine residues in the trypanosomal trans-sialidase. The residues in *S. typhimurium*, which change to cysteines in the trans-sialidase, are Lys 94 and Gly 229. Note, neither the Lys or Gly residues are conserved in the *C. perfringens* sialidase.

On the basis of the proposed sequence alignment, the active site residues of the *Salmonella* structure were replaced with the trans-sialidase residues identified from the sequence alignment. The program SAM in the FRODO package was used to construct the trans-sialidase homology model (Jones, 1985). SAM builds the new residues using the atom positions of the starting *S. typhimurium* residues as a template. The position of atoms, which were could not be derived from the starting crystal structure, were built from a dictionary of sidechain conformers. The resulting trans-sialidase homology model was subjected to one round of Powell energy minimization. Figure 2 shows the active site of trypanosomal trans-sialidase homology model in comparison to the *S. typhimurium* bacterial sialidase.

Figure 2. Homology model of trypanosomal *T cruzi* trans-sialidase domain-DANA complex created using *Salmonella typhimurium-DANA* crystal structure and bacterial sialidase amino acid alignment. The active site residues, which could interact with the substrate, are shown. Note, Arg 37, which was not identified from the amino acid sequence alignment, is missing from the right-hand side of the arginine triad.

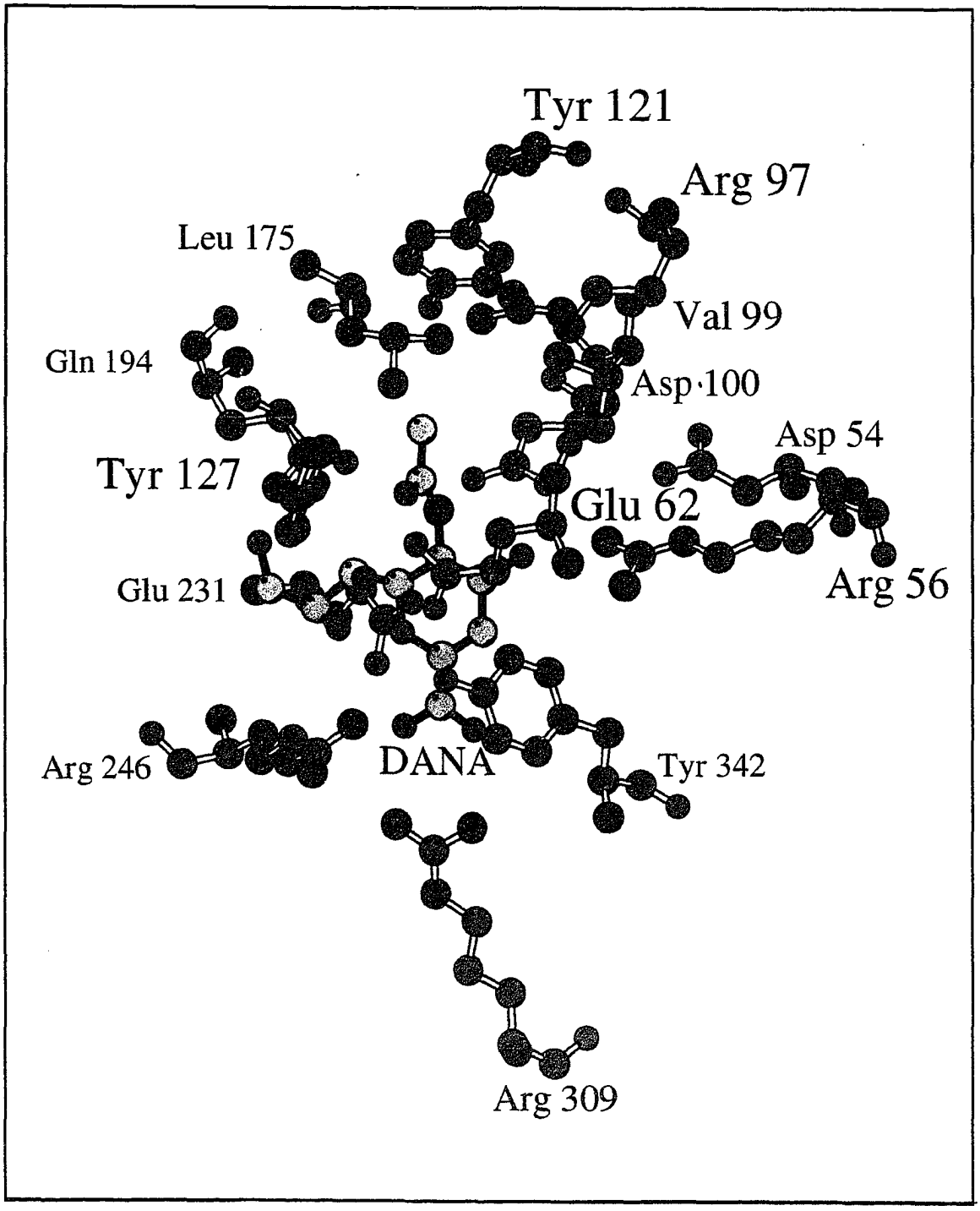

LIST OF REFERENCES FOR APPENDICES

Air, G. M. & Laver, W. G. (1989). The neuraminidase of influenza virus. *Proteins: Struct. Func. Genet.* **6**, 341-356.

Akimoto, S., Ono, T., Tsutsui, H., Kinouchi, T., Kataoka, K. & Ohnishi, Y. (1994). Complete sequence of the *Bacteroides fragilis* YCH46 neuraminidase-encoding gene. *Biochem. Biophys. Res. Comm.* **203**(2), 914-921.

Alhadeff, J. A. & Wolfe, S. (1981). Characterization of human liver (4-mythylumbelliferyl-alpha-*D*-*N*-acetylneuraminic acid) neuraminidase activity. *Int. J. Biochem.* **13**(9), 975-980.

Baricos, W. H., Cortez-Schwartz, S. & Shah, S. V. (1986). Renal neuraminidase. Characterization in normal rat kidney and measurement in experimentally induced nephrotic syndrome. *Biochem. J.* **239**(3), 705-710.

Beighton, D. & Whiley, R. A. (1990). Sialidase activity of the "Streptococcus milleri group" and other viridans group *streptococci. J. Clin. Microbiol.* **28**(6), 1431-1433.

Berg, J. O., Lindqvist, L., Andersson, G. & Nord, C. E. (1983). Neuraminidase in *Bacteroides fragilis. Appl. Environ. Microbiol.* **46**(1), 75-80.

Bieringer, K. & Zoch, E. (1990). Neuraminidase in juvenile calf thymus: Determination and characterization by a continuous fluorometric assay procedure. *Thymus,* **15**(4), 233-240.

Bilosky, H. S. & Burks, C. (1988). The GenBank (R) genetic sequence data bank. *Nucl. Acid Res.* **16**, 1861-1864.

Blumberg, B. S. & Warren, L. (1961). The effect of sialidase on transferrins and other serum proteins. *Biochim. Biophy. Acta* **50**, 90.

Bouwstra, J. B., Deyl, C. M. & Vliegenthart, J. F. (1987). Purification and kinetic properties of sialidase from *Clostridium perfringens. Biol. Chem. Hoppe-Seyler* **368**(3), 269-275.

Breen, K. C., Nolan, P. M. & Regan, C. M. (1988). Soluble rat brain sialidase does not influence intracellular glycosylation of Golgi sialyltransferase or its constitutive glycoproteins. *Neurosci. Lett.* **88**(3), 308-312.

Briselden, A. M., Moncla, B. J., Stevens, C. E. & Hillier, S. L. (1992). Sialidases (neuraminidases) in bacterial vaginosis and bacterial vaginosis-associated microflora. *J. Clin. Microbiol.* **30**(3), 663-666.

Brossmer, R. & Nebelin, E. (1958). Synthesis of *N*-formyl- and *N*-succinyl-*D*-neuraminic acid on the specificity of neuraminidase. *FEBS Lett.* **4**, 335.

Brown, J. G. & Straus, D. C. (1987). Characterization of neuraminidases produced by various serotypes of group B *streptococci. Infect. Immun.* **55**(1), 1-6.

Buschiazzo, A., Cremona, M. L., Campetella, O., Frasch, A. C. & Sanchez, D. O. (1993). Sequence of a *Trypanosoma rangeli* gene closely related to *Trypanosoma cruzi* trans-sialidase. *Mol. Biochem. Parasitol.* **62**(1), 115-116.

Cacalano, G., Kays, M., Saiman, L. & Prince, A. (1992). Production of the *Pseudomonas aeruginosa* neuraminidase is increased under hyperosmolar conditions and is regulated by genes involved in alginate expression. *J. Clin. Invest.* **89**(6), 1866-1874.

Camara, M., Boulnois, G. J., Andrew, P. W. & Mitchell, T. J. (1994). A neuraminidase from *Streptococcus pneumoniae* has the features of a surface protein. *Infect. Immun.* **62**(9), 3688-3695.

Camara, M., Mitchell, T. J., Andrew, P. W. & Boulnois, G. J. (1991). *Streptococcus pneumoniae* produces at least two distinct enzymes with neuraminidase activity: Cloning and expression of a second neuraminidase gene in *Escherichia coli. Infect. Immun.* **59**(8), 2856-2858.

Chaves, L. B., Briones, M. R. & Schenkman, S. (1993). Trans-sialidase from *Trypanosoma cruzi* epimastigotes is expressed at the stationary phase and is different from the enzyme expressed in trypomastigotes. *Mol. Biochem. Parasitol.* **61**(1), 97-106.

Chen, X. G., Nagai, T. & Yamada, H. (1994). Sialidase in rabbit blood. Characterization of sialidase purified from rabbit erythrocyte membrane. *Eur. J. Biochem.* **221**(2), 655-664.

Chiarini, A., Fiorilli, A., Di Francesco, L., Venerando, B. & Tettamanti, G. (1993). Human erythrocyte sialidase is linked to the plasma membrane by a glycosylphosphatidylinositol anchor and partly located on the outer surface. *Glycoconj. J.* **10**(1), 64-71.

Chuang, N. N. & Yang, B. C. (1990). A sialidase from the hepatopancreas of the shrimp *Penaeus japonicus* (Crustacea: Decapoda): Reversible binding with the acidic beta-galactosidase. *Comp. Biochem. Physiol.* **97**(2), 353-356.

Cohen-Forterre, L., Mozere, G., Andre, J. & Sternberg, M. (1984). Studies on kidney sialidase in normal and diabetic rats. *Biochim. Biophy. Acta,* **801**(1), 138-145.

Colli, W. (1993). Trans-sialidase: A unique enzyme activity discovered in the protozoan *Trypanosoma cruzi. FASEB J.* **7**(13), 1257-1264.

Corfield, A. P., Veh, R. W., Wember, M., Michalski, J. C. & Schauer, R. (1981). The release of *N*-acetyl- and *N*-glycolloyl-neuraminic acid from soluble complex carbohydrates and erythrocytes by bacterial, viral and mammalian sialidases. *Biochem. J.* **197**(2), 293-299.

Corfield, A. P., Higa, H., Paulson, J. C. & Schauer, R. (1983). The specificity of viral and bacterial sialidases for alpha(2-3)- and alpha(2-6)-linked sialic acids in glycoproteins. *Biochim. Biophy. Acta,* **744**(2), 121-126.

Corfield, A. P. & Clamp, J. R. (1984). Mucin sialidase in the rat large intestine. *Biochem. Soc. Trans.* **12**(4), 605-607.

Costa e Silva Filho, F., Breier-Saraiva, E. M., Tosta, M. X. & de Souza, W. (1989). *Trichomonas vaginalis* and *Tritrichomonas foetus* secrete neuraminidase into the culture medium. *Mol. Biochem. Parasitol.* **35**(1), 73-78.

Crampen, M., von Nicolai, H. & Zilliken, F. (1979). Properties and substrate specificities of two neuraminidases from

Trichomonas fetus. Hoppe-Seyler's Z. Physiol. Chem. **360**(12), 1703-1712.

Crennell, S., Garman, E., Laver, G., Vimr, E. & Taylor, G. (1994). Crystal structure of *Vibrio cholerae* neuraminidase reveals dual lectin-like domains in addition to the catalytic domain. *Structure,* **2**(6), 535-544.

Crennell, S. J., Garman, E. F., Laver, W. G., Vimr, E. R. & Taylor, G. L. (1993). Crystal structure of a bacterial sialidase (from *Salmonella typhimurium* LT2) shows the same fold as an influenza virus neuraminidase. *Proc. Nat. Acad. Sci. USA,* **90**(21), 9852-9856.

Cross, A. S. & Wright, D. G. (1991). Mobilization of sialidase from intracellular stores to the surface of human neutrophils and its role in stimulated adhesion responses of these cells. *J. Clin. Invest.* **88**(6), 2067-2076.

Dairaku, K., Miyagi, T., Wakui, A. & Tsuiki, S. (1986). Cytosolic sialidases of rat tissues with special reference to skeletal muscle enzyme. *Biochem. Int.* **13**(5), 741-748.

Davis, L., Baig, M. M. & Ayoub, E. M. (1979). Properties of extracellular neuraminidase produced by group A streptococcus. *Infect. Immun.* **24**(3), 780-786.

Dawson, P. S. & Patterson, D. (1967). Neuraminidase activity of a bovine parainfluenza 3 virus. *Nature (London),* **213**, 185.

Den Tandt, W. R. & Brossmer, R. (1984). Determination of methylumbelliferyl-*N*-acetylneuraminic acid sialidase for clinical purposes. *J. Clin. Chem. Clin. Biochem.* **22**(2), 189-193.

Den Tandt, W. R. & Scharpe, S. (1984). Methylumbelliferyl-*N*-acetylneuraminic acid sialidase in human liver. *Biochem. Med.* **31**(3), 287-293.

Den Tandt, W. R., Adriaenssens, K. & Scharpe, S. (1987). Characteristics of human intestinal acid sialidase. *Enzyme,* **37**(3), 155-158.

Dreyfus, H., Preti, A., Harth, S., Pellicone, C. & Virmaux, N. (1983). Neuraminidase in calf retinal outer segment membranes. *J. Neurochem.* **40**(1), 184-188.

Drzeniek, R. & Gauhe, A. (1970). Differences in substrate specificity of myxovirus neuraminidase. *Biochem. Biophys. Res. Comm.* **38**, 651.

Drzeniek, R. (1972). Viral and bacterial neuraminidases. *Curr. Top. Microbiol. Immunol.* **59**, 35-74.

Engstler, M., Reuter, G. & Schauer, R. (1992). Purification and characterization of a novel sialidase found in procyclic culture forms of *Trypanosoma brucei*. *Mol. Biochem. Parasitol.* **54**(1), 21-30.

Engstler, M., Reuter, G. & Schauer, R. (1993). The developmentally regulated trans-sialidase from *Trypanosoma brucei* sialylates the procyclic acidic repetitive protein. *Mol. Biochem. Parasitol.* **61**(1), 1-13.

Esievo, K. A. N. (1979). *16th Meeting of the OAU/STRC International Council for Trypanosomiasis Research and Control, Yaunde, Cameroun.*

Ferrari, J., Harris, R. & Warner, T. G. (1994). Cloning and expression of a soluble sialidase from Chinese hamster ovary cells: Sequence alignment similarities to bacterial sialidases. *Glycobiology,* **4**(3), 367-373.

Finne, J. & Makela, P. H. (1985). Cleavage of the polysialosyl units of brain glycoproteins by a bacteriophage endosialidase. Involvement of a long oligosaccharide segment in molecular interactions of polysialic acid. *J. Biol. Chem.* **260**(2), 1265-1270.

Fiorilli, A., Venerando, B., Siniscalco, C., Monti, E., Bresciani, R., Caimi, L., Preti, A. & Tettamanti, G. (1989). Occurrence in brain lysosomes of a sialidase active on ganglioside. *J. Neurochem.* **53**(3), 672-680.

Flashner, M., Wang, P., Hurley, J. B. & Tanenbaum, S. W. (1977). Properties of an inducible extracellular neuraminidase from an Arthrobacter isolate. *J. Bacteriol.* **129**(3), 1457-1465.

Frank, G. H. & Tabatabai, L. B. (1981). Neuraminidase activity of *Pasteurella haemolytica* isolates. *Infect. Immun.* **32**(3), 1119-1122.

Fraser. (1978). Neuraminidase production by *Clostridia. J. Med. Microbiol.* **11**(3), 269-280.

Fraser, A. G. & Brown, R. (1981). Neuraminidase production by *Bacteroidaceae. J. Med. Microbiol.* **14**(1), 63-76.

Godoy, V. G., Dallas, M. M., Russo, T. A. & Malamy, M. H. (1993). A role for *Bacteroides fragilis* neuraminidase in bacterial growth in two model systems. *Infect. Immun.* **61**(10), 4415-4426.

Gottschalk, A. (1957). Neuraminidase: the specific enzyme of influenza virus and *Vibrio cholerae. Biochim. Biophys. Acta,* **23**, 645-646.

Greffard, A., Pairon, J. C., Terzidis-Trabelsi, H., Heslan, J. M., Bignon, J., Lambre, C. R. & Pilatte, Y. (1994). Initial characterization of human thymocyte sialidase activity: Evidence that this enzymatic system is not altered during the course of T-cell maturation. *Int. J. Biochem.* **26**(6), 769-776.

Guo, X. & Sinnott, M. L. (1993). *Salmonella typhimurium* neuraminidase acts with inversion of configuration. *Biochem. J.* **296**(Pt 2), 291-292.

Guzman, C. A., Plate, M. & Pruzzo, C. (1990). Role of neuraminidase-dependent adherence in *Bacteroides fragilis* attachment to human epithelial cells. *FEMS Microbiol. Lett.* **59**(1-2), 187-192.

Hallenbeck, P. C., Vimr, E. R., Yu, F., Bassler, B. & Troy, F. A. (1987). Purification and properties of a bacteriophage-induced endo-*N*-acetylneuraminidase specific for poly-alpha-2,8-sialosyl carbohydrate units. *J. Biol. Chem.* **262**(8), 3553-3561.

Hammann, R., von Nicolai, H. & Werner, H. (1981). Neuraminidases of *Bacteroidaceae. Z. Bakteriol.* **248**(4), 526-531.

Harth, G., Haidaris, C. G. & So, M. (1987). Neuraminidase from *Trypanosoma cruzi*: Analysis of enhanced expression of the enzyme in infectious forms. *Proc. Nat. Acad. Sci. USA,* **84**(23), 8320-8324.

Hayano, S. & Tanaka, A. (1967). Streptococcal sialidase I: Isolation and properties of sialidase produced by group K streptococcus. *J. Bacteriol.* **93**, 1753.

Hayano, S. & Tanaka, A. (1968). Streptococcal sialidase II: Kinetic and immunological studies of sialidase produced by group K streptococcus. *J. Bacteriol.* **95**, 1551.

Hayano, S. & Tanaka, A. (1969). Sialidase-like enzymes produced by group A, B, C, G and L *streptococci* and by *streptococcus sanguis. J. Bacteriol.* **97**, 1328.

Heimer, R. & Meyer, K. (1956). Studies on sialic acid of submaxillary mucoid. *Proc. Nat. Acad. Sci. USA,* **42**, 728.

Henningsen, M., Roggentin, P. & Schauer, R. (1991). Cloning, sequencing and expression of the sialidase gene from *Actinomyces viscosus* DSM 43798. *Biol. Chem. Hoppe-Seyler,* **372**(12), 1065-1072.

Heuermann, D., Roggentin, P., Kleineidam, R. G. & Schauer, R. (1991). Purification and characterization of a sialidase from *Clostridium chauvoei* NC08596. *Glycoconj. J.* **8**(2), 95-101.

Hiraiwa, M., Uda, Y., Nishizawa, M. & Miyatake, T. (1987). Human placental sialidase: Partial purification and characterization. *J. Biochem.* **101**(5), 1273-1279.

Hiraiwa, M., Nishizawa, M., Uda, Y., Nakajima, T. & Miyatake, T. (1988). Human placental sialidase: Further purification and characterization. *J. Biochem.* **103**(1), 86-90.

Hoffler, U., Gloor, M. & von Nicolai, H. (1981). Neuraminidase production by *Propionibacterium acnes*-strains isolated from patients with acne vulgaris, seborrheic eczema and healthy subjects. *Z. Bakteriol. Mikrobiol. Hygiene,* **250**(1-2), 122-126.

Holzer, C. T., von Itzstein, M., Jin, B., Pegg, M. S., Stewart, W. P. & Wu, W. Y. (1993). Inhibition of sialidases from viral, bacterial and mammalian sources by analogues of 2-deoxy-2,3-didehydro-*N*-acetylneuraminic acid modified at the C-4 position. *Glycoconj. J.* **10**(1), 40-44.

Hong, V. N., Beauregard, G., Potier, M., Belisle, M., Mameli, L., Gatti, R. & Durand, P. (1980). Studies on the sialidoses: properties of human leucocyte neuraminidases. *Biochim. Biophy. Acta,* **616**(2), 259-270.

Hoyer, L. L., Hamilton, A. C., Steenbergen, S. M. & Vimr, E. R. (1992). Cloning, sequencing and distribution of the *Salmonella typhimurium* LT2 sialidase gene, nanH, provides evidence for interspecies gene transfer. *Mol. Microbiol.* **6**(7), 873-884.

Hoyer, L. L., Roggentin, P., Schauer, R. & Vimr, E. R. (1991). Purification and properties of cloned *Salmonella typhimurium* LT2 sialidase with virus-typical kinetic preference for sialyl alpha 2→3 linkages. *J. Biochem.* **110**(3), 462-467.

Ifeanyi, F. I. & Bailie, W. E. (1992). Passive protection of mice with antiserum to neuraminidase from *Pasteurella multocida* serotype A:3. *Vet. Res. Comm.* **16**(2), 97-105.

Kabayo, J. P. & Hutchinson, D. W. (1977). Studies on a neuraminidase from *Streptomyces griseus. FEBS Lett.* **78**(2), 221-224.

Kopitz, J., von Reitzenstein, C., Muhl, C. & Cantz, M. (1994). Role of plasma membrane ganglioside sialidase of human neuroblastoma cells in growth control and differentiation. *Biochem. Biophys. Res. Commun.* **199**(3), 1188-1193.

Laurell, A. B. (1959). Neuraminidase-like factors in cultures of *pneumococci, a-streptococci,* and *pasturella pseudotuberculosis. Acta Pathol. Microbiol. Scand.* **47**, 182.

Leprat, R. & Michel-Briand, Y. (1980). Extracellular neuraminidase production by a strain of *Pseudomonas aeruginosa* isolated from cystic fibrosis. *Ann. Microbiol.* **3**, 209-222.

Li, Y. T., Nakagawa, H., Ross, S. A., Hansson, G. C. & Li, S. C. (1990). A novel sialidase which releases 2,7-anhydro-alpha-*N*-

acetylneuraminic acid from sialoglycoconjugates. *J. Biol. Chem.* **265**(35), 21629-21633.

Li, Y. T., Yuziuk, J. A., Li, S. C., Nematalla, A., Hasegawa, A., Kimura, M. & Nakagawa, H. (1994). A novel sialidase capable of cleaving 3-deoxy-*D*-glycero-*D*-galacto-2-nonulosonic acid (KDN). *Arch. Biochem. Biophys* **310**(1), 243-246.

Libby, P., Alroy, J. & Pereira, M. E. (1986). A neuraminidase from *Trypanosoma cruzi* removes sialic acid from the surface of mammalian myocardial and endothelial cells. *J. Clin. Invest.* **77**(1), 127-135.

Lieser, M., Harms, E., Kern, H., Bach, G. & Cantz, M. (1989). Ganglioside GM3 sialidase activity in fibroblasts of normal individuals and of patients with sialidosis and mucolipidosis IV. Subcellular distribution and and some properties. *Biochem. J.* **260**(1), 69-74.

Liljemark, W. F., Bloomquist, C. G., Fenner, L. J., Antonelli, P. J. & Coulter, M. C. (1989). Effect of neuraminidase on the adherence to salivary pellicle of *Streptococcus sanguis* and *Streptococcus mitis*. *Caries Res.* **23**(3), 141-145.

Lock, R. A., Paton, J. C. & Hansman, D. (1988). Purification and immunological characterization of neuraminidase produced by *Streptococcus pneumoniae*. *Microbial Pathol.* **4**(1), 33-43.

Marchesini, S., Cestaro, B., Lombardo, A., Sciorelli, G. & Preti, A. (1984). Human blood cells sialidases. *Biochem. Int.* **8**(1), 151-158.

Mattingly, S. J., Milligan, T. W., Pierpont, A. A. & Straus, D. C. (1980). Extracellular neuraminidase production by clinical isolates of group B *streptococci* from infected neonates. *J. Clin. Microbiol.* **12**(4), 633-635.

McNamara, D., Beauregard, G., Nguyen, H. V., Yan, D. L., Belisle, M. & Potier, M. (1982). Characterization of human placental neuraminidases. Stability, substrate specificity and molecular weight. *Biochem. J.* **205**(2), 345-351.

Medina-Acosta, E., Franco, A. M., Jansen, A. M., Sampol, M., Neves, N., Pontes-de-Carvalho, L., Grimaldi Junior, G. & Nussenzweig, V. (1994a). Trans-sialidase and sialidase activities discriminate between morphologically indistinguishable trypanosomatids. *Eur. J. Biochem.* **225**(1), 333-339.

Medina-Acosta, E., Paul, S., Tomlinson, S. & Pontes-de-Carvalho, L. C. (1994b). Combined occurrence of trypanosomal sialidase/trans-sialidase activities and leishmanial metalloproteinase gene homologues in *Endotrypanum* sp. *Mol. Biochem. Parasitol.* **64**(2), 273-282.

Mendla, K. & Cantz, M. (1984). Specificity studies on the oligosaccharide neuraminidase of human fibroblasts. *Biochem. J.* **218**(2), 625-628.

Meyer, D. M., Lemonnier, M. & Bourrillon, R. (1981). Human liver neuraminidase. *Biochem. Biophys. Res. Commun.* **103**(4), 1302-1309.

Michalski, J. C., Corfield, A. P. & Schauer, R. (1982). Solubilization and affinity chromatography of a sialidase from human liver. *Hoppe-Seyler's Z. Physiol. Chem.* **363**(9), 1097-2002.

Michalski, J. C., Corfield, A. P. & Schauer, R. (1986). Properties of human liver lysosomal sialidase. *Biol. Chem. Hoppe-Seyler,* **367**(8), 715-722.

Miller, C. A., Wang, P. & Flashner, M. (1978). Mechanism of Arthrobacter sialophilus neuraminidase: The binding of substrates and transition-state analogs. *Biochem. Biophys. Res. Comm.* **83**(4), 1479-1487.

Milligan, T. W., Baker, C. J., Straus, D. C. & Mattingly, S. J. (1978). Association of elevated levels of extracellular neuraminidase with clinical isolates of type III group B *streptococci. Infect. Immun.* **21**(3), 738-746.

Milligan, T. W., Mattingly, S. J. & Straus, D. C. (1980). Purification and partial characterization of neuraminidase from type III group B *streptococci. J. Bacteriol.* **144**(1), 164-171.

Milligan, T. W., Straus, D. C. & Mattingly, S. J. (1977). Extracellular neuraminidase production by group B *streptococci*. *Infect. Immun.* **18**(1), 189-195.

Miyagi, T., Goto, T. & Tsuiki, S. (1984). Sialidase of rat hepatomas: qualitative and quantitative comparison with rat liver sialidase. *Gann*, **75**(12), 1076-1082.

Miyagi, T., Konno, K., Emori, Y., Kawasaki, H., Suzuki, K., Yasui, A. & Tsuik, S. (1993). Molecular cloning and expression of cDNA encoding rat skeletal muscle cytosolic sialidase. *J. Biol. Chem.* **268**(35), 26435-26440.

Miyagi, T., Sagawa, J., Konno, K., Handa, S. & Tsuiki, S. (1990). Biochemical and immunological studies on two distinct ganglioside-hydrolyzing sialidases from the particulate fraction of rat brain. *J. Biochem.* **107**(5), 787-793.

Miyagi, T. & Tsuiki, S. (1984). Rat-liver lysosomal sialidase. Solubilization, substrate specificity and comparison with the cytosolic sialidase. *Eur. J. Biochem.* **141**(1), 75-81.

Miyagi, T. & Tsuiki, S. (1985). Purification and characterization of cytosolic sialidase from rat liver. *J. Biol. Chem.* **260**(11), 6710-6716.

Moncla, B. J. & Braham, P. (1989). Detection of sialidase (neuraminidase) activity in *Actinomyces* species by using 2'-(4-methylumbelliferyl)alpha-*D*-*N*-acetylneuraminic acid in a filter paper spot test. *J. Clin. Microbiol.* **27**(1), 182-184.

Moncla, B. J., Braham, P. & Hillier, S. L. (1990). Sialidase (neuraminidase) activity among gram-negative anaerobic and capnophilic bacteria. *J. Clin. Microbiol.* **28**(3), 422-425.

Moran, N. M., Breen, K. C. & Regan, C. M. (1986). Characterization and cellular localization of a developmentally regulated rat neural sialidase. *J. Neurochem.* **47**(1), 18-22.

Nakato, H., Shinomiya, K. & Mikawa, H. (1986). Possible role of neuraminidase in the pathogenesis of arteritis and thrombocytopenia induced in rats by *Erysipelothrix rhusiopathiae*. *Pathol. Res. Pract.* **181**(3), 311-319.

Nonaka, H., Ishikawa, Y., Otsuka, M., Toda, K., Sato, M. & Nakamura, R. (1983). Purification and some properties of neuraminidase isolated from the culture medium of oral bacterium *Streptococcus mitis* ATCC 9811. *J. Dental Res.* **62**(7), 792-797.

Ono, T., Akimoto, S., Kinouchi, T., Kataoka, K. & Ohnishi, Y. (1994). Cloning and expression of the *Bacteroides fragilis* YCH46 neuraminidase gene in *Escherichia coli* and *Bacteroides uniformis*. *FEMS Microbiol. Lett.* **121**(2), 153-158.

Pardoe, G. J. (1970). The inducible neuraminidase (N-acyl-neuraminyl hydrolase EC 3.2.1.18) of *Klebsiella aerogenes* NCIB 9479. *Pathol. Microbiol.* **35**, 361.

Pellegrin, J. L., Ortega-Barria, E., Barza, M., Baum, J. & Pereira, M. E. (1991). Neuraminidase activity in acanthamoeba species trophozoites and cysts. *Invest. Opthalmol. Visual Sci.* **32**(12), 3061-3066.

Pellegrin, J. L., Ortega-Barria, E., Prioli, R. P., Buerger, M., Strout, R. G., Alroy, J. & Pereira, M. E. (1993). Identification of a developmentally regulated sialidase in *Eimeria tenella* that is immunologically related to the *Trypanosoma cruzi* enzyme. *Glycoconj. J.* **10**(1), 57-63.

Pereira, M. E. (1983). A developmentally regulated neuraminidase activity in *Trypanosoma cruzi*. *Science*, **219**(4591), 1444-1446.

Pereira, M. E., Mejia, J. S., Ortega-Barria, E., Matzilevich, D. & Prioli, R. P. (1991). The *Trypanosoma cruzi* neuraminidase contains sequences similar to bacterial neuraminidases, YWTD repeats of the low density lipoprotein receptor, and type III modules of fibronectin. *J. Exp. Med.* **174**(1), 179-191.

Pereira, M. E. & Moss, D. (1985). Neuraminidase activity in *Trypanosoma rangeli*. *Mol. Biochem. Parasitol.* **15**(1), 95-103.

Pilatte, Y., Bignon, J. & Lambre, C. R. (1987). Lysosomal and cytosolic sialidases in rabbit alveolar macrophages: Demonstration of increased lysosomal activity after in vivo activation with bacillus Calmette-Guerin. *Biochim. Biophy. Acta*, **923**(1), 150-155.

Pitto, M., Chigorno, V., Giglioni, A., Valsecchi, M. & Tettamanti, G. (1989). Sialidase in cerebellar granule cells differentiating in culture. *J. Neurochem.* **53**(5), 1464-1470.

Pontes-de-Carvalho, L. C., Tomlinson, S. & Nussenzweig, V. (1993). *Trypanosoma rangeli* sialidase lacks trans-sialidase activity. *Mol. Biochem. Parasitol.* **62**(1), 19-25.

Popoff, M. R. & Dodin, A. (1985). Survey of neuraminidase production by *Clostridium butyricum*, *Clostridium beijerinckii*, and *Clostridium difficile* strains from clinical and nonclinical sources. *J. Clin. Microbiol.* **22**(5), 873-876.

Potier, M., Michaud, L., Tranchemontagne, J. & Thauvette, L. (1990). Structure of the lysosomal neuraminidase-beta-galactosidase-carboxypeptidase multienzymic complex. *Biochem. J.* **267**(1), 197-202.

Roggentin, P., Rothe, B., Kaper, J., Galen, J., Lawrisuk, L., Vimr, E. & Schauer, R. (1989). Conserved sequences in bacterial and viral sialidases. *Glycoconj. J.* **6**(3), 349-353.

Rood, J. I. & Wilkinson, R. G. (1976). Relationship between hemagglutinin and sialidase from *Clostridium perfringens* CN3870: Chromatographic characterization of the biologically active proteins. *J. Bacteriol.* **126**(2), 831-844.

Rothe, B., Rothe, B., Roggentin, P. & Schauer, R. (1991). The sialidase gene from *Clostridium septicum*: Cloning, sequencing, expression in *Escherichia coli* and identification of conserved sequences in sialidases and other proteins. *Mol. Gen. Genet.* **226**(1-2), 190-197.

Royal, G. J., Nandedkar, A. K., Sampson, C. C. & Faggett, T. (1984). Neuraminidase production by *Candida albicans*. *J. Nat. Med. Assoc.* **76**(2), 143-145.

Sagawa, J., Miyagi, T. & Tsuiki, S. (1988). Membrane-associated sialidase of rat liver and its decrease in hepatomas. *Jap. J. Cancer Res.* **79**(1), 69-73.

Sagawa, J., Miyagi, T. & Tsuiki, S. (1990). Characterization of the major sialidases of various types of rat blood cells: Their

comparison with rat liver sialidases. *J. Biochem.* **107**(3), 452-456.

Saito, M., Sugano, K. & Nagai, Y. (1979). Action of *Arthrobacter ureafaciens* sialidase on sialoglycolipid substrates. Mode of action and highly specific recognition of the oligosaccharide moiety of ganglioside GM1. *J. Biol. Chem.* **254**(16), 7845-7854.

Saito, M. & Yu, R. K. (1986). Further characterization of a myelin-associated neuraminidase: Properties and substrate specificity. *J. Neurochem.* **47**(2), 632-641.

Saito, M. & Yu, R. K. (1993). Possible role of myelin-associated neuraminidase in membrane adhesion. *J. Neurosci. Res.* **36**(2), 127-32.

Sakurada, K., Ohta, T. & Hasegawa, M. (1992). Cloning, expression, and characterization of the *Micromonospora viridifaciens* neuraminidase gene in *Streptomyces lividans. J. Bacteriol.* **174**(21), 6896-6903.

Samollow, P. B., Ford, A. L. & VandeBerg, J. L. (1990). Biochemical characteristics and subcellular localizations of rat liver neuraminidase isozymes: A paradox resolved. *Biochem. Genet.* **28**(5-6), 283-298.

Sato, A., Hiramatsu, M., Kashimata, M., Murayama, M., Minami, N. & Minami, N. (1989). Characteristics of sialidase in the rat salivary glands. *Enzyme,* **41**(4), 200-208.

Saunders, J. M. & Miller, C. H. (1983). Neuraminidase-activated attachment of *Actinomyces naeslundii* ATCC 12104 to human buccal epithelial cells. *J. Dental Res.* **62**(10), 1038-40.

Scanlon, K. L., Diven, W. F. & Glew, R. H. (1989). Purification and properties of *Streptococcus pneumoniae* neuraminidase. *Enzyme,* **41**(3), 143-150.

Schauer, R. & Wember, M. (1989). Isolation and characterization of a sialidase from the starfish *Asterias rubens. Biol. Chem. Hoppe-Seyler,* **370**(3), 183-190.

Schauer, R., Wember, M. & Tschesche, H. (1984). Isolation and characterization of an oligosaccharide- and glycoprotein-specific sialidase from human leucocytes. *Hoppe-Seyler's Z. Physiol. Chem.* **365**(4), 419-426.

Schengrund, C. L., Repman, M. A. & Nelson, J. T. (1979). Distribution in spleen subcellular organelles of sialidase active towards natural sialogylcolipid and sialoglycoprotein substrates. *Biochim. Biophy. Acta,* **568**(2), 377-385.

Schenkman, S., Jiang, M. S., Hart, G. W. & Nussenzweig, V. (1991). A novel cell surface trans-sialidase of *Trypanosoma cruzi* generates a stage-specific epitope required for invasion of mammalian cells. *Cell,* **65**(7), 1117-1125.

Schenkman, S., Pontes de Carvalho, L. & Nussenzweig, V. (1992). *Trypanosoma cruzi* trans-sialidase and neuraminidase activities can be mediated by the same enzymes. *J. Exp. Med.* **175**(2), 567-575.

Scudder, P., Doom, J. P., Chuenkova, M., Manger, I. D. & Pereira, M. E. (1993). Enzymatic characterization of beta-*D*-galactoside alpha 2,3-trans-sialidase from *Trypanosoma cruzi. J. Biol. Chem.* **268**(13), 9886-9891.

Sharma, A., Biswas, S. & Sarin, K. (1992). *Plasmodium falciparum* invades human red cells via a parasite produced glycosidase. *Ind. J. Exp. Biol.* **30**(10), 923-924.

Shilo, M. (1957). Breadkdown of lactose derivative by bacteria. *Biochem. J.* **66**, 48.

Sokol, F., Blaskovic, D. & Krizanova, O. (1961). Subunits of myxoviruses II. Properties of haemagglutinin of Newcastledisease, parainfluenza I, and mumps viruses. *Acta Virol.* **5**, 153.

Sondag-Thull, D., Levene, N. A., Levene, C., Manny, N., Liew, Y. W., Bird, G. W., Schechter, Y., Francois-Gerard, C., Huet, M. & Blanchard, D. (1989). Characterization of a neuraminidase from *Corynebacterium aquaticum* responsible for Th polyagglutination. *Vox Sanguinis,* **57**(3), 193-198.

Spaltro, J. & Alhadeff, J. A. (1987). Cellular localization and substrate specificity of isoelectric forms of human liver neuraminidase activity. *Biochem. J.* **241**(1), 137-143.

Srivastava, P. N. & Abou-Issa, H. (1977). Purification and properties of rabbit spermatozoal acrosomal neuraminidase. *Biochem. J.* **161**(2), 193-200.

Straus, D. C., Jolley, W. L. & Purdy, C. W. (1993). Characterization of neuraminidases produced by various serotypes of *Pasteurella haemolytica*. *Infect. Immun.* **61**(11), 4669-4674.

Straus, D. C. & Portnoy-Duran, C. (1983). Neuraminidase production by a *Streptococcus sanguis* strain associated with subacute bacterial endocarditis. *Infect. Immun.* **41**(2), 507-515.

Takeshita, T., Takagaki, M., Amano, A., Murakami, Y., Nagata, H. & Shizukuishi, S. (1991). Purification and properties of neuraminidase from the culture medium of *Bacteroides loescheii*. *Oral Microbiol. Immunol.* **6**(5), 316-319.

Tanaka, H., Ito, F. & Iwasaki, T. (1992). Purification and characterization of a sialidase from *Bacteroides fragilis* SBT3182. *Biochem. Biophys. Res. Comm.* **189**(1), 524-529.

Tanaka, H., Ito, F. & Iwasaki, T. (1994). Two sialidases which preferentially hydrolyze sialyl alpha 2-8 linkage from *Bacteroides fragilis* SBT3182. *J. Biochem.* **115**(2), 318-321.

Terzidis-Trabelsi, H., Pilatte, Y., Greffard, A., Bignon, J. & Lambre, C. (1991). Sialidase in the guinea pig pulmonary parenchyma. Increased activity in the cytosolic and microsomal subcellular fractions after stimulation with *Bacillus Calmette Guerin*. *Biol. Chem. Hoppe-Seyler*, **372**(6), 437-442.

Teufel, M., Roggentin, P. & Schauer, R. (1989). Properties of sialidase isolated from *Actinomyces viscosus* DSM 43798. *Biol. Chem. Hoppe-Seyler*, **370**(5), 435-443.

Uchida, Y., Tsukada, Y. & Sugimori, T. (1977). Distribution of neuraminidase in *Arthrobacter* and its purification by affinity chromatography. *J. Biochem.* **82**(5), 1425-1433.

Uchida, Y., Tsukada, Y. & Sugimori, T. (1979). Enzymatic properties of neuraminidases from *Arthrobacter ureafaciens*. *J. Biochem.* **86**(5), 1573-1585.

Usuki, S., Lyu, S. C. & Sweeley, C. C. (1988). Sialidase activities of cultured human fibroblasts and the metabolism of GM3 ganglioside. *J. Biol. Chem.* **263**(14), 6847-6853.

Usuki, S. & Sweeley, C. C. (1988). Consideration of a functional role of an extracellular sialidase secreted by cultured fibroblasts. *Ind. J. Biochem. Biophys.* **25**(1-2), 102-105.

van der Horst, G. T., Galjart, N. J., d'Azzo, A., Galjaard, H. & Verheijen, F. W. (1989). Identification and in vitro reconstitution of lysosomal neuraminidase from human placenta. *J. Biol. Chem.* **264**(2), 1317-1322.

Van Dessel, G., De Wolf, M., Lagrou, A., Hilderson, H. & Dierick, W. (1984). Characterization, purification, and subcellular localization of bovine thyroid sialidases. *J. Biochem.* **96**(4), 937-947.

Venerando, B., Cestaro, B., Fiorilli, A., Ghidoni, R., Preti, A. & Tettamanti, G. (1982). Kinetics of *Vibrio cholerae* sialidase action on gangliosidic substrates at different supramolecular-organizational levels. *Biochem. J.* **203**(3), 735-742.

Venerando, B., Fiorilli, A., Di Francesco, L., Chiarini, A., Monti, E., Zizioli, D. & Tettamanti, G. (1994). Cytosolic sialidase from pig brain: A 'protein complex' containing catalytic and protective units. *Biochim. Biophy. Acta,* **1208**(2), 229-237.

Venerando, B., Fiorilli, A., Masserini, M., Giuliani, A. & Tettamanti, G. (1985). Interactions of pig brain cytosolic sialidase with gangliosides. Formation of catalytically inactive enzyme-ganglioside complexes. *Biochim. Biophy. Acta* **833**(1), 82-92.

Verheijen, F. W., Palmeri, S. & Galjaard, H. (1987). Purification and partial characterization of lysosomal neuraminidase from human placenta. *Eur. J. Biochem.* **162**(1), 63-67.

Vertiev, Y. V. & Ezepchuk, Y. V. (1981). Purification and characterization of some enzymatic properties of

neuraminidase from *Corynebacterium ulcerans*. *Hoppe-Seyler's Z. Physiol. Chem.* **362**(10), 1339-1344.

von Nicolai, H., Esser, P. & Lauer, E. (1981). Partial purification and properties of neuraminidase from *Bifidobacterium lactentis*. *Hoppe-Seyler's Z. Physiol. Chem.* **362**(2), 153-162.

von Nicolai, H., Hoffler, U. & Zilliken, F. (1980a). Isolation, purification, and properties of neuraminidase from *Propionibacterium acnes*. *Z. Bakteriol.* **247**(1), 84-94.

von Nicolai, H., Muller, H. E. & Zilliken, F. (1978). Substrate specificity of neuraminidase from *Erysipelothrix rhusiopathiae*. *Hoppe-Seyler's Z. Physiol. Chem.* **359**(3), 393-398.

von Nicolai, H., Muller, H. E. & Zilliken, F. (1980b). Purification and properties of two neuraminidases from *Streptococcus viridans* II. *FEBS Lett.* **117**(1), 107-110.

Wang, P., Tanenbaum, S. W. & Flashner, M. (1978). Purification and properties of *Arthrobacter* neuraminidase. *Biochim. Biophy. Acta* **523**(1), 170-180.

Warner, T. G., Chang, J., Ferrari, J., Harris, R., McNerney, T., Bennett, G., Burnier, J. & Sliwkowski, M. B. (1993). Isolation and properties of a soluble sialidase from the culture fluid of Chinese hamster ovary cells. *Glycobiology*, **3**(5), 455-463.

Waters, P. J., Corfield, A. P., Eisenthal, R. & Pennock, C. A. (1994). Freeze-stable sialidase activity in human leucocytes: Substrate specificity, inhibitor susceptibility, detergent requirements and subcellular localization. *Biochem. J.* **301**(Pt 3), 777-784.

Waxham, M. N. & Aronowski, J. (1988). Identification of amino acids involved in the sialidase activity of the mumps virus hemagglutinin-neuraminadase protein. *Virology*, **167**(1), 226-232.

Wyler, D. J. & Suzuki, K. (1983). In vitro parasite-monocyte interactions in human leishmaniasis: Effect of enzyme treatments on attachment. *Infect. Immun.* **42**(1), 356-61.

Yamamoto, Y. & Nishimura, K. (1987). Copurification and separation of beta-galactosidase and sialidase from porcine testis. *Int. J. Biochem.* **19**(5), 435-442.

Yeung, M. K. & Fernandez, S. R. (1991). Isolation of a neuraminidase gene from *Actinomyces viscosus* T14V. *Appl. Environ. Microbiol.* **57**(11), 3062-3069.

Yohe, H. C., Saito, M., Ledeen, R. W., Kunishita, T., Sclafani, J. R. & Yu, R. K. (1986). Further evidence for an intrinsic neuraminidase in CNS myelin. *J. Neurochem.* **46**(2), 623-629.

Zeigler, M. & Bach, G. (1981). Cellular localization of neuraminidases in cultured human fibroblasts. *Biochem. J.* **198**(3), 505-508.

Zenz, K. I., Roggentin, P. & Schauer, R. (1993). Isolation and properties of the natural and the recombinant sialidase from *Clostridium septicum* NC 0054714. *Glycoconj. J.* **10**(1), 50-56.

GRADUATE SCHOOL
UNIVERSITY OF ALABAMA AT BIRMINGHAM
DISSERTATION APPROVAL FORM

Name of Candidate Clinton Livingston White

Major Subject Biochemistry

Title of Dissertation Crystallographic Studies of Sialidase and Structure-based Design of Inhibitors

Dissertation Committee:

_____, Chairman

Director of Graduate Program _____

Dean, UAB Graduate School _____

Date 7/11/95

PS-1428